UNIVERSITAT POLITÈCNICA DE VALÈNCIA

INSTITUTO INTERUNIVERSITARIO DE RECONOCIMIENTO MOLECULAR Y DESARROLLO TECNOLÓGICO

Design of new nanostructured systems with applications in the field of recognition and diagnosis

PhD. THESIS

Submitted by

Àngela Ribes Momparler

PhD. Supervisors:

Prof. Ramón Martínez Máñez
Dr. Elena Aznar Gimeno

Valencia, July 2018

RAMÓN MARTÍNEZ MÁÑEZ, PhD in Chemistry and Professor at the *Universitat Politècnica de València*, and ELENA AZNAR GIMENO, PhD in Chemistry and researcher at *Centro de Investigación Biomédica en Red*.

CERTIFY:

That the work ***"Design of new nanostructured systems with applications in the field of recognition and diagnosis"*** has been developed by Àngela Ribes Momparler under their supervision in the Instituto Interuniversitario de Investigación de Reconocimiento Molecular y Desarrollo Tecnológico (IDM) at *Universitat Politècnica de València*, as a Thesis Project in order to obtain the degree of PhD in Chemistry at the *Universitat Politècnica de València.*

Valencia, 13th July 2018.

Prof. Ramón Martínez Máñez Dra. Elena Aznar Gimeno

A la meua família

Li ho digueren i ho va oblidar,

ho va veure i ho va entendre,

ho va fer i ho va aprendre.

Acknowledgements

Una vegada et poses a escriure aquestes línies significa que una etapa de la vida científica esta a punt d'acabar. Bé vida científica i personal ja que durant tots aquestos anys moltes persones, han passat a formar part de la meua vida i que d'una manera o altra quedaran per sempre. Per açò este apartat va dedicat a totes elles.

Primerament agraïr a Ramón, que em deixara formar part del seu grup i poder portar a terme el treball que ací presente. D'esta manera m'he format i he anat adquirint coneixements que de ben segur em serviràn per sempre. A Elena, que sempre has estat ahí des del primer minut que vaig posar un peu en l'edifici 5M, portant-me de la maneta quasi quasi i que sempre que l'he necessitat ha estat, donant-me els seus consells i gràcies a l'experiència que m'ha transmes he sabut com encaminar tots els entrebancs que han anat apareguent-me. També agraïr-li a Félix els seus consells que sempre ha estat dispost a donar. A Loles que tantes coses en el mon de la microscopia m'ha ensenyat. Andrea tu també moltes gràcies per haver estat ahí, i haver-me aconsellat i ajudat en tot moment des de que ens vam conèixer.

Com no al meu "Comando Fe", Sara, Mari Carmen que juntetes vam iniciar una nova etapa en el grup, sent les pioneres a La Fe i on l'estilisme sabeu que teniu que cuidar!! A Luís, la recent incorporació al "Comando". Als tres gràcies per tantes rises i moments que hem compartit i un bon llegat de feina en el món dels oligos vos he deixat!! Cuideu molt bé el lab de la Fe eeeh!!

A totes les personetes que formaven part del lab 2.6 i que per raons d'espai ens vam separar a Bea Lozano, sigue así y pon orden que tu vales para eso, a las principesas, Alba, Irene, Amelia (tu a medias,jjj) i Mónica. A Lorena i Xente que algún que altre consell els vaig donar als seus inicis. Toni i Santi, grans cervellets i millors persones. A la tècnic Marta que feies un gran treball! Iris, Borja, Bea de Luis, Eva y Maria a vosotros también muchas gracias! I a Luis Villaescusa que també és uno més del 2.6 i que algun que altre mal de cap del raig X hem compartit.

Tampoc m'olvide de la gent de la CPI, Cris T, seguirem trobant-nos en algún triatló de segur, Elisa, Adrián, Edgar y Maria Ruiz.

Al sector internacional Sameh, Mª Elena, Ismael, Hazem, Tania i Andy.
A les noves incorporacions Sara, Alejandra, Gema, Araceli i Juanfran que ja no he coincit molt amb ells.
També m'agradaria dedicar unes línies a esta gent que també va formar part del 2.6 i que poc a poc van anar acabant les seues tesis però que tant em va ensenyar al començament d'aquesta etapa Cris G, Maria, Nuria, LLuis, Carmen, Mar i Cris M.
A unes altres persones a les quals els estic molt agraïda son a les que formen part del servei de microscòpia de la UPV i que em van dir que no m'olvidara d'ells i vegeu que no ho he fet, gràcies Manolo i Jose Luis per tot el temps que meu dedicat.
A la gent de la tercera planta Eva, Quique i Pablo per l'ajuda que he tingut d'ells en els tràmits burocràtics que han fet falta.
També agrair a Geles i Javier del grup d' Infecció Greu de la Fe, la seua hospitalitat i ajuda quan vaig haver d'anar allí a realitzar proves.
Dir-vos que espere que açò no siga un adeu, si no, un fins prompte!!
I fora de l'àmbit laboral, com no, als meus pares que sempre han estat ahí, dia rere dia, preguntant-me que com va? I ara en que investigues? I podem ajudar-te en alguna cosa? Sempre donant-me recolzament i sobretot estant ahi! També a la meua germaneta, Teresa, que sempre esta ahí i m'escolta i soc la seua científica; gràcies per la portada tan xula que m'ha fet!! Paco a tu també moltes gràcies per aguantar-me, ajudar-me i acompanyar-me allà on ha fet falta. Tampoc vull de deixar-me a la meua iaia, cosins i tios que també sempre han mostrat interès per tot allò que he fet.
I ja per finalitzar agraïr també a amigues, amics, companys de la banda, companys del club de triatló i altres coneguts que sempre han mostrat interès i motivació per allò que estava fent.

MOLTES GRÀCIES!!

Resum

La present tesi doctoral titulada "Design of new nanostructured systems with applications in the field of recognition and diagnosis" està enfocada en el disseny i síntesi de nous materials híbrids amb funció de porta molecular utilitzant diferents suports inorgànics, basats en sílice i alúmina i que poden ser aplicats al camp del reconeixement i diagnòstic.

Així en aquesta tesi es presenta el disseny d'un nou nanodispositiu per a la detecció de Bisfenol A que és una toxina letal. En aquest sistema s'han utilitzat nanopartícules de sílice mesoporoses carregades amb rodamina B i funcionalitzades amb grups isocianat. El disseny es basa en l'utilització d'un aptàmer, que és una seqüència curta d'ADN que reconeix específicament al Bisfenol A, com a porta molecular. Aquest aptàmer s'uneix a la superfície de les nanopartícules bloquejant els porus. Únicament en presència de Bisfenol A, s'activa l'alliberament del colorant, que pot mesurar-se mitjançant espectroscòpia de fluorescència, degut a l'elevada especificitat i selectivitat de l'aptàmer per aquesta toxina. Fins el moment, no s'havia descrit cap material que utilitzara el concepte de porta molecular per a la detecció fluorogènica de Bisfenol A.

En el següent capítol s'han dissenyat dos nous nanodispositius per a la detecció d'Ocratoxina A, que és una molècula carcinògena. El sistema es compon de nanopartícules de sílice mesoporosa on els porus es tapen amb un aptàmer específic per a aquest analit. Aquestes nanopartícules es carreguen amb rodamina B i la seua superfície es funcionalitza amb grups isocianat o amino, que permeten unir l'aptàmer per via covalent o electrostàtica respectivament. En presència de la molècula d'Ocratoxina A, l'aptàmer reconeix l'analit separant-se de la superfície i permetent l'alliberament del colorant que pot analitzar-se mitjançant espectroscòpia de fluorescència. El sistema presenta elevada eficàcia en medis reals, a més d'aportar un mètode senzill i de baix cost per a poder realitzar les anàlisis.

En un altre capítol de la tesi, s'ha desenvolupat un nanodispositiu per a la detecció de cocaïna basat en suports d'alúmina anòdica nanoporosa, carregats

amb el colorant rodamina B i on els porus es tanquen fent servir un aptàmer específic per a cocaïna. En presència de l'estupefaent, l'aptàmer es desplaça de la superfície nanoporosa, permetent que la rodamina B ixca de l'interior dels porus a la dissolució. El sistema respon amb alta eficiència en medis reals com la saliva, on és habitual realitzar els test de drogues. A més, també es va estudiar la possible reutilització del suport d'alúmina, sent això un avantatge, que redueix costos i mà d'obra.

En el següent capítol s'ha desenvolupat un nou nanodispositiu capaç de detectar ADN de *Candida albicans* i que podria ser utilitzat per al diagnòstic de la infecció produïda per aquest fong. En particular, s'ha emprat alúmina anòdica nanoporosa com a suport, que s'ha carregat amb rodamina B i funcionalitzat amb grups isocianat. Per al bloqueig dels porus s'ha utilitzat una seqüència d'oligonucleòtids específica per a *Candida albicans*. D'aquesta manera, en presència d'ADN de *Candida albicans* l'oligonucleòtid que bloqueja l'entrada dels porus presenta més afinitat per l'ADN que per la unió a la superfície d'alumina funcionalitzada i conseqüentment es separa de la superfície produint l'alliberament del colorant al medi exterior. El sistema presenta molt bons resultats de sensibilitat en comparació amb altres mètodes convencionals. A més, s'ha realitzat un ampli estudi d'aquest sistema en presència d'ADN d'altres soques de l'espècie *Candida spp*. i d'altres patògens, demostrant-se la gran selectivitat del sistema desenvolupat. Com a prova de concepte, el sistema s'ha validat en mostres reals de pacients infectats per *Candida albicans*, obtenint resultats que milloren en temps als que de manera rutinària s'utilitzen per a la seua detecció. Tenint en compte aquests resultats prometedors, el sistema desenvolupat ha sigut protegit a través d'una patent.

En el setè capítol de la tesi es descriu la síntesi, caracterització i capacitats sensores de nanopartícules de sílice per a la detecció de miRNA-145. El disseny del sistema consisteix en nanopartícules de sílice mesoporoses carregades amb rodamina B, funcionalitzades amb grups isocianat o amino i que empren diverses seqüències específiques i selectives a aquest miRNA per bloquejar els porus de les nanopartícules. En presència de miRNA-145, la formació d'estructures dúplex o tríplex entre les seqüències que tapen els porus i el miRNA-145 desencadena

l'alliberament del colorant que pot seguir-se per espectroscòpia de fluorescència. A més, es mostra el funcionament del sistema en sèrum humà. Es tracta d'un mètode simple, transportable que pot ser fàcilment modificat per a diferents tipus de miRNA, oferint així un gran potencial per a aplicacions clíniques.

Els nous sistemes que es presenten en esta tesis suposen un avanç en el camp del reconeixement i diagnòstic ja que es tracta de sistemes que son ràpids, que presenten una sensibilitat i selectivitat elevades i que a més son versàtils, per això poden servir de model per a la preparació de nous sistemes per al reconeixement ràpid, sensible i selectiu d'un ampli ventall d'espècies.

Resumen

La presente tesis doctoral titulada *"Design of new nanostructured systems with applications in the field of recognition and diagnosis"* está enfocada en el diseño y sintesis de nuevos materiales híbridos con función de puerta molecular empleando diferentes soportes inorgánicos, basados en sílice y alúmina y que pueden ser aplicados al campo del reconocimiento y diagnóstico.

Así en esta tesis se presenta el diseño de un nuevo nanodispositivo para la detección del Bisfenol A que es una toxina letal. En este sistema se han utilizado nanopartículas de sílice mesoporosas cargadas con rodamina B y funcionalizadas con grupos isocioanato. El diseño se basa en el empleo de un áptamero, que es una secuencia corta de ADN que reconoce específicamente al Bisfenol A, como puerta molecular. Este aptámero se une a la superficie de las nanopartículas bloqueando los poros. Únicamente en presencia de Bisfenol A, se activa la liberación del colorante, que puede medirse mediante espectroscopía de fluorescencia, debido a la elevada especificidad y selectividad del aptámero por esta toxina. Hasta el momento, no se había descrito ningún material que utilizara el concepto de puerta molecular para la detección fluorogénica del Bisfenol A.

En siguiente capítulo se han diseñado dos nuevos nanodispositivos para la detección de Ocratoxina A, que es una molécula carcinógena. El sistema se compone de nanopartículas de silicie mesoporosa cuyos poros se bloquean con un aptámero específico para dicho analito. Estas nanopartículas se cargan con rodamina B y su superficie se funcionaliza con grupos isocianato o amina, que permiten unir el aptámero por via covalente o electrostática respectivamente. En presencia de la molécula de Ocratoxina A, el aptámero reconoce al analito separándose de la superficie y permitiendo la liberación del colorante que puede medirse mediante espectroscopía de fluorescencia. El sistema presenta elevada eficacia en medios reales, además de aportar un método sencillo y de bajo coste para poder realizar los análisis.

En otro capítulo de la tesis, se ha desarrollado un nanodispositivo para la detección de cocaína basado en soportes de alúmina anódica nanoporosa, cargados con el colorante rodamina B y cuyos poros se bloquean utilizando un aptámero específico para cocaína. En presencia del estupefaciente, el aptámero se desplaza de la superificie nanoporosa, permitiendo que la rodamina B salga del interior de los poros a la disolución. El sistema responde con alta eficiencia en medios reales como la saliva, donde es habitual realizar los test de drogas. Además, también se estudió la posible reutilización del soporte de alumina, siendo esto una ventaja, que reduce costes y mano de obra.

En el siguiente capítulo se ha desarrollado un nuevo nanodispositivo capaz de detectar ADN de *Candida albicans* y que podría ser empleado para el diagnóstico de la infección producida por este hongo. En particular, se ha empleado alúmina anódica nanoporosa como soporte, que se ha cargado con rodamina B y funcionalizado con grupos isocianato. Para el bloqueo de los poros se ha utilizado una secuencia oligonucleotídica específica para *Candida albicans*. De esta manera, en presencia de ADN de *Candida albicans* el oligonucleótido que bloquea la entrada de los poros presenta más afinidad por el ADN que por la unión a la superficie de alumina funcionalizada y consecuentemente se separa de la superficie induciendo la liberación del colorante al medio exterior. El sistema presenta muy buenos resultados de sensibilidad en comparacion con otros metodos convencionales. Además, se ha realizado un amplio estudio de este sistema en presencia de ADN de otras cepas de la especie *Candida* spp. y de otros patógenos, demostrándose la gran selectividad del sistema desarrollado. Como prueba de concepto, el sistema se ha validado en muestras reales de pacientes infectados por *Candida albicans*, obteniéndose resultados que mejoran en tiempo a los que de manera rutinaria se utilizan para su detección. Teniendo en cuenta estos resultados prometedores, el sistema desarrollado ha sido protegido mendiante una patente.

En el séptimo capítulo de la tesis se describe la síntesis, caracterización y capacidades sensoras de nanopartículas de sílice para la detección de miRNA-145. El diseño del sistema consiste en nanopartículas de sílice mesoporosas cargadas con rodamina B, funcionalizadas con grupos isocianato o amino y que emplean

varias secuencias específicas y selectivas a este miRNA para bloquear los poros de las nanopartículas. En presencia de miRNA-145, la formación de estructuras dúplex o triplex entre las secuencias que tapan los poros y el miRNA-145 activa la liberación del colorante que puede seguirse por espectroscopía de fluorescencia. Además, se muestra el funcionamiento del sistema en suero humano. Se trata de un método simple, transportable que puede ser fácilmente modificado para diferentes tipos de miRNA, ofreciendo así un gran potencial para aplicaciones clínicas.

Los nuevos sistemas que se presentan en esta tesis suponen un avance en los campos del reconocimiento y diagnóstico, ya que se trata de sistemas que son rápidos, que presentan una sensibilidad y selectividad elevadas y que son versátiles, por lo que pueden servir de modelo para la preparación de nuevos sistemas para el reconocimiento rápido, sensible y selectivo de un amplio abanico de especies.

Abstract

The present doctoral thesis entitled *Design of new nanostructured systems with applications in the field of recognition and diagnosis* is focused on the design and synthesis of new hybrid materials with molecular gate function using different inorganic supports, based on silica and alumina and that can be applied to the field of recognition and diagnosis.

This thesis presents the design of a new nanodevice for the detection of Bisphenol A, which is a lethal toxin. In this system, mesoporous silica nanoparticles loaded with rhodamine B and functionalized with isocyanate groups have been used. The design is based on the use of an aptamer, which is a short DNA sequence that specifically recognizes Bisphenol A, as a molecular gate. This aptamer is attached to the surface of the nanoparticles blocking the pores. Only in the presence of Bisphenol A, the release of the dye is observed, which can be measured by fluorescence spectroscopy, due to the high specificity and selectivity of the aptamer for this toxin. As far as we know, any material using the molecular gate concept for the fluorogenic detection of Bisphenol A has been previously described.

In the next chapter two new nanodevices for the detection of Ochratoxin A, which is a carcinogenic molecule have been designed. The system consists of mesoporous silica nanoparticles whose pores are blocked with a specific aptamer for this analyte. These nanoparticles are loaded with rhodamine B and its surface is functionalized with isocyanate or amine groups, which allow the aptamer to be attached covalently or electrostatically, respectively. In the presence of the molecule of Ochratoxin A, the aptamer recognizes the analyte by displacement from the surface and allows the release of the dye that can be measured by fluorescence spectroscopy. The system has high efficiency in real media. In addition, it provides a simple and low cost method to perform the measurements.

In another chapter of the thesis, a nanodevice for the detection of cocaine based on nanoporous anodic alumina supports, loaded with the rhodamine B dye and

whose pores are blocked using a specific aptamer for cocaine have been developed. In the presence of the narcotic drug, the aptamer is displaced from the nanoporous surface, allowing rhodamine B to escape from the pores voids to the solution. The system responds with high efficiency in real media such as saliva, where it is usual to perform drug tests. In addition, the possible reuse of the alumina support was also studied. This is an advantage, which reduces costs and labor.

In the following chapter a new nanodevice capable of detecting DNA of *Candida albicans* and that could be used for the diagnosis of the infection produced by this fungus has been developed. In particular, nanoporous anodic alumina has been used as support. It has been loaded with rhodamine B and functionalized with isocyanate groups. To block the pores, an oligonucleotide sequence specific for *Candida albicans* was used. In this way, in the presence of *Candida albicans* DNA, the oligonucleotide that blocks the entry of the pores presents more affinity for the DNA than for binding to the functionalized alumina surface and consequently it separates from the surface, inducing the release of the dye to the medium. The system presents very good sensitivity in comparison with other conventional methods. In addition, an extensive study of this system has been carried out in the presence of DNA of other strains of the species *Candida spp.* and other pathogens, demonstrating the great selectivity of the developed system. As proof of concept, the system has been validated in real samples of patients infected by *Candida albicans*, obtaining results that improve in time to those that are routinely used for their detection. Taking into account these promising results, the developed system has been protected by a patent.

The seventh chapter of the thesis describes the synthesis, characterization and sensory capacities of silica nanoparticles for the detection of miRNA-145. The system design consists of mesoporous silica nanoparticles loaded with rhodamine B, functionalized with isocyanate or amino groups and that employ several specific and selective sequences to this miRNA to block the pores of the nanoparticles. In the presence of miRNA-145, the formation of duplex or triplex structures between the pore-blocking sequences and the miRNA-145 triggers the release of the dye that can be followed by fluorescence spectroscopy. In addition,

the performance of the system in human serum is shown. It is a simple, transportable method that can be easily modified for different types of miRNA, thus offering great potential for clinical applications.

The new systems presented in this thesis represent an advance in the fields of recognition and diagnosis, as they are fast, show high sensitivity and selectivity and are versatile. Therefore they can serve as example for the preparation of new systems for rapid, sensitive and selective recognition of a wide variety of species.

Publications

Results of the present PhD thesis and other contributions have led to the following scientific publications:

Àngela Ribes, Elena Aznar, Andrea Bernardos, María Dolores Marcos, Pedro Amorós, Ramón Martínez Máñez, Felix Sancenón, *Fluorogenic Sensing of Carcinogenic Bisphenol A using Aptamer-Capped Mesoporous Silica Nanoparticles*, Chem. Eur. J. 2017, 23, 1-5.

Àngela Ribes, Sara Santiago Felipe, Andrea Bernardos, María Dolores Marcos, Teresa Pardo, Félix Sancenón, Ramón Martínez Máñez, Elena Aznar, *Two new fluorogenic aptasensors to detect Ochratoxin A based on capped mesoporous silica nanoparticles*, ChemistryOpen 2017, 6, 653-659.

Àngela Ribes, Elisabet Xifré Pérez, Elena Aznar, Felix Sancenón, Teresa Pardo, Lluís Francisco Marsal, Ramón Martínez Máñez, *Molecular gated nanoporous anodic alumina for the detection of cocaine*, Sci. Rep. 2016, 6, 38649.

Àngela Ribes, Elena Aznar, Sara Santiago-Felipe, Elisabet Xifré-Pérez, María Angeles Tormo-Más, Javier Pemán, F. Lluís Marsal and Ramón Martínez-Máñez, *New rapid and selective chromofluorogenic kit able to detect infection produced by fungi Candida albicans*, submitted.

Àngela Ribes, Maria Angeles Tormo-Mas, Elisabet Xifre Perez, Ramón Martínez-Mañez, Elena Aznar, F. Lluis Marsal, Javier Pemán, María Dolores Marcos, Félix Sancenón, "Material poroso para la detección de *Candida albicans*, método de diagnóstico que lo utiliza y método de preparación del mismo", patent application P201731069. Date: November 2017.

Àngela Ribes, Sara Santiago-Felipe, Anna Aviñó, Vicente Candela-Noguera, Ramón Eritja, Félix Sancenón, Ramón Martínez-Máñez, Elena Aznar, *Design of Oligonucleotide-capped Mesoporous Silica Nanoparticles for the detection of miRNA-145 by Duplex and Triplex formation,* Subbmited.

Pavel Bartovsky, Àngela Ribes, Alessandro Agostini Ángel Francisco Benito Beorlegui, Ramón Martínez Mañez, *Delivery modulation in silica mesoporous supports via functionalization in the pore outlets with aZn(II) bis(2-pyridylmethyl)amine complex*. Inirg. Chimic. Acta. 2014, 417, 263-269.

Abbreviations and Acronyms

A

ATP	Adenosine 5'-triphosphate
AuNPs	Gold Nanoparticles

B

BET model	Brunauer, Emmet and Teller model
BJH model	Barret, Joyner and Halenda model
BPA	Bisphenol A
BPC	Bisphenol C
BPE	Bisphenol E
BHI	Brain Heart Infusion

C

CD-GOx	Cyclodextrin-modified glucose oxidase
CIBER-BBN	Centro de Investigación biomedical en red de Bioingeniería, Biomateriales y Nanomedicina
CTABr	n-cetyltrimethylammonium bromide
CRS	Cozart® Rapid Scan
c.a.	approximately
CSF	Cerebrospinal Fluid

D

dint	Interpore distance
DNA	Deoxyribonucleic acid

DLS	Dinamyc Light Scatering
DNP	1,5- dioxynaphthalene
Dp	Nanopore diameter

E

EXC	Excitation
EDTA	Ethylendiaminetetraacetic acid

F

FESEM	Field Emision Scanning Electronic Microscopy
FITC	Fluorescein isothiocyanate
FT-IR	Fourier Transform Infrared Radiation

G

GC	Gas Chromatography
GO	Graphene Oxide
Gox	Glucose Oxidase
GSH	Glutathione
GTP	guanosine 5’-triphosphate

H

h	hours
HA	Hard anodisation
HPLC	High Pressure Liquid Chromatography

I

ICMUV	Institut de Ciència dels Materials, Universitat de València
IDM	Instituto de Reconocimiento Molecurar y Desarrollo Tecnológico
i.e.	In essence
IUPAC	International Union Pure ans Applied Chemistry

L

LOD	Limit Of Detection

M

MA	Mild anodisation
min	Minutes
MCM	Mobil Cristallyne Material
ME	Mercaptoethanol
MS	Mass Spectrometry
MSNs	Mesoporous Silica Nanoparticles
MALDI-TOF	Matrix-Assisted Laser Desorption/Ionization Time-Of-Flight

N

NAA	Nanoporous Anodic Alumina

O

Ochratoxin A	OTA

P

P	Pression
PMOs	Periodic Mesoporous organosilicas

PNIPAAm	N-Isopropylacrylamide Polymer
P_0	Absolute Pression
ppm	Parts Per Million
PXRD	Power X-Ray Diffraction
PBS	Phosphate Buffer Saline
PCR	Polymerase Chain Reaction
PNA-FISH	Peptide Nucleic Acid Fluorescent In-Situ Hybridization

R

RNA	Ribonucleic acid
SELEX	Systematic Evolution of Ligands by Exponential enrichment
SDA	Structure-Directing Agent
SMS	Silica Mesoporous Support
Rh	Rhodamine

S

SDS	Sodium Dodecyl Sulfate

T

T	Temperature
TEA	Triethylamine
TEM	Transmission Electron Microscopy
TEOS	Tetraethylorthosilicate
TGA	Thermogravimetric Analysis
TLCT	True Liquid Crystal
TMOS	Tetramethylorthosilica
TRIS	Tris(hydroxymethyl)aminomethane
TE	TRIS-EDTA

U

UV	Ultraviolet
UVM	Universidad Valencia Material
UFC	Unite forming colony

V

V	Volt

Table of Contents

1. General introduction

1.1 Supramolecular chemistry

The concept of supramolecular chemistry was firstly described in 1960 with the pioneering works of Pedersen, Cram and Lehn, who received the Nobel Prize in 1987 for their contributions to the development of this new area. According to Dr. Lehn, a 'supermolecule' is an organized complex entity that is created from the association of two or more chemical species held together by intermolecular forces. In this context, the term 'Supramolecular Chemistry' may be defined as "chemistry beyond the molecule", focusing on the organized entities of higher complexity that result from the association of two or more chemical species held together by intermolecular forces.[1] Also, 'chemistry of molecular assemblies and of the intermolecular bonds', 'chemistry of non-covalent bond' or 'non-molecular chemistry' are other expressions used for its definition.[2]

While the main basis of chemistry is the creation of molecular assemblies employing a controlled formation or breaking of bonds, supramolecular chemistry examines the weaker and reversible noncovalent interactions between molecules. These forces include hydrogen bonding, metal coordination, hydrophobic forces, van der Waals forces, π-π interactions and electrostatic effects,[3] with the aim to easily generate unique supermolecules. Development of supramolecular chemistry was inspired mainly by nature, which displays a wide variety of complex structures originated during biological processes, such as substrate binding to a receptor protein, enzymatic reactions, assembling of protein-protein complexes, immunological antigen-antibody association, intermolecular reading, translation and transcription of the genetic code, signal induction by neurotransmitters, etc. [4]

---

[1] J. M. Lehn, *Supramolecular Chemistry*, Ed. VCH, Weinheim, **1995**; J.M. Lehn, Nobel lecture, **1987**.

[2] J.W. Steed, J.L. Atwood, *Supramolecular Chemistry*, 2nd Ed., *John Wiley & Sons. Inc.* West Sussex (UK*),* **2009**.

[3] J.L. Atwood, J.L. Steed, *Encyclopedia of Supramolecular Chemistry,* 1st Ed. *Taylor & Francis Group*, New York, **2004**.

[4] K. Ariga, T. Kunitake, *Supramolecular Chemistry–Fundamentals and application*, 1st Ed., *Springer–Verlag*, Heidelberg, **2006**.

The emergence of supramolecular chemistry had a deep effect on how efficiently chemists prepare structures of different sizes and shapes with dimensions in the range of 1 to 100 nm. Following supramolecular chemistry principles, molecules can be associated by their geometric or electronic affinity yielding supramolecular aggregates that presented new properties and characteristics that are very difficult to achieve by the isolated molecular entities. These new supermolecules can be used to create even more sophisticated structures such as mesoporous materials. In a step forward, the incorporation of molecules or supermolecules onto preorganized materials offers the possibility to prepare new supramolecular chemistry-based functional systems with advanced functionality that can be a valuable tool in a wide range of fields.

1.2 Molecular recognition

Supramolecular chemistry has also made a great contribution in the development of molecular recognition systems. Recognition happens when a molecule is identified by another molecule that acts as a receptor and is spatially arranged to interact thereby minimizing the overall energy of the new supramolecular structure. In scientific terms, molecular recognition can be defined as the selective interaction between a host or receptor molecule and a guest or substrate through non-covalent interactions. In order to form a supermolecule, receptor and guest must have mutual spatial and electronic complementary binding sites, or, in other words, they must follow the lock and key principle, (Figure 1) in which the guest has a geometric size or shape complementary to the receptor or host. This concept lays the basis for molecular recognition; i.e. the discrimination by a host between a number of guests.

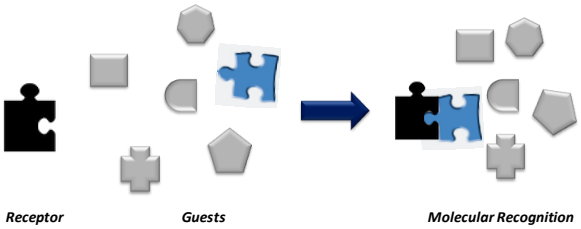

Figure 1. Molecular recognition event by a specific host-guest interaction.

Chemosensors

A molecular sensor or chemosensor is a system that interacts with an analyte producing a measurable signal. Chemosensors combine molecular recognition events with the generation of a macroscopic signal (by a reporter moiety) that reveals the presence of the guest.[5] This phenomenon should be selective and fast in order to be applicable. Whereas chemical sensors or chemosensors usually refer to systems that typically use coordinating forces for guest binding the term chemodosimeter is related with the use of specific irreversible reactions between host and guest.[6]

In general, a molecular chemical sensor or chemosensor is composed, at least, for two units which are, (i) binding subunit and (ii) signaling subunit:

(i) Binding subunit: is the unit responsible of recognition and also of the efficiency of the interaction with the selected substrate. The binding subunit, also known as receptor, must be designed with the aim to achieve a selective coordination with the target guest. To obtain this selectivity a high degree of complementarity between the receptor and the guest (in terms of size, shape, charge, etc.) is mandatory.

(ii) Signaling subunit: is the unit that acts as a signal transducer and informs of the recognition process that occurs at molecular level through changes in a measurable macroscopic signal. Traditionally, changes in color, fluorescence or redox potential have been used as signal outputs.

In particular, chromo-fluorogenic sensors offer significative advantages over other analytical methods. For example the signal is measured by a non-destructive detection method, which involves simple and extended instrumentation. Additionally, the measurements need small amounts of samples and allow, in some cases, *in situ* and real-time detection. Colorimetric sensors can be used to the naked eye sensing of analytes. While fluorogenic sensors have in general a high degree of sensitivity and specificity due to the possibility of selecting

[5] a) W.C. Rogers, M.O. Wolf, *Coord. Chem. Rev.,* **2002**, *233*, 341–350; b) S. Akine, F. Utsuno, S. Piao, H. Orita, S. Tsuzuki, T. Nabeshima, *Inorg. Chem*., **2016**, *55*, 810–821.

[6] a) R. Martínez–Máñez, F. Sancenón, *Chem. Rev.*, **2003**, *103*, 4419–4476; b) M. Moragues, R. Martínez–Máñez, F. Sancenón, *Chem. Soc. Rev.*, **2011**, *40*, 2593–2643.

excitation and emission wavelengths, and normally allow to achieve lower detection limits when compared with colorimetric techniques.

Practically, all reported examples of chromo-fluorogenic chemosensors described in the literature are constructed by the application of one of the three main approaches described below:

- **Binding site–signaling subunit approach**: In this case both units are linked through a covalent bond. The interaction of a target molecule with the binding site changes the electronic properties of the signaling subunit (a dye or a fluorophore) resulting in a sensing event via color or emission modulation.[7] Figure 2a represents this approach.
- **Displacement approach:** This protocol uses binding sites and signaling subunits forming a coordination complex (molecular ensemble), not covalently linked. This approach relies in a displacement reaction that takes place when the target molecule is coordinated with the binding site and then the signaling subunit returns to the solution. An optical response is obtained because the color or emission of the signaling subunit in the sensing ensemble is different to that presented when it is free in solution.[8] In figure 2b this approach is represented.
- **"Chemodosimeter'' approach**: The main difference between this approach and the others is that an irreversible chemical reaction takes place. This way takes advantage of target induced specific chemical reactions that generate fluorescence or color changes to signal the recognition event. This type of systems usually presents a high selectivity.[9] Figure 2c explains this approach.

[7] a) T. Gunnlaugsson, M. Glynn, G.M. Tocci, P.E. Kruger, F.M. Pfeffer, *Coord. Chem. Rev*., **2006**, *250*, 3094–3117; b) V. Amendola, D. Esteban–Gómez, L. Fabbrizzi, M. Lichelli, *Acc. Chem. Res*., **2006**, *39*, 343–353; c) T. Gunnlaugsson, H.D.P. Ali, M. Glynn, P.E. Kruger, G.M. Hussey, F.M. Pfeffer, C.M.G. Dos Santos, J. Tierney, *J. Fluoresc*., **2005**, *15,* 287–299; d) T. I. Kim, H. Jin, J. Bae, Y. Kim, *Anal. Chem*., **2017**, 89, 10566–10569.

[8] a) S.L. Wiskur, H. Ait–Haddou, J.J. Lavigne, E.V. Anslyn, *Acc. Chem. Res*., **2001**, *34*, 963–972; b) B.T. Nguyen, E.V. Anslyn, *Coord. Chem. Rev*., **2006**, *250*, 3118–3127.

[9] Z. Xu, X. Chen, H. N. Kim, J. Yoon, *Chem. Soc. Rev*., **2010**, *39*, 127–137.

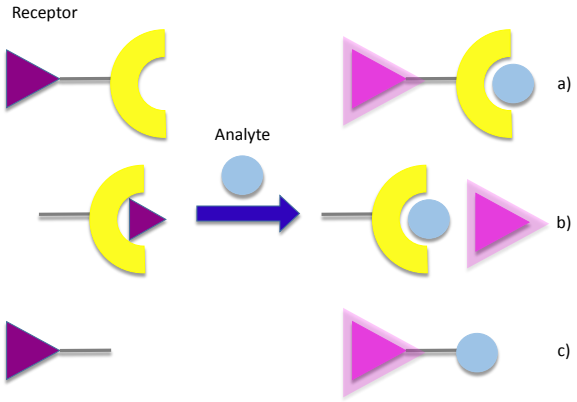

Figure 2. Representative scheme of the three main approaches used in the development of optical chemosensors. a) Binding site-signaling subunit approach; b) Displacement protocol; c) Chemodosimeter approach.

1.3 Nanotechnology: the tool of 21st century

The first definition of the term nanotechnology is attributed to Professor Norio Taniguchi that defined it in 1974 as: "*production technology to get extra high accuracy and ultra-fine dimensions, that is, the preciseness and fineness on the order of 1 nm, 10^{-9} m in length*."[10] Another definition of nanotechnology was stated as "the construction and use of functional structures designed from atomic or molecular scale with a least one characteristic dimension measured in nanometers".[11] The particular size of these entities allows them to exhibit new and significantly improved physical, chemical and biological properties, phenomena and processes. This discipline involves research and development measuring and manipulating matter at the atomic, molecular and supramolecular levels with the peculiarity that one of these dimensions is at the same escale than antibodies and viruses as despicted in Figure 3.

[10] N. Taniguchi, *in Proc. Intl. Conf. Prod.* Eng. Part II, 1st Ed., *Japan Society of Precision Engineering*, Tokyo, **1974**.
[11] K. Narendra, S. Kumbhat, *Essentials in Nanoscience and Nanotechnology*; 1st Ed. *John Wiley & Sons*, UK, **2016**.

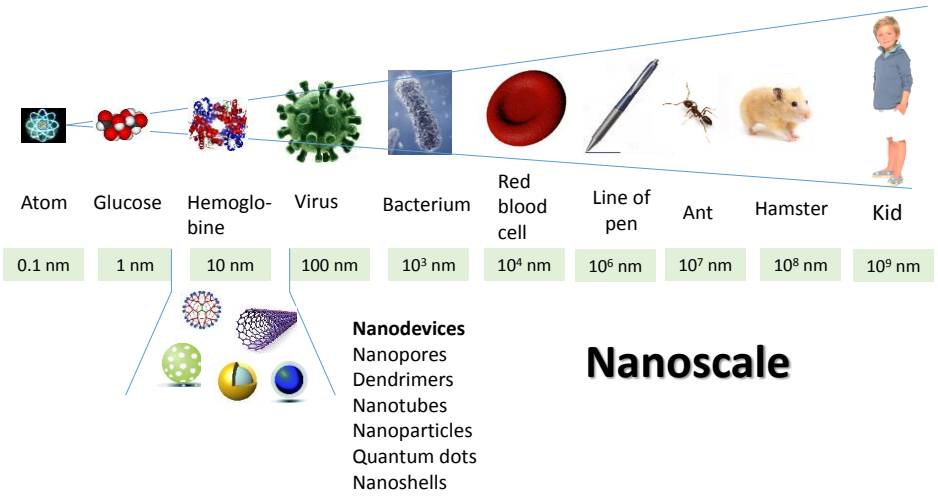

Figure 3. Illustration to compare sizes of selected objects, biomolecules and nanomaterials

Supramolecular chemistry and molecular recognition have contributed to the field adding extra functionality to the new nano-objects. Thus, a multitude of nanosystems based on nanoparticles, nanotubes or nanostructured surfaces have been developed and continue being developed in fields as nanobiotechnology, nanomaterials, nanoelectronics, nanomagnetism, nanophotonics among others. Literally, nanotechnology means any technology performed at nanoscale range that has application in the real world. Nowadays, we can found plenty of examples of nanotechnology being developed on almost every research field and industrial area.

1.4 Organic-inorganic hybrid porous materials

The development of organic-inorganic hybrid materials started with the aim to synthesize complex systems with innovative synergic effects and improved features. These materials are easily obtained by the covalent anchoring of molecular (organic) functional groups into inorganic materials as supporting

platforms.[12] In particular, this thesis is focused in the development of hybrid organic-inorganic nanomaterials.

Hybrid organic inorganic nanomaterials are not simply physical mixtures. They can be broadly defined as molecular or nano-composites with (bio)organic and inorganic components, intimately mixed where at least one of the component domains has a dimension ranging from a few Å to several nanometers. Consequently the properties of hybrid materials are not only the sum of the individual contributions of both phases, but the role of their inner interfaces could be predominant.[13] Moreover, the incorporation of functional organic molecules on solid supports by covalent bonding offers certains advantages:

- ✓ Functional group units can be in some way organized into the inorganic surface as a monolayer (depending of the functionalization degree).
- ✓ It is possible to perform subsequent anchoring processes to obtain a surface functionalized with different organic molecules and thus modulate its properties according with the nature of the anchored functional molecules.
- ✓ Leaching processes involving the organic group are avoided.
- ✓ If the solid support is functionalized with an organic group that could give a reversible coordination process it can be reused several times without lost of functionality.

These heterogenous materials are usually easy to handle. Furthermore, the possible control of size, shape and surface area of the materials, can provide interesting changes on physical and chemical properties of the inorganic surface.

The combination of supramolecular principles and nanoscopic solid structures enables the design of new hybrid sensing ensembles with improved sensitivity and/or selectivity for target of analytes for which selectivity is hard to achieve by

[12] a) K. Rurack, R. Martínez-Máñez, *The supramolecular chemistry of organic-inorganic hybrid materials*, ed. John Wiley & Sons, **2010**; b) A.P. Gale*, R. Quesada, Coord. Chem. Rev.*, **2006**, *250,* 3219–3244; c) J. F. Callan, A. P. de Silva, D. C. Magri, *Tetrahedron,* **2005**, *61*, 8551–8588; d) G. J. Mohr, *Sens. Actuators B,* **2005**, *107*, 2–13.

[13] C. Sánchez, *J. Mater. Chem.*, **2005**, *15*, 3557–3558.

conventional methods.[14] This is especially so when tridimensional supports are used as supports. Using 3D-architectured inorganic supports improves exponentially the repository of possibilities to design new functional nanodevices. For example, there is a wide range of silica materials with porous structure able to incorporate novel potential features onto hybrid materials (i.e. control of special acces to certain region, flux control inside channels, double functionalization in the inner and outer regions of the material, etc.) with respect to the possibilities of planar silica materials. Next section will be centered in the description of porous scaffolds as a class of hybrid nanomaterial.

1.4.1 Types of porous materials

Porous materials are materials with pores that can be cavities, channels or interstices. The features of a porous material vary depending on the size, arrangement and shape of the pores, as well as the porosity (the ratio of the total pore volume relative to the apparent volume of the material) and composition of the material itself. In this thesis, two different nanoporous materials are used: i) mesoporous silica materials (MSM) and ii) nanoporous anodic alumnia (NAA). In the followings sections, both will be explained in detail.

1.4.1.1 Mesoporous silica materials

The International Union of Pure and Applied Chemistry (IUPAC) classifies porous materials in three classes according to the pore size: microporous (pore size < 2 nm), mesoporous (pore size in the 2-50 nm range) and macroporous (pore size > 50 nm).[15] Well-known members of the microporous class are zeolites, which provide excellent catalytic properties by virtue of their crystalline aluminosilicate

[14] a) A. Verma, V.M. Rotello, *Chem. Commun.*, **2005**, *3*, 303–312; b) U. Drechsler, B. Erdogan, V.M. Rotello, *Chem. Eur. J.*, **2004**, *10*, 5570–5579; c) A.B. Descalzo, R. Martínez–Máñez, F. Sancenón, K. Hoffmann, K. Rurack, *Angew. Chem. Int. Ed.*, **2006**, *45*, 5924–5948. d) F. Mancin, E. Rampazzo, P. Tecilla, U. Tonellato, *Chem. Eur. J.*, **2006**, *12*, 1844–1854. e) I. Willner, B. Basnar, B. Willner, *Adv. Funct. Mater.,* **2007**, *17*, 702–717.

[15] X.S. Zhao, *J. Mater. Chem.,* **2006**, *16*, 623–625.

network.[16] However, their applications are somehow limited by the relatively small pore openings. Larger pores are found in mesoporous materials. Member of this family are, for instance porous glasses and porous gels.[17] However, they show disordered pore systems with broad pore-size distributions. Other mesoporous solids can, for instance, be prepared via intercalation of layered materials, such as double hydroxides, metal (titanium, zirconium) phosphates and clays, but they also have very broad mesopore-size distributions, as well as additional micropores.[18]

The first mesoporous solid that showed a regular ordered pore arrangement and a very narrow pore-size distribution, was MCM-41 material (where MCM stands for Mobil Composition of Matter), prepared in 1992 by the Mobil Oil Company.[19] Within their work, the authors demonstrated that depending on the synthesis conditions (solvent, pH, temperature, concentration), it was possible to obtain different phases (known as M41S phase materials): MCM-41 (with a hexagonal arrangement of the mesopores), MCM-48 (with a cubic arrangement of mesopores) and MCM-50 (with a lamellar structure).

These materials are a new class of solids characterized by large specific surface areas, between 500 and 1000 $m^2\ g^{-1}$, homogeneous pore size, and high pore volume (in the order of 1 $cm^3\ g^{-1}$). Moreover, they are inert and possess high thermal stability. Applications of these materials can be found in the areas of catalysis,[20] filtration and separation,[21] gas adsorption and storage,[22] enzyme

[16] J. Yang, Y.B. Zhang, Q. Liu, C.A. Trickett, E. Gutiérrez–Puebla, M.A. Monge, M. H. Cong, A. Aldossary, H.Deng, O.M. Yaghi, , *J. Am. Chem. Soc.* **2017**, *139*, 6448–6455.
[17] D.J. Mulder, L.M. Scheres, J. Dong, G. Portale, D.J. Broer, A.P. Schenning, *Chem. Mater.*, **2017**, *29*, 6601–6605.
[18] a) D. Gu, F. Schüth, *Chem. Soc. Rev.*, **2014**, *43*, 313–344. b) G.J. D.A. Soler–Illia, C. Sanchez, B. Lebeau, J. Patarin, *Chem. Rev.*, **2002**. *102*, 4093–4138.
[19] C.T. Kresge, M.E. Leonowicz, W.J. Roth, J.C. Vartuli, J.S. Beck, *Nature*, **1992**, *359*, 710–712.
[20] a) D.E. De Vos, M. Dams, B.F. Sels, P.A. Jacobs, *Chem. Rev.,* **2002**, *102*, 3615–3640; b) A. Mavrogiorgou, M. Baikousi, V. Costas, E. Mouzourakis, Y. Deligiannakis, M.A. Karakassides, M. Louloudi*, J. Mol. Catal. A: Chem*., **2016**, *413*, 40–55.
[21] G. Bayramoglu, M.Y. Arica, *Microporous Mesoporous Mater*., **2016**, *226*, 117–124.
[22] M. Kruk, M. Jaroniec, *Chem. Mater.*, **2001**, *13*, 3169–3183.

immobilization,[23] biomedical tissue regeneration,[24] drug delivery,[25] and chemical/biochemical sensing.[26]

- Synthesis

The usual method for building up a system that presents a high ordered mesoporous structure with homogeneous pore dimensions requires two main components:

✓ A template acting as structure-directing agent of the porous network

✓ A polymeric precursor able to self-organize around the template and, upon polymerization, build up the final rigid structure

From the literature it is obvious that the formation of ordered mesoporous materials largely depends on parameters related with the specific chemistry and chemical interactions involved in the studied system, but also on the physical conditions employed in their synthesis. Some of these parameters are, for example, the type of inorganic material and its propensity to crystallise in the walls, type of precursors used and the kinetics of their hydrolysis and condensation, type of surface-active molecules, the respective and relative concentrations of surfactant and inorganic species, pH, temperature, synthesis time, type of solvent, etc.

Generally, the synthesis of these inorganic silica based scaffolds is accomplished by the use of a template such as a surfactant that acts as a structure-directing agent, and is able to form micelles in water solution.

---

[23] a) M. Vallet–Regi, M. Colilla, I.J. Izquierdo–Barba, *Biomed. Nanotechnol.*, **2008**, *4*, 1–15; b) Y. Xu, D. Gao, P. Feng, C. Gao, S. Peng, H.T. Ma, S. Yang, C. Shuai, *Appl. Surf. Sci*. **2017**, *423*, 30, 314–321.

[24] a) I.I. Slowing, B. G. Trewyn, S. Giri, V.S.Y. Lin, *Adv. Funct. Mater*., **2007**, *17*, 1225–1236; b) J.E. Lee, N. Lee, H. Kim, J. Kim, S.H. Choi, J.H. Kim, T. Hyeon, *J. Am. Chem. Soc*., **2009**, *132*, 552–557.

[25] a) M. Vallet–Regi, F. Balas, D. Arcos, *Angew. Chem., Int. Ed.*, **2007**, *46*, 7548–7558; b) A.H. Teruel, C. Coll, A.M. Costero, D. Ferri, M. Parra, P. Gaviña, M. González-Álvarez, V. Merino, M.D. Marcos R. Martínez-Máñez, F. Sancenón, *Biomolecules*, **2018**, *23*, 375; c) C. De La Torre, I. Casanova, G. Acosta, C. Coll, M.J. Moreno, F. Albericio, E. Aznar, R. Mangues, M. Royo, F. Sancenón, R. Martínez-Máñez, *Adv. Funct. Mat*., **2015**, *25*, 687–695; d) R. Bhat, A. Ribes, N. Mas, E. Aznar, F. Sancenón, M.D. Marcos, J.R. Murguía., A. Venkatarman, R. Martínez-Máñez, *Langmuir*, **2016**, *32*, 1195–1200.

[26] K. A. Kilian, T. Boecking, K. Gaus, M. Gal, J. J. Gooding, *ACS Nano* **2007**, *1*, 355–361.

Depending on factors described above, such as concentration and dimensions of the surfactant, temperature, pH solution, ionic force, etc. different kind of micelles can be obtained. These micelles organize themselves into supermicellar structures and depending on the same factors reported before different kind of supermicellar aggregates can be obtained. In the synthesis of silica based ordered inorganic scaffolds, oligomeric silicates, wich are present in the reaction mixture, are able to condensate around the template, obtaining as a result a mesoporous solid that contains in its pores larger quantities of surfactant molecules. The subsequent elimination of the surfactant from the pores of the materials gives the desired inorganic mesoporous scaffold. The surfactant elimination can be carried out by aerobic high temperature calcination or by extraction with adequate solvents.

Researchers have found that two different mechanisms are involved on the formation process of these composite materials. In the first mechanism, named as true liquid-crystal templating (TLCT) mechanism, the concentration of the surfactant is very high and, as a consequence, a lyotropic liquid-crystalline phase is formed without requiring the presence of the precursor inorganic framework materials (normally tetraethyl- (TEOS) or tetramethylorthosilica (TMOS)). [27] The other mechanism considers that liquid-crystalline phase is formed even at lower concentrations of surfactant molecules, for example, in a cooperative self assembly of the template molecules and the added inorganic species. [28]

By small changes in the synthesis route, it is possible to modify the features of the final solid. For example, the nature of the structure directing agent can be used to modulate the pore size (from 2 up to 50 nm).[29] The particle morphology

[27] G.S. Attard, J.C. Glyde, C.G. Göltner, *Nature*, **1995**, *378*, 366–368.

[28] A. Monnier, F. Scheth, Q. Huo, D. Kumar, D. Margolese, R.S. Maxwell, G. Stucky, M. Krishnamurty, P. Petroff, A. Firouzi, M. Janicke, B. Chmelka, *Science*, **1993**, *261*, 1299–1303.

[29] a) A. Bagshaw, E. Prouzet, T.J. Pinnavaia, *Science*, **1995**, *269*, 1242–1244; b) M.H. Kim, H.K. Na, Y.K. Kim, S.R. Ryoo, H.S. Cho, K.E. Lee, H. Jeon, R. Ryoo, D.H. Min, *ACS nano*, **2011**, *5*, 3568–3576.

can also be tuned from micrometric and heterogeneous particles to thin films, nanoparticles or monoliths.[30]

MCM-41 is one of the best known common mesoporous silica materials and most widely studied. The MCM-41 synthesis is schematically represented in Figure 4. As it can be observed the synthesis deals with the polymerization of tetrahethylortosilicate (TEOS), used as inorganic siliceous precursor, around super-micellar-template previously formed in water solution. The mesoporous material obtained by subsequent removal of the surfactant by extraction with adequate solvents or by aerobic high temperature calcination (500-600^{o}C), presents cylindrical unidirectional empty channels of approximately 3 nm of diameter (when CTAB is used as surfactant) arranged in a hexagonal distribution. The final solid presents a delicate structural order that is very difficult to obtain following traditional synthetic routes. The principal advantage of this method is that the high grade of homogeneity of the initial elements is transmitted to the final material, showing a system of pores not only homogeneous in size but also in form and regularity.

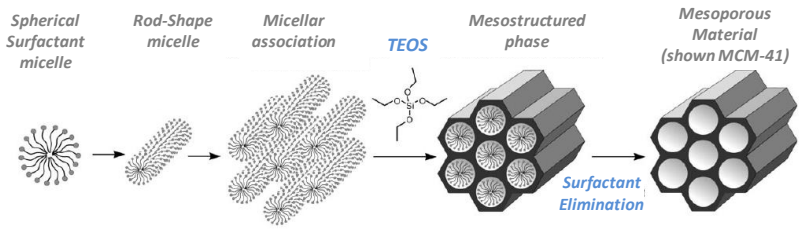

Figure 4. Synthesis pathways of MCM-41 by true liquid-crystal template mechanism.

[30] H.B.S. Chan, P.M. Budd, T.D.V. Naylor, *J. Mater. Chem*., **2001,** *11*, 951–957; b) Q. Cai, Z.S. Luo, W.Q. Pang, Y.W. Fan, X.H. Chen, F.Z. Cui, *Chem. Mater*., **2001**, *13*, 258–263. c) S.P. Naik, W. Fan, T. Yokoi, T. Okubo, *Langmuir*, **2006**, *22*, 6391–6397; d) J. Kobler, K. Moller, T. Bein, *ACS Nano*, **2008**, *2*, 791–799.

Furthermore, this approach has been extended to non-silica oxides, such as TiO_2 and ZrO_2, using several types of templating agents, including non-ionic surfactants and block copolymers.

To characterize these materials conventional techniques as powder X-ray diffraction to ensure the prescence of ordered or disordered structures, transmission electron microscopy (TEM) and scaning emission microscopy (SEM) to obtain the morphology, adsorption-desorption isotherms, to calculate specific surface and pore size, thermogravimmetry analyses (TG) to obtain the amount of organic content, dynamic light scattering (DLS) to measure size and Z-potential, are used. Moreover techniques as infrared spectroscopy and magnetic nuclear resonance have also been employed.

- Functionalization

The mechanism in which organic groups are chemically anchored to an inorganic support to form hybrid materials is known as functionalization. This procedure comprises the incorporation of organic functional components[31] which lead to modify the physical and chemical properties of mesoporous silica materials, either on the silica surface, or within the channels. Organic modification of the silica permits precise control over the surface properties and pore sizes of the mesoporous materials for specific applications and stabilize the materials towards hydrolysis. Through the development of hybrid inorganic-organic mesoporous solids, much progress has been made in the last few years in a number of applications in different of fields.

The incorporation of organic functionalities in mesoporous silica materials can be achieved in three ways: 1) by subsequent modification of the pore surface by attachment of organic components onto a pure silica matrix (*grafting*, postsynthetic functionalization of silica), (Figure 5), 2) by simultaneous

[31] a) J. Ding, C.J. Hudalla, J.T. Cook, D.P. Walsh, C.E. Boissel, P.C. Iraneta, J.E. O´Gara, *Chem. Mater*., **2004**, *16*, 670–681; b) X. Feng, G.E. Fryxell, L.Q. Wang, A.Y. Kim, J. Liu, K.M. Kremer, *Science*, **1997**, *276*, 923–926; c) A. Walcarius, C. Delacôte, *Chem. Mater*., **2003**, *15*, 4181–4192; d) Y.V.S. Rao, D.E. De Vos, T. Bein, P.A. Jacob, *Chem. Commun*., **1997**, 355–356.

condensation of inorganic silica species and organosilica precursors (co-condensation, one-pot synthesis) (Figure 6), and 3) by the incorporation of organic groups as bridging components directly and specifically into the pore walls using bissilylated organic precursors that lead to periodic mesoporous organosilicas (PMOs), (Figure 7).

Thereupon, the three methods of functionalization will be explained in more detail.[32]

✓ Post-synthetic functionalization of silicas ("*grafting*"): In this case a post functionalization of the inorganic silica material with selected trialkoxysilanes takes place. With this mechanism, a superficial modification is usually obtained.[33] This method of modification has the advantage that, under the synthetic conditions used, the mesostructure of the starting silica phase is usually retained. However, as the organosilanes react preferentially at the pore openings during the initial stages of the synthetic process, the diffusion of further molecules into the deep part of the pores is somehow impaired. This lead to a non-homogeneous distribution of the organic groups, with the pores having a lower degree of functionalization.

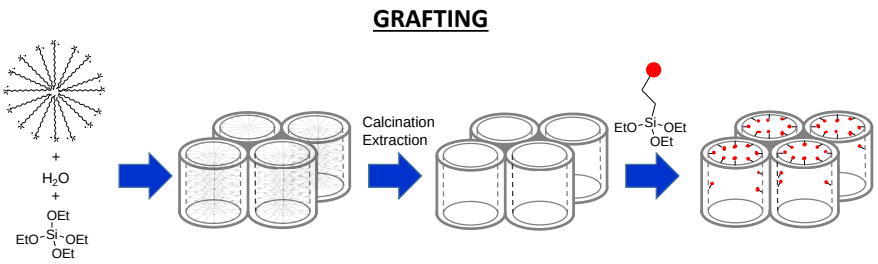

Figure 5. Schematic representation of functionalization of MCM-41 material through grafting procedure.

✓ Co-condensation procedure or direct synthesis: In this case a simultaneous condensation of silica and organosilica precursors takes place. This

[32] M.H. Lim, C.F. Blanford, A. Stein, *Chem. Mater*. **1998**, 10, 467–470.
[33] A. Stein, B.J. Melde, R.C. Schroden, *Adv. Mater*. **2000**, *12*, 19, 1403–1419.

method allows to obtain an internal and external covalent modification of the scaffold, and organic units are generally more homogeneously distributed compared with the grafting process. Some drawbacks of this method are:

a) The degree of mesoscopic order of the products decreases with increasing concentration of organosilica precursors in the reaction mixture.

b) Homocondensation reactions between silane groups are increased. The proportion of terminal organic groups that are incorporated into the pore-wall network is generally lower than the amount that would correspond to the starting concentration of the reaction mixture

c) The homogeneous distribution of different organic functionalities in the framework cannot be guaranteed.

d) The incorporated organic groups can lead to a reduction in the pore diameter, pore volume, and specific surface area. In this method, care must be taken not to destroy the organic functionality during removal of the surfactant, using a lesser aggressive method such as extraction instead of the calcination.

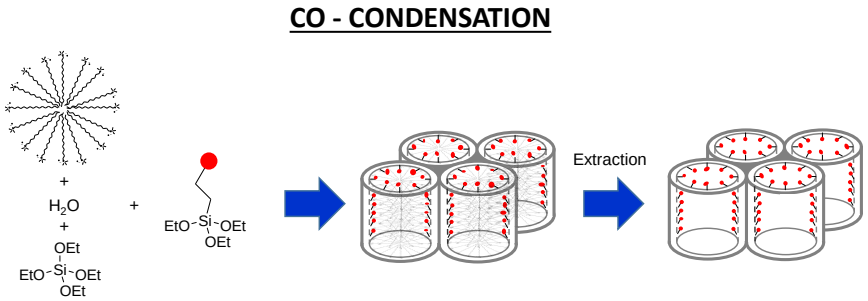

Figure 6. Schematic representation of co-condensation synthetic procedure for MCM-41.

✓ Preparation of Periodic Mesoporous Organosilicas (“PMOs”): Another way to incorporate organic compounds onto mesoporous silicas is the preparation of PMOs. This method is similar to the co-condensation protocol but using bridging bis-silylated trialkoxysilane agents. This procedure allows to incorporate organic groups as components of the material structure by the use of single-source

organosillica precursors. The first example of PMOs was discovered by three independent groups at the same year.[34]

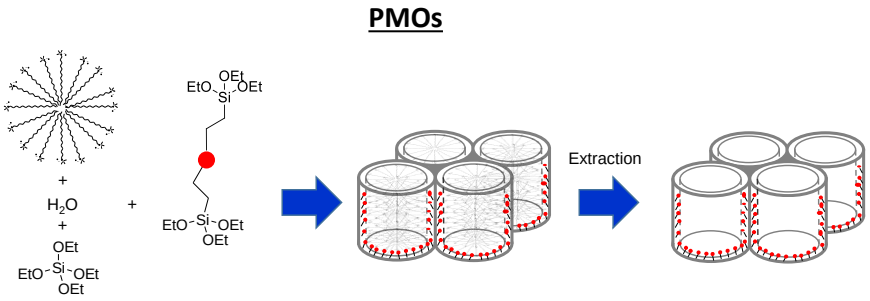

Figure 7. Schematic representation of PMOs formation.

Commonly, the grafting method is the most used. This is the easiest way to introduce of organic groups mantaining the original mesostructure of the silica.

The surface modification opens new opportunities, creating new hybrid materials with new functionalities.[35] The incorporation of different organic groups to this kind of porous materials are used in the preparation of material for applications such as drug delivery and sensing.

1.4.1.2 Nanoporous anodic alumina

As mentioned above, the second nanoporous material used in this thesis is Nanoporous anodic alumina (NAA). The first reports of nanoporous anodic alumina date at earliest decades of century 20st mainly for decorative and protective purposes. In the next years several scientists developed new routes of synthesis and applications of this material.[36] In 1953, Keller characterized the nanoporous anodic alumina structure for the first time by electron microscopy. In his work, he describes the NAA structure as hexagonally arranged arrays of

[34] a) S. Inagaki, S. Guan, Y. Fukushima, T. Ohsuna, O. Terasaki, *J. Am. Chem. Soc.*, **1999**, *121*, 9611–9614. b) B.J. Melde, B.T. Holland, C.F. Blanford, A. Stein, *Chem. Mater.*, **1999**, *11*, 3302–3308. c) T. Asefa, M.J. MacLachlan, N. Coombs, G.A. Ozin, *Nature*, **1999**, *402*, 867–871.

[35] a) M. Baranowska, A.J. Slota, P.J. Eravuchira, *Colloids Surf B Biointerfaces*, **2014**, *122*, 375–383; b) S. Kapoor, R. Hegde, A.J Bhattacharyya , *J. Control Release*, **2009**, *140*, 34–39.

[36] a) British Patent 223994 (1923); b) Italian Patent 741753 (1936).

nanometric pores, in which the interpore distance (i.e. the distance between the centres of adjacent pores) is directly proportional to the anodization voltage.[37] This work was the key for many studies about chemical and physical properties of NAA. The first theoretical approach about formation mechanisms of both barrier and porous type of aluminium oxide was developed by Diggle.[38]

Numerous theoretical models about pore nucleation and growth in NAA have been put forward,[39] but the actual mechanism of NAA growth has yet to be completely clarified. The scientific community agrees that pore nucleation starts to take place in the oxide thin film formed on the aluminium surface at the beginning of the anodization process. Instabilities in the electric field across the oxide thin film generate electric field concentrations at certain sites on the oxide film surface. At these sites, which act as nucleating centres, ionic conduction is enhanced and local temperature is increased by the Joule effect. In these conditions, oxide is preferentially dissolved and pores are generated through the oxide film surface, growing from these nucleating centres.

The discovery of the two-step anodization process[40] in 1995 and the nanoimprint process[41] two years later by Masuda and Fukuda are two turning points in the history of NAA. These fabrication processes are relatively inexpensive ways of fabricating polydomain and monodomain nanoporous structures based on aluminium oxide. The pore size distribution of these types of NAA is extremely narrow and can be fabricated with a high pore length/pore diameter ratio. This fact opened a new window on the fabrication of a new generation of nanostructures.

- Synthesis

[37] F. Keller, M.S. Hunter, D.L. Robinson, *J. Electrochem. Soc.*, **1953** *100* 411–419.
[38] J.W. Diggle, T.C. Downie, C.W. Coulding, *Chem. Rev.*, **1969**, *69*, 305–405.
[39] a) T.P. Hoar, N.F. Mott, *J. Phys. Chem. Solids*, **1959**, *9*, 97–99; b) G. Patermarakis, N. Papandreadis, *Electrochim. Acta*, **1993**, *38*, 2351–2361.
[40] H. Masuda, K. Fukuda, *Science*, **1995**, *268*,1466–1468.
[41] H. Masuda, H. Yamada, M. Satoh, H. Asoh, M. Nakao, T. Tamamura, Highly, Appl. Phys. Lett., **1997**, *71,* 2770–2772.

The fabrication of NAA is constructed through an anodization process. It consists of an electrolyte which normally is an aqueous solution of sulphuric, oxalic or phosphoric acid, in which both the anode (i.e. aluminium foil) and the cathode (i.e. platinum wire) are partially immersed. When the anodization voltage is applied between the anode and cathode, pores nucleate and start growing on the aluminium surface. The growth mechanism in steady state is the result of competing oxidation (i.e. formation of oxide) and dissolution (i.e. dissolution of oxide) through the anodization process. First, aluminium oxide grows at the aluminium alumina interface and within the oxide barrier layer because of the countermigration of ionic species (i.e. Al^{3+} and O^{2-}) (see Figure 8A). Second, as despicted in Figure 8B aluminium oxide (Al_2O_3) is dissolved at the alumina-electrolyte interface. Finally, the current density is decreased and consequently the pores grow at constant rate (Figure 8C).

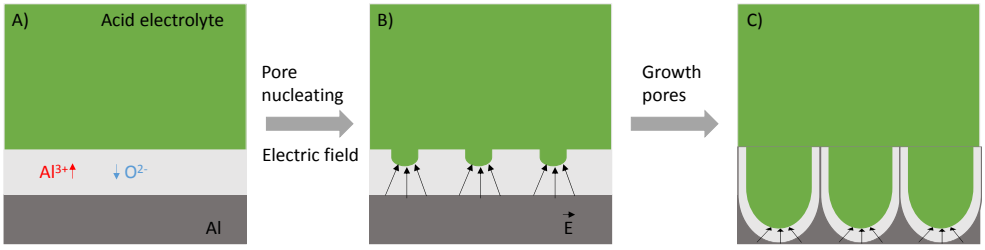

Figure 8. Schematic representation of fabrication of NAA: A) aluminium oxide interface is growing, B) an electric field is applied where aluminium oxide is dissolved and pore nucleating starts and C) pores grow.

Concretely, in this thesis the material used is prepared by two-step anodization process. It consists of applying a long first anodization step (i.e. about 24 h) to high purity annealed and electropolished aluminium substrates. In the course of this anodization step, the initially disordered pores are hexagonally ordered inside domains of several μm^2 by the self-ordering mechanism. Then, the Al_2O_3 film, which has disordered pores on the top and ordered pores on the bottom, is removed by wet chemical etching. The remaining aluminium substrate presents a patterned surface with hexagonally ordered concavities. Subsequently, the

second anodization step is applied under the same conditions as the first step. Then, pores start to grow from the concavities located on the patterned Al surface, which act as nucleating centres concentrating the electric field. The pores remain hexagonally arranged throughout the second anodization step.

The next figure clarifies the difference between one-step and two-step anodization to fabricate NAA.

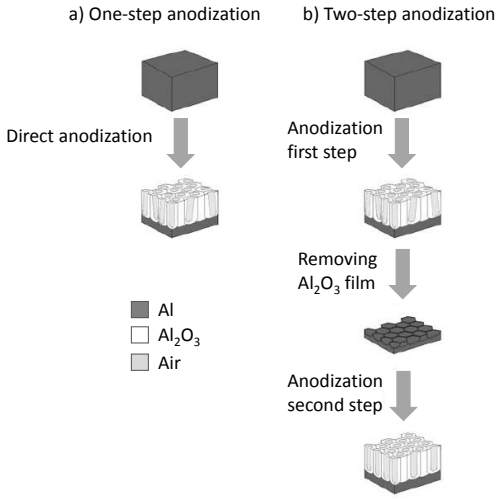

Figure 9. Schematic diagram describing the most widely used methods for fabricating NAA a) one step anodization (disordered pores) and b) two-step anodization (ordered pores).

Depending on the depth of NAA, this material is used for different applications. The mechanisms of pore modulation are directly related to the pore formation mechanisms. It is widely accepted that the pore formation is driven by the electric field at the pore bottom and through the barrier layer,[42] which is responsible for the drift of ionic species, which leads to the formation of aluminum oxide at the oxide-metal interface. At the same time, the characteristic dimensions of the

[42] J. Oh, C.V. Thompson, *Electrochim. Acta,* **2011**, *56*, 4044–4051.

porous alumina is also related to the plasticity of the barrier layer and to the need of stress relief as it is being formed.[43]

Additionally, depending on the anodization conditions, aluminium can be anodised under mild (MA) or hard anodization (HA) regimes.[44] While the first is carried out at moderate voltages and temperatures, the latter is performed at high voltages and low temperatures. The different anodization conditions for each of these regimes will be established by the acid electrolyte. Table 1 summarises the most representative MA and HA anodization conditions (i.e andodization voltage, V and temperature, T), as well as geometric features (i.e. nanopore distance, Dp and interpore distance, d_{int}) of the resulting NAA.

Table 1. MA and HA anodization conditions for the synthesis of NAA

Acid electrolyte (0.3M)	Anodization regime	V (V)	T (°C)	Dp (nm)	d_{int} (nm)	Growth rate (μm h^{-1})	Ref.
H_2SO_4	MA	25	5-8	25	63	7.5	[45]
H_2SO_4	HA	40	0-1	30	78	85	[46]
$H_2C_2O_4$	MA	40	5-8	30	100	3.5	[47]
$H_2C_2O_4$	HA	140	0-1	50	280	50	[38]
H_3PO_4	MA	195	0-1	160	500	2	[39b]

In terms of crystallography, as-produced NAA basically consists of an amorphous phase. However, the NAA crystallographic phase evolves by being

[43] a) S. Lee, D Kim, E. Gillette, J. Oh, S.W Han, *Phys. Chem.,* **2013**, *15*, 10659–10665; b) B He, S.J. Son, S.B. Lee, *Langmuir,* **2006**, *22*, 8263–8265.
[44] F. Keller, M.S. Hunter, D.L. Robinson, *J. Elect. Soc.,* **1953**, 9, 411–419.
[45] G. Patermarakis, P. Lenas, C. Karavassilis, G. Papayiannis, *Electrochim. Acta*, **1991**, *36,* 709–725.
[46] S.K. Thamida, H.C. Chang, *Chaos*, **2002**, *12*, 240–251.
[47] V.P. Parkhutik, V.I. Shershulsky, *Appl. Phys.*, **1992**, *25*, 1258–1263.

subjected to a thermal treatment.[48] First, the crystallographic phase transition from amorphous to gamma alumina (γ- Al_2O_3) starts at 700^oC, becoming entirely γ-Al_2O_3 at 1000^oC. If the temperature increases, a new crystallographic phase transition is initialized at 1100^oC from gamma alumina to alpha alumina (α - Al_2O_3 or corundum). Finally, at 1200^oC the NAA crystallographic phase becomes pure α-alumina.

Chemically, two main regions can be distinguished in the structure of a nanoporous anodic alumina pore.[49] The first one is an inner layer close to the aluminium-alumina interface, which is basically composed of pure alumina. The second one is an outer layer located between the inner layer and the alumina-electrolyte interface, which is contaminated by anionic species, which are provided by the acid electrolyte (i.e. phosphate, sulphate, oxalate, etc).

- Functionalization

As mesoporous silica materials, the surface modification of nanoporous anodic alumina is easy and it is of great interest in various fields such as biomedical applications and surface coating.[50]

The incorporation of organic functionalities in nanoporous anodic alumina can be achieved by the grafting method (postsynthetic functionalization of alumina). In order to develop a surface able to attach the organic group, the NAA is treated with boiling hydroxyperoxide (H_2O_2) to obtain hydroxyl (-OH) groups on the surface. Figure 10 represents this process.

---

[48] a) P.P. Mardilovich, A.N. Govyadinov, N.I. Mukhurov, A.M. Rzhevskii, R. Paterson, *J. Membr. Sci.*, **1995**, *98*, 131–142; b) W.L. Xu, M.J. Zheng, S. Wu, W.Z. Shen, *Appl. Phys. Lett.*, **2004**, *85*, 4364–4366; c) A. Kirchner, K.J.D. MacKenzie, I.W.M. Brown, T. Kemmitt, M.E. Bowden, *J. Membr. Sci.,* 2007, *287*, 264–270; d) Y Li, G.H. Li, G.W. Meng, L.D. Zhang, F. Phillip, *J. Phys. Condens. Matter*, **2001**, *13*, 2691–2699; e) N.M. Yakovleva, A.N. Yakovlev, E.A. Chupakhina, *Thin Solid Films,* **2000***, 366*, 37–42; f) L.F. Marsal, L. Vojkuvka, P. Formentín, J. Pallarès, J. Ferré–Borrull, *Opt. Mater.*, **2009**, *31*, 860–864.

[49] a) J. Lee, S. Nigo, Y. Nakano, S. Kato, H. Kitazawa, G. Kido, *Sci. Tech. Adv. Mater* , **2010**, *11*, 1–4; b) F. Le Coz, L. Arurault, S. Fontorbes, V. Vilar, L. Datas, P. Winterton, *Surf. Interface Anal.*, **2010**, *42*, 227–233; c) K. Nielsch, J. Choi, K. Schwim, R.B. Wehrspohn, U. Gösele, *Nano Lett.*, **2002**, *2*, 677– 680.

[50] a) D.A. Javaid, D.M. Krapchetov, J. Ford, *J. Membr. Sci*., **2005**, *246*, 181–191; b) J. Salonen, V.P. Lehto, *Chem. Eng. J*., **2008**, *137*, 162–172.

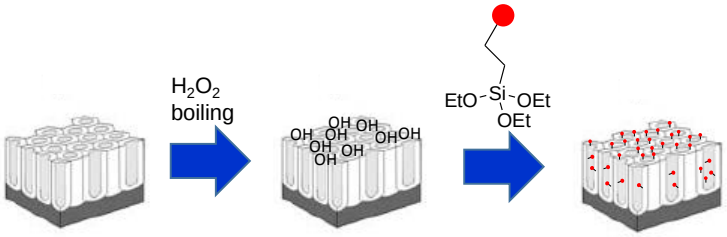

Figure 10. Schematic representation of functionalization of NAA through graftinc procedure.

1.5 Gated Materials

As cited in the last section, anchoring organic molecules or supermolecules onto certain inorganic scaffoldings has led to the development of some hybrid materials, which show cooperative functional behaviors not found in free molecules or in the unfunctionalized solids alone.

One appealing concept in this fertile field is related with the design of gated materials. These materials are constructed to tune the transport of chemical or biochemical species from voids of porous supports to a solution, and vice versa, in response to a predefined stimulus.[51] Following this concept, several research groups have been involved in the synthesis and characterization of imaginative nanodevices in which the delivery of a certain cargo stored in a container can be triggered by applying selected external stimuli.[52] Such gated materials are composed mainly of two subunits: (i) a porous inorganic support in which a cargo is loaded and (ii) certain molecular or supramolecular entities (commonly known molecular gates), generally grafted onto the external surface, which can control mass transport from pores. As depicted in Figure 11, the application of an external stimulus allows the release of the entrapped guest.

---

[51] a) K. Ariga, S. Ishihara, J. Labuta, J.P. Hill, *Curr. Org. Chem*. **2011**, *15*, 3719−3733; b) A. B. Descalzo, R. Martínez–Máñez, F. Sancenón, K. Hoffmann, K. Rurack, Angew. *Chem., Int. Ed*. **2006**, *45*, 5924−5948,

[52] E. Aznar, M. Oroval, L. Pascual, J.R. Murguía, R. Martínez-Máñez, F. Sancenón, *Chem. Rev.,* **2016**, *116*, 561–718.

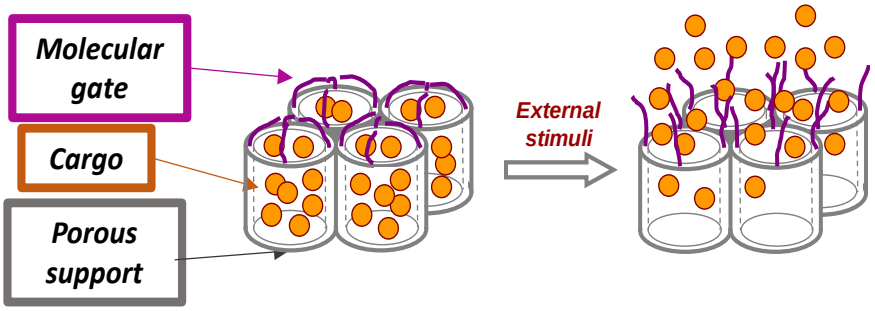

Figure 11. Schematic representation of a nanoscopic gated support.

When dealing with the inorganic support one of the most commonly used material for preparing gated nanodevices is mesoporous silica. Moreoever in this thesis, nanoporous anodic alumina is also used to prepare gated materials.

The first example of gated material was described in 2003 by Fujiwara and coworkers.[53] The gate consisted of 7-[(3-triethoxysilyl)-propoxy]coumarin groups attached to the mesoporous silica surface. Coumarin undergoes a [2 + 2] photodimerization in which there is a cycloaddition reaction that involves carbon−carbon double bonds of two neighboring molecules to result in a cyclobutane dimer. Photodimerization of coumarin is performed in the presence of light and is, in most cases, a reversible process that can be controlled by selecting the irradiation wavelength (> 310 nm). The functionalized material was loaded with selected cargos (phenanthrene, cholestane, and progesterone). Capped solids showed no cargo release; however, when the system was irradiated with a 250 nm UV-light, pore opening and cargo release was observed, as shown in Figure 12. Years later, the authors loaded the pores of mesoporous bioactive glasses with phenanthrene, and pore outlets were functionalized with a coumarin derivative. When n-hexane suspensions of the material were irradiated with light of wavelength >310 nm, negligible phenanthrene release was observed due to the

[53] a) N.K. Mal, M. Fujiwara, Y. Tanaka *Nature,* **2003**, *421*, 350; b) N.K. Mal, M. Fujiwara, Y. Tanaka, T. Taguchi, M. Matsukata, *Chem. Mater.* **2003**, *15*, 3385–3394.

formation of coumarin dimers, whereas irradiation with 250 nm light induced cargo release.[54]

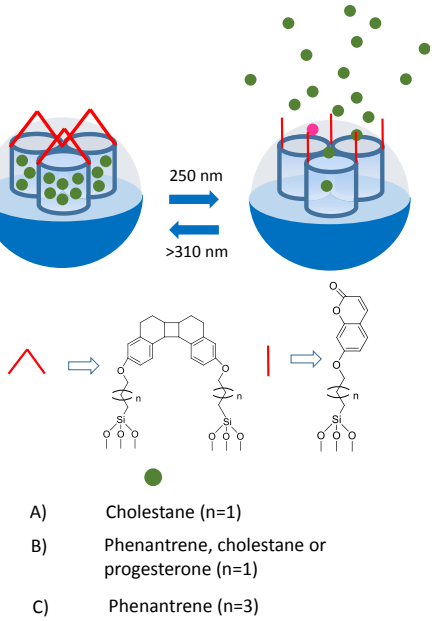

Figure 12. (A and B) MCM-41 support or (C) mesoporous bioactive glasses loaded with (A) cholestane, (B) phenantrene, cholestane, or progesterone or (C) phenantrene and capped with cyclobutane dimers of coumarin. Upon irradiation at 250 nm, the selected cargos were released due to the regeneration of the coumarin monomers. Cargo release could be once again stopped by irradiation at 310 nm.

Other example of gated material was reported by R. Casasús, R. Martínez and coworkers, in 2004. They described one of the first examples of a pH-controlled gated silica mesoporous support. This example was also the first reported capped system that worked in an aqueous environment. Whereas most published examples in gated materials are used for delivery applications, this example focused on using a gated system to control the entry of a certain molecule (a

[54] H.M. Lin, W.K. Wang, P.A. Hsiung, S.G. Shyu, *Acta Biomater*. **2010**, *6*, 3256−3263.

squaraine dye) to the inner pores of the mesoporous scaffold.[55] The authors used a micrometric MCM-41 support that was functionalized on the outer surface with 3-[2-(2-aminoethylamino)ethylamino]propylmethoxysilane (a linear polyamine) and with mercaptopropyl chains grafted inside the pores (see Figure 13). The entrance of the dye into pores was indicated by the reaction of squaraine (blue) with the thiol groups placed inside pores, which gave a colorless derivative. At an acidic pH, the nitrogen atoms of the polyamine molecules were protonated and adopted a rigid-like conformation due to the Coulombic repulsions between the ammonium groups. This resulted in pore blockage and inhibited squaraine access to the thiol moieties (the solution remained blue). However, at a neutral pH, amines were partly protonated, adopted a more flexible conformation, and squaraine dye was able to enter into inner pores (the solution turned colorless). A synergic anion controlled outcome also resulted from the interaction between protonated amines and certain anions.

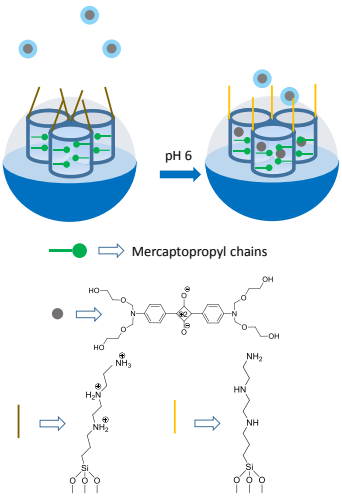

Figure 13. Micrometric MCM-41 support functionalized with polyamines on the outer surface and with mercaptopropyl groups on the inner surface. Changes in pH controlled squaraine access to the pores.

[55] R. Casasús, M.D. Marcos, R. Martínez–Máñez, J.V. Ros–Lis, J. Soto, L. A. Villaescusa, P. Amorós, D. Beltran, C. Guillem, J. Latorre, *J. Am. Chem. Soc*. **2004**, *126*, 8612–8613.

The first example of temperature-controlled nanoscopic gated hybrid material was described in 2003 by G. P. López and co-workers.[56] These authors used mesoporous silica nanoparticles, and the N-isopropylacrylamide (PNIPAAm) polymer was grown on the inner pores of the mesoporous support by atom transfer radical polymerization of N-isopropylacrylamide (Figure 14). At a low temperature (below the less than lower critical solution temperature of the polymer (LCST) at 32 °C), the polymer was hydrated and extended closing the pores and inhibiting dye (fluorescein and Rh 6G) delivery. In contrast at high temperatures (50 °C, above the LCST), the polymer was in a hydrophobic collapsed form, which allowed dye delivery.

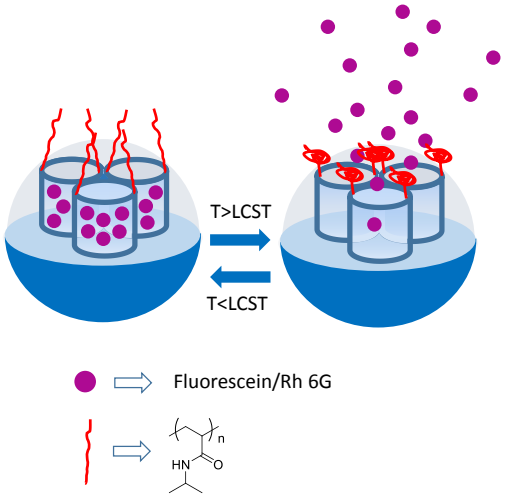

Figure 14. MSNs capped with N-isopropylacrylamide-derivative polymers or copolymers. Temperature changes induced cargo release

Apart from the examples explained above, to date numerous gated systems using mesoporous hybrid scaffoldings have been reported.[57] Among others,

[56] Q. Fu, G.V.R. Rao, L.W. Ista, Y. Wu, B.P. Andrzejewski, L.A. Sklar, T.L. Ward, G.P. Lopez, G. P. *Adv. Mater*. **2003**, *15*, 1262−1266

[57] a) W.H. Chen, G.F. Luo, Q. Lei, F.Y. Cao, J.X. Fan, W.X. Qiu, R.X. Zhuo, *Biomaterials*, **2016**, *76*, 87–101; b) A. Baeza, R.R. Castillo, A. Torres–Pardo, J.M. Gonzalez–Calbet, M. Vallet–Regi, *J. Mater. Chem. B*, **2017**, *5*, 2714–2725; c) J.A. Gruenhagen, C.Y. Lai, D.R. Radu, V. S.Y. Lin, E.S. Yeung, *Appl. Spectrosc.*, **2005**, *59*, 424–431.

supramolecular assemblies,[58] inorganic nanoparticles,[59] and polymers[60] have been used as blocking caps that controls the opening/closing of pore entrances in mesoporous scaffolds. Moreover, different stimuli, such as pH,[61] light,[62] redox potential,[63] temperature[64] and target small molecules[65] have been applied as

[58] a) T.D. Nguyen, Y. Liu, S. Saha, K.C.F. Leung, J.F. Stoddart, J.I. Zink, *J. Am. Chem. Soc.* **2007**, *129*, *626–634*. b) R. Liu, Y. Zhang, P.Y. Feng, *J. Am. Chem. Soc.* **2009**, *131*, 15128–15129.

[59] a) C.Y. Lai, B. G. Trewyn, D.M. Jeftinija, K. Jeftinija, S. Xu, S. Jeftinija, V.S.Y. Lin, *J. Am. Chem. Soc.* **2003**, *125*, 4451–4459; b) S. Giri, B.G. Trewyn, M.P. Stellmaker, V.S.Y. Lin, *Angew. Chem., Int. Ed.*, **2005**, *44*, 5038–5044; c) E. Aznar, M.D. Marcos, R. Martínez–Máñez, F. Sancenón, J. Soto, P. Amorós, P. Guillem*, J. Am. Chem. Soc.*, **2009**, *131*, 6833–6843. d) J.L. Vivero–Escoto, I.I. Slowing, C. Wu, V.S.Y. Lin, *J. Am. Chem. Soc.* **2009**, *131*, 3462–3463.

[60] a) R. Liu, X. Zhao, T. Wu., P. Y. Feng*, J. Am. Chem. Soc*. **2008**, *130*, 14418–14419; b) C.L. Zhu, X.Y. Song, W.H. Zhou, H H. Yang, X.R. Wang, *J. Mater. Chem.,* **2009**, **19**, 7765–7770.

[61] a) R. Casasús, M.D. Marcos, R. Martínez–Máñez, J.V. Ros–Lis, J. Soto, L.A. Villaescusa, P. Amorós, D. Beltrán, C. Guillem, J. Latorre, *J. Am. Chem. Soc.,* **2004**, *126*, 8612–8613; b) M. Ruiz–Rico, É. Pérez–Esteve, M.J. Lerma–García, M.D. Marcos, R. Martínez–Máñez, J.M. Barat, *Food chem.*, **2017**, *218*, 471–478; c) Q.Yang, S. Wang, P. Fan, L. Wang, Y. Di, K. Lin, F. S. Xiao, *Chem. Mater.,* **2005**, *17*, 5999–6003; d)V. Cauda, C. Argyo, A. Schlossbauer, T.J. Bein, *J. Mater. Chem.*, **2010**, *20*, 4305–4311; e) B. Tian, S. Liu, S. Wu, W. Lu, D. Wang, L. Jin, Z. Quan, *Colloids Surf., B*, **2017**, *154*, 287–296; f) H. Meng, M. Xue, T. Xia, Y. L. Zhao, F. Tamanoi, J.F. Stoddart, J.I. Zink, E.A. Nel, *J. Am. Chem. Soc.*, **2010**, *132*, 12690–12697; g) A. Llopis–Lorente, B. Lozano–Torres, A. Bernardos, R. Martínez–Máñez, F. Sancenón, *J. Mat. Chem. B*, **2017**, *5*, 3069–3083; h) W. Guo, J. Wang, S.J. Lee, F. Dong, S.S. Park, C.S. Ha, *Chem. Eur. J.*, **2010**, *16*, 8641–8646; i) A. Popat, J. Liu, G. Q. Lu, S. Z. Qiao, *J. Mater. Chem.,* **2012**, *22*, 11173–11178.

[62] a) E. Johansson, E. Choi, S. Angelos, M. Liong, J. I. Zink, *Sol–Gel Sci. Technol.*, **2008**, *46*, 313–317; b) Q. Lin, Q. Huang, C. Li, C. Bao, Z. Liu, F. Li, L. Zhu, L. *J. Am. Chem. Soc.*, **2010**, *132*, 10645–10647; c) J. Lai, X. Mu, Y. Xu, X. Wu, C. Wu, C. Li, J. Chen, Y. Zhao, *Chem. Commun.,* **2010**, *46*, 7370–7294.

[63] a) R. Liu, X. Zhao, T. Wu, P. Feng, *J. Am. Chem. Soc.*, **2008**, *130*, 14418–14419; b) R. Mortera, J. Vivero–Escoto, I.I. Slowing, E. Garrone, B. Onida, V.S.Y. Lin, *Chem. Commun.,* **2009***,* 3219–3221.

[64] a) C. Liu, J. Guo, W. Yang, J. Hu, C. Wang, S. Fu, *J. Mat. Chem.*, **2009***, 19*, 4764–4770; b) J. Lai, X. Mu, Y. Xu, X. Wu, C. Wu, C. Li, J. Chen, Y. Zhao, *Chem. Commun.,* **2010**, *46*, 7370–7372; c) C.R. Thomas, D.P. Ferris, J.H. Lee, E. Choi, M.H. Cho, E.S. Kim, J.F. Stoddart, J.S. Shin, J. Cheon, J.I. Zink, *J. Am. Chem. Soc.,* **2010**, *132*, 10623–10625.

[65] a) R. Casasús, E. Aznar, M. D. Marcos, R. Martínez–Máñez, F. Sancenón, J. Soto, P. Amorós, *Angew. Chem. Int. Ed.*, **2006,** *45*, 6661–6664; b) L. Zhang, Y. Li, C.Y. Jimmy, *J. Mat. Chem. B*, **2014**, *2*, 452–470; c) N. Song, Y.W. Yang, *Chem. Soc. Rev.*, 2015, *44*, 3474–3504; d) E. Aznar, C. Coll, M.D. Marcos, R. Martínez–Máñez, F. Sancenón, J. Soto, P. Amorós, J.

"triggers" for uncapping the pores and releasing different guest molecules from mesoporous scaffolds. Most recently, design of stimuli-responsive nanoscopic gated systems involving biomolecules became an important field. Specially, the controlled release of bioactive molecules is a very interesting issue, from a pharmaceutical point of view. It opens new possibilities to direct the nanoscopic vehicle to specific cell using a specific external stimulus and/or can prevent degradation of the internal entrapped cargo due to metabolic processes. Also, some biomolecules, especially enzymes,[66] have been used as stimuli to uncap gated scaffolds. In the same line, enzymes and other biomolecules, such as sachharides,[67] peptides,[68] aptamers[69] or DNA,[70] have also been used as capping agents. To have a broad overview of this fertile area, Table 2, summarizes different types of external stimuli and the mechanism used to induce cargo delivery. Selected references are included.

Cano, E. Ruiz, *Chem. Eur. J.*, **2009**, *15*, 6877–6888; e) Y. Zhao, B. G. Trewyn, I.I. Slowing, V. S.Y. Lin, *J. Am. Chem. Soc.,* **2009***, 131*, 8398–8400; f) Y.L. Choi, J. Jaworsky, M.L. Seo, S.J. Lee, J.H. Jung, *J. Mater. Chem.,* **2011**, *21*, 7882–7885; g) A. Schulz, R. Woolley, T. Tabarin, C. McDonagh, *Analyst*, **2011**, *136*, 1722–1727; h) J. Lee, J. Lee, S. Kim, C.J. Kim, S. Lee, B. Min, Y. Shin, C. Kim, *Bull. Korean Chem. Soc.*, **2011**, 32, 1357–1358; i) I. Candel, A. Bernardos, E. Climent, M.D. Marcos, R. Martínez–Máñez, F. Sancenón, J. Soto, A. Costero, S. Gil, M. Parra, *Chem. Commun*. **2011**, *47*, 8313–8315.

[66] a) K. Patel, S. Angelos, W.R. Dichtel, A. Coskun, Y.W. Yang, J.I. Zink, J.F. Stoddart, *J. Am. Chem. Soc.,* **2008***, 130*, 2382–2383; b) A. Schlossbauer, J. Kecht, T. Bein, *Angew. Chem. Int. Ed.*, **2009**, *48*, 3092–3095; c) A. Bernardos, E. Aznar, M. D. Marcos, R. Martínez–Máñez, F. Sancenón, J. Soto, J. M. Barat, P. Amorós, P. *Angew. Chem. Int. Ed.*, **2009**, *48*, 5884–5887; d) C. Park, H. Kim, S. Kim, C. Kim, *J. Am. Chem. Soc.,* **2009***, 131*, 16614–16615; e) P.D. Thornton, A. Heise, *J. Am. Chem. Soc.,* **2010**, *132*, 2024–2028.

[67] A. Bernardos, L. Mondragón, E. Aznar, M. D. Marcos, R. Martínez–Máñez, F. Sancenón, J. Soto, J. M. Barat, E. Pérez–Payá, C. Guillem, P. Amorós, *ACS Nano*, **2010**, *4*, 6353–6368.

[68] a) C. Coll, L. Mondragón, R. Martínez–Máñez, F. Sancenón, M.D. Marcos, J. Soto, P. Amorós, E. Pérez–Payá, *Angew*. *Chem*. *Int*. *Ed*., **2011**, 50, 2138–2140; b) F. Porta, G.E.M. Lamers, J.I. Zink, A. Kros, *Phys. Chem. Chem. Phys.,* **2011**, *13*, 9982–9985.

[69] a) C.L. Zhu, C.H. Lu, X.Y. Song, H.H. Yang, X.R. Wang, *J. Am. Chem. Soc.*, **2011**, *133*, 1278–1281

[70] a) A. Schossbauer, S. Warncke, P.M.E. Gramlich, J. Kecht, A. Manetto, T. Carell, T. Bein, *Angew. Chem. Int. Ed.*, **2010**, *49*, 4734–4743; b) Y. Zhang, Q. Yuan, T. Chen, X. Zhang, Y. Chen, W. Tan, *Anal. Chem.*, **2012**, *84*, 1956–1962.

Table 2. Types of external stimulus, and mechanism through molecular gates

External stimulus	Mechanism	Ref.
Light	• Photodimerization of molecules.	71
	• Photoisomerization of molecules	72,73
	• Photocleaveage of covalently linked caps	74
	• Generation of Reactive Oxygen Species able to cause the rupture of chemical bonds	75
	• Use of gold nanoclusters which absorb optical energy and generate heating enough to induce the destabilization of the capping	76
Temperature	• Use of temperature-responsive polymers	68,77
	• Melting of grafted double-stranded DNA.	78
Magnetic fields	• Changes on the conformation/structure of thermosensitive molecules	79
Ultrasound	• Molecular destabilization by cavitation	80
Redox	• Reduction of inclusion complexes such as rotaxanes and pseudorotaxanes	81
	• Reduction of disulfide bonds	82
pH	• Changes in conformation of molecules from a rigid to flexible a form due to pH.	55,83
	• Coordination or rupture of metal complexes	84,85
	• Changes on volume of pH-sensitive polymers	86
	• Destabilization of layer-by-layer depositions	87
	• Conformational changes on DNA and peptide structures	88
	• Destabilization of lipid bilayers	89
	• Rupture of pH-sensitive bonds	90
	• Dissolution of inorganic caps	91
Molecules and Biomolecules	• Use of specific molecular recognition interactions between organic functionalized groups and anions, cations or small neutral molecules	92-94
	• Hybridization of oligonucleotides	95
Enzymes	• Hydrolysis of specific chemical groups	96-101

are switched between “open” and “closed” states.

[71] a) N.K. Mal, M. Fujiwara, Y. Tanaka, *Nature,* **2003**, *421*, 350−353; b) H.M.Lin, W.K. Wang, P.A. Hsiung, S.G. Shyu, *Acta Biomater.,* **2010**, *6,* 3256−3263; c) J. Yang, W.D. He, C. He, J.

Tao, S.Q. Chen, S.M. Niu, S.L. Zhu, S.L.J. Polym. Sci., *Part A: Polym. Chem.,* **2013**, *51*, 3791−3799.

[72] a) D.P. Ferris, Y.P. Zhao, N.M. Khashab, H.A. Khatib, J.F. Stoddart, J.I. Zink, *J. Am. Chem. Soc*., **2009**, *131*, 1686−1688; b) J. Croissant, A. Chaix, O. Mongin, M. Wang, S. Clement, L. Raehm, J.O. Durand, V. Hugues, M. Blanchard–Desce, M. Maynadier, A. Gaullud, M. Gary-Bobo, M. García, J. Lu, F. Tamanoi, D.P. Ferris. D. Tarn, J.I. Zink, *Small*, **2014**, *10*, 1752−1755; c) J. Liu, W. Bu, L. Pan, J. Shi, *Angew. Chem., Int. Ed*. **2013**, *52*, 4375−4379.

[73] a) E. Aznar, R. Casasús, B. García–Acosta, M.D. Marcos, R. Martínez–Máñez, F. Sancenón, J. Soto, P. Amorós, *Adv. Mater*., **2007**, *19*, 2228−2231; b) Q. Xing, N. Li, D. Chen, W. Sha, Y. Jiao, X. Qi, Q. Xu, J. Lu, *J. Mater. Chem. B,* **2014**, *2*, 1182−1189; c) L. Chen, W. Wang, B. Su, Y. Wen, C. Li, Y. Zhou, M. Li, X. Shi, H. Du, Y. Song, L. Jiang, *Nano,* **2014**, *8*, 744−751.

[74] a) J.L. Vivero–Escoto, I.I. Slowing, C. W. Wu, V.S.Y. Lin, *J. Am. Chem. Soc*., **2009**, *131*, 3462−3463; b) T.M. Guardado–Alvarez, L.S. Devi, J.M. Vabre, T.A. Pecorelli, B.J. Schwartz, J.O. Durand, O. Mongin, M. Blanchard–Desce, J.I. Zink, *Nanoscale,* **2014**, *6*, 4652−4658; c) Y. Yang, B. Velmurugan, X. Liu, B. Xing, *Small,* **2013**, *9*, 2937−2944.

[75] a) S. Yang, N. Li, Z. Liu, W. Sha, D. Chen, Q. Xu, J. Lu, *Nanoscale,* **2014**, *6*, 14903−14910; b) P.M. Dobay, A. Schmidt, E. Mendoza, T. Bein, J. Rädler, *Nano Lett*., **2013**, *13*, 1047−1052.

[76] a) P. Shi, Z. Liu, K. Dong, E. Ju, J. Ren, Y. Du, Z. Li, X. A. Qu, *Adv. Mater*., **2014**, *26*, 6635−6641; b) P. Shi, E. Ju, J. Ren, X. Qu, *Adv. Funct. Mater*., **2014**, *24*, 826−834.

[77] a).; b) M.M. Russell, L. Raboin, T.M. Guardado–Alvarez, J.I. Zink, *J. Sol–Gel Sci. Technol*., **2014**, *70*, 278−285; c) C.L. Wu, X. Wang, L.Z. Zhao, Y.H. Gao, R.J. Ma, Y.L. An, L.Q. Shi, *Langmuir,* **2010**, *26*, 18503−18507.

[78] a) C. Chen, J. Geng, F. Pu, X. Yang, J. Ren, X. Qu, Angew. *Chem., Int. Ed*., **2011**, *50*, 882−886; b) Z.Z. Yu, N. Li, P.P. Zheng, W. Pan, B. Tang, *Chem. Commun*., **2014**, *50*, 3494−3497

[79] a) A. Baeza, E. Guisasola, E. Ruiz–Hernandez, M. Vallet–Regí, *Chem. Mater*., **2012**, *24*, 517−524; b) D.H. Kim, Y. Guo, Z.L. Zhang, D. Procissi, J. Nicolai, R.A.Omary, A.C. Larson, *Adv. Healthcare Mater*., **2014**, *3*, 714−724.

[80] X. Wang, H. Chen, Y. Zheng, M. Ma, Y. Chen, K. Zhang, D. Zeng, J. Shi, *Biomaterials,* **2013**, *34*, 2057−2068; b) X. Wang, H. Chen, K. Zhang, M. Ma, F. Li, D. Zeng, S Zheng, Y. Chen, L. Jiang, H. Xu, J. Shi, *Small,* **2014**, *10*, 1403−1411.

[81] a) G.Q. Silveira, M.D. Vargas, C.M. Ronconi, *J. Mater. Chem*., **2011**, *21*, 6034−6039; b) B. Lozano–Torres, L. Pascual, A. Bernardos, M.D. Marcos, J.O. Jeppesen, Y.Salinas, R. Martínez–Máñez, F.Sancenón *Chem. Comm*., **2017**, 53,*25* 3559–3562.

[82] a) S.Y. Tan, C.Y. Ang, P.Z. Li, Q.M. Yap, Y.L. Zhao, *Chem. Eur. J*. 2014, *20*, 11276−11282; b) S.R. Gayam, S.P. Wu, *J. Mater. Chem. B,* **2014**, *2*, 7009−7016; c) B.Y. Lee, Z. Li, D.L. Clemens, B.J. Dillon, A.A. Hwang, J.I. Zink, M.A. Horwitz, *Small*, **2016**, *12*, 27, 3690–3702.

[83] V. Morales, M. Gutiérrez-Salmerón, M. Balabasquer, J. Ortiz-Bustos, A. Chocarro-Calvo, C. García-Jiménez, R.A. García-Muñoz, *Adv. Funct. Mat.*, **2016**, *40*, 7291–7303.

[84] a) S. Wu, Q. Deng, X. Huang, X. Du, *ACS Appl. Mater. Interfaces,* **2014**, *6*, 15217−15223; b) Z. Zou, S. Li, D. He, X. He, K. Wang, L. Li, *J. Mat. Chem. B*, **2017**, *11*, 2126–2132; c) G.M.

Bao, L. Wang, H.Q. Yuan, X. Y. Wang, T.X. Mei, M.R. Qu, *RSC Advances*, **2016**, *111*, 109453–109459.

[85] a) S. Angelos, Y.W. Yang, K. Patel, J.F. Stoddart, J.I. Zink*, Angew. Chem., Int. Ed*., **2008**, *47*, 2222−2226; b) B. Tian, S. Liu, S. Wu, W. Lu, D. Wang, L. Jin, B. Hu, K. Li, Z. Whang, Z. Quan, *Colloids Surf., B*, **2017**, *154*, 287–296.

[86] a) J.K. Fu, Y.C. Zhu, Y.J. Zhao*, Mater. Chem. B,* **2014**, *2*, 3538−3548; b) Y., Sun, Z.P. Ran, H.Y. Tang, Y. Li, W.S. Song, Q.G. Ren, W.L. Yang, J.L. Kong, *J. Chin. Chem*. **2013**, *31*, 787−793; c) C. Samart, P. Prawingwong, S. Amnuaypanich, H.B. Zhang, K. Kajiyoshi, P.J Reubroycharoen, *Ind. Eng. Chem*., **2014**, *20*, 2153−2158.

[87] a) W. Feng, W. Nie, C. He, X. Zhou, L. Chen, K. Qiu, W. Wang, Z. Yin, *ACS Appl. Mater. Interfaces,* **2014**, *6*, 8447−8460; b) Y.F. Zhu, J.L. Shi, W.H. Shen, X.P. Dong, J.W. Feng, M.L. Ruan, Y.S. Li, *Angew. Chem., Int. Ed*., **2005***, 44*, 5083−5087.

[88] a) C.E. Chen, F. Pu, Z.Z. Huang, Z. Liu, J.S. Ren, X.G. Qu, *Nucleic Acids Res*., **2011**, *39*, 1638−1644; b) Y. Tang, Z. Teng, Y. Liu, Y. Tian, J. Sun, S. Wang, C. Wang, J. Wang, G.J. Lu, *Mater. Chem. B,* **2014**, *2*, 4356−4362.

[89] a) Z. Luo, K. Cai, Y. Hu, B. Zhang, D. Xu, *Adv. Healthcare Mater*. **2012**, *1*, 321−325; b) J. Zhang, D. Desai, J.M. Rosenholm, *Adv. Funct. Mater*., **2014**, *24*, 2352−2360.

[90] a) L. Zhou, Z.H. Li, Z. Liu, J.S. Ren, X.G. Qu, *Langmuir*, **2013**, *29*, 6396−6403; b) Q. Gan, X. Lu, Y. Yuan, J. Qian, H. Zhou, X. Lu, J. Shi, C.A. Liu,C. *Biomaterials,* **2011**, *32*, 1932−1942.; c) Z. Zheng, X. Huang, D.A. Shchukin, *Chem. Commun*., **2014**, *50*, 13936−13939.

[91] a) H.P. Rim, K.H. Min, H.J. Lee, S.Y. Jeong, S. C. Lee, *Angew. Chem., Int. Ed*., **2011**, *50*, 8853−8857; b) C. Yang, W. Guo, L. Cui, D. Xiang, K. Cai, H. Lin, F. Qu, *Mater. Sci. Eng. C,* **2014**, *36*, 237−243; c) Q.S. Zheng, Y.L. Hao, P.R. Ye, L.Q. Guo, H.Y. Wu, Q.Q. Guo, J.Z. Jiang, F.F. Fu, G.N. Chen, *J. Mater. Chem. B,* **2013**, *1*, 1644−1648

[92] a) E. Aznar, C. Coll, M.D. Marcos, R. Martínez–Máñez, F. Sancenón, J. Soto, P. Amorós, J. Cano, E. Ruiz, *Chem. Eur. J.,* **2009**, *15*, 6877−6888; b) L. Hou, C. Zhu, X. Wu, G. Chen, D. Tang, *Chem. Commun*., **2014**, *50*, 1441−1444.

[93] a) E. Climent, M.D. Marcos, R. Martínez–Máñez, F. Sancenón, J. Soto, K. Rurack, P. Amorós, *Angew. Chem., Int. Ed*., **2009**, *48*, 8519−8522; b) L. Tan, Z. Chen, C. Zhang, X. Wei, T. Lou, Y. Zhao, *Small*, **2017**,14 ; c) N. Hao, L. Li, L., F.Tang, *Int. Mater. Rev.*, **2017**, *2*, 57–77.

[94] a) M. Chen, C. Huang, C. He, W. Zhu, Y. Xu, Y. Lu, *Chem. Commun*., **2012***, 48*, 9522–9524; b) L. Sun, X.G. Zhang, Z.M. Wu, C. Zheng, C.X. Li, *Polym. Chem*., **2014**, *5*, 1999−2009; c) M. Yu, Z. Gu, T. Ottewell, C. Yu, *J. Mat. Chem.,* **2017**, 18, 3241–3252.

[95] a) E. Climent, R. Martínez–Máñez, F. Sancenón, M.D. Marcos, J. Soto, A. Maquieira, P. Amorós, *Angew. Chem., Int. Ed*., **2010**, *49*, 7281−7283.

[96] a) L. Pascual, S. Sayed, M.D. Marcos, R. Martínez-Máñez, F. Sancenón, *Asian J. Chem.*, **2017**, *7*, 775–784; b) A. Llopis–Lorente, B. Lozano–Torres, A. Bernardos, R. Martínez–Máñez, F. Sancenón, *J. Mat. Chem,*. **2017**,*17*, 3069–3083.

[97] a) W. Guo, C. Yang, L. Cui, H. Lin, F. Qu, *Langmuir* 2014, *30*, 243−249; b) C. Hu, P. Huang, Z. Zheng, Z. Yang, X. Wang, *Langmuir,* **2017**, *22*, 5511–5518.

[98] a) A. Schlossbauer, J. Kecht, T. Bein, *Angew. Chem., Int. Ed.,* **2009**, *48*, 3092−3095; b) A. Popat, S. Jambhrunkar, J. Zhang, J. Yang, H. Zhang, A. Meka, C. Yu, *Chem. Commun*., **2014**, *50*, 5547−5550.

1.5.1 Sensing application

Recognition using gated materials is a new merging application which has been developed in the last years.[102] A great variety of anions, cations, neutral molecules and biomolecules have been selected to trigger the release of entrapped cargos from mesoporous support. In recent years, the development of this type of applications has increased significantly.[103]

The core concept of applying gated materials to sensing protocols is to load the support with a reporter and to design the capping mechanism in such a way that a target analyte is able to selectively trigger uncapping and the delivery of the cargo (a reporter).[103,104] This concept differs for the classic supramolecular "binding site–signaling subunit" systems because the new protocol disconnects the recognition step from the signaling event, which therefore makes the amount of signal independent of the host–guest interaction.[105] Additionally, these systems are very flexible and can be adapted as required for a selected application. For example, they can be implanted in differents supports. Also, they have the possibility of using diferent molecules as reporter. Moreover, amplification features can be achieved due to large loading capacity of the used supports. This means that a few molecules of analyte can induce the release of a large quantity of signaling molecules, previously entrapped on the pores.

---

[99] N. Más, A. Agostini, L. Mondragón, A. Bernardos, F. Sancenón, M.D. Marcos, R. Martínez–Máñez, A.M. Costero, S. Gil, M. Merino–Sanjuan, M.; P. Amorós, M. Orzaez, E. Perez–Payá, *Chem. Eur. J.,* **2013**, *19*, 1346−1356.

[100] Y.F. Zhu, W. Meng, N. Hanagata, *Dalton Trans*., **2011**, *40*, 10203−10208.

[101] S. Zong, Z. Wang, H. Chen, D. Zhu, P. Chen, Y. Cui, *IEEE Trans. Nanobiosci.,* **2014**, *13*, 55−60.

[102] E. Aznar, R. Martínez–Máñez, F. Sancenón, *Expert Opin. Drug Deliver.,* **2009**, *6*, 643–655

[103] F. Sancenón, Ll. Pascual, M. Oroval, E. Aznar, R. Martínez–Máñez, *ChemistryOpen,* **2015**, 4, 418–437.

[104] C. Coll, A. Bernardos, R. Martínez–Máñez, F. Sancenón, *Acc. Chem. Res*., **2013**, *46*, 339–349.

[105] a) L.E. Santos–Figueroa, M.E. Moragues, E. Climent, A. Agostini, R. Martínez–Máñez, F. Sancenón, *Chem. Soc. Rev*., **2013,** *42*, 3489–3613; b) M.E. Moragues, R. Martínez–Máñez, F. Sancenón, *Chem. Soc. Rev*., **2011**, *40*, 2593–2643; c) Y. Salinas, R. Martínez–Máñez, M.D. Marcos, F. Sancenón, A.M. Costero, M. Parra, S. Gil, *Chem. Soc. Rev*., **2012**, *41*, 1261–1296.

When using gating concepts for sensing, two possible situations are envisioned (see Figure 15). In one, pores are open and the reporter is delivered to the solution, whereas in the presence of a given analyte, this molecule can bind to receptors on the external surface of the mesoporous support and close the gate. As far as capping of the mesoporous support is selectively achieved in the presence of a target analyte, the design of a probe can be envisioned (See Figure 15A). In the second approach, the starting material is capped, and the presence of a target guest induces pore opening and dye delivery due to competitive binding as the Figure 15B shows.

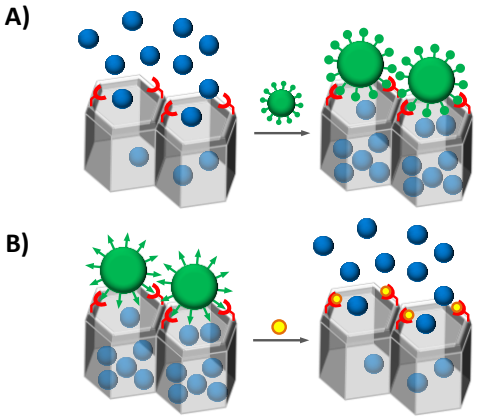

Figure 15. Scheme of the recognition paradigm using nanoscopic gate-like scaffoldings: A) inhibition of dye release due to analyte coordination with grafted binding sites; B) uncapping of the pores by an analyte-induced displacement reaction.

Of the two approaches, the second is perhaps the most interesting because it is able to show a signal in the presence of a target analyte (i.e. off–on behavior), which is generally easier to measure than dye delivery inhibition (i.e. on–off behavior).

Nowadays, some researchers have envisioned the potential of this application. Although the amount of current literature regarding gated materials devoted to sensing applications is not very huge, the research field is experiencing a big

advance in the last years. As summarized in Table 3, different mechanisms to develop gated materials to detect selected analytes have been described.

Table 3. Summary of different mechanisms to develop sensing materials.

Type of analytes	Mechanism	Ref.
Anions	• Formation of complexes between the molecular gate and the triggered anion.	106
	• Recognition with selective DNA sequences	107
Cations	• Interaction with thiol groups	108
	• Formation of complexes	109
	• Recognition of selective DNA sequences	110
Small neutral molecules	• Displacement reactions	111
	• Nucleophilic substitution	112
	• pH changes	113
	• Reduction of disulfide bonds	114
	• Formation of complexes	115
	• Specific recognition using biomolecules	116
Biomolecules	• DNA sequence recognition	117

[106] a) R. Casasús, E. Aznar, M. D. Marcos, R. Martínez–Máñez, F. Sancenón, J. Soto, P. Amorós, *Angew. Chem. Int. Ed*., **2006**, *45*, 6661–6664; *Angew. Chem*., **2006**, *118*, 6813–6816; b) S. El Sayed, M. Milani, C. Milanese, M. Licchelli, R. Martínez-Máñez, F. Sancenón, *Chem. Eur. J.,* **2016,** *39*, 13935–13945.

[107] a) V.C. Özalp, T. Schäfer, *Chem. Eur. J*., **2011**, *17*, 9893–9896; b) V.C. Özalp, D. Çam, F. Hernandez, L.I., Hernandez, T. Schäfer, H.A. Öktem, *Analyst*, **2016,** *8*, 2595–2599.

[108] a) E. Climent, M. D. Marcos, R. Martínez–Máñez, F. Sancenûn, J. Soto, K. Rurack, P. Amorós, *Angew. Chem. Int. Ed*., **2009**, *48*, 8519–8522; *Angew. Chem*., **2009**, *121*, 8671–8674.

[109] Y. L. Choi, J. Jaworski, M. L. Seo, S. J. Lee, J. H. Jung, *J. Mater. Chem*., **2011,** *21*, 7882–7885

[110] a) Z. Zhang, D. Balogh, F. Wang, I. Willner, *J. Am. Chem. Soc*., **2013**, *135*, 1934–1940; b) L. Fu, J. Zhuang, W. Lai, X. Que, M. Lu, D. Tang, *J. Mater. Chem. B,* **2013**, *1*, 6123–6128.

Next, some representative examples cited in the Table 3, are explained in more detail.

- ✓ Sensing of anions

Due to the importance of anions in several chemical and biological processes, many researchers have focused their projects to the chemistry of anion recognition and host molecules for anions.[103,118] The first work where silica mesoporous supports (SMSs) were used for sensing applications was reported by

---

[111] a) Y.N. Zhao, B.G. Trewyn, I.I. Slowing, V.S.Y. Lin, *J. Am. Chem. Soc.,* **2009**, *131*, 8398−8400; b) T. Yadavalli, D. Shukla, *Nanomedicine: NBM*, **2017,** *1*, 219–230.

[112] P. Díez, A. Sánchez, M. Gamella, P. Martínez–Ruíz, E. Aznar, C. de La Torre, J. R. Murguía, R. Martínez–Máñez, R. Villalonga, M. J. Pingarrón, *J. Am.Chem. Soc*., **2014**, *136*, 9116–9123.

[113] R. Villalonga, P. Díez, A. Sánchez, E. Aznar, R. Martínez–Máñez, J. M. Pingarrón, *Chem. Eur. J*., **2013**, *19*, 7889–7894.

[114] S. El Sayed, C. Giménez, E. Aznar, R. Martínez–Máñez, F. Sancenón, M.Licchelli, *Org. Biomol. Chem*., **2015**, *13*, 1017–1021

[115] a) I. Candel, A. Bernardos, E. Climent, M. D. Marcos, R. Martínez–Máñez, F.Sancenón, J. Soto, A. M. Costero, S. Gil, M. Parra, *Chem. Commun*. **2011**,*47*, 8313–8315; b) N. Idros, M.Y. Ho, M. Pivnenko, M., Qasim, H. Xu, Z. Gu, D. Chu, *Procedia Technology*, **2017**, *27*, 312–314; c)

[116] a) E. Climent, A. Bernardos, R. Martínez–Máñez, A. Maquieira, M. D. Marcos, N. Pastor–Navarro, R. Puchades, F. Sancenón, J. Soto, P. Amorós, *J. Am.Chem. Soc*., **2009**, *131*, 14075–14080; b) B. Ruehle, D.L. Clemens, B.Y. Lee, M.A. Horwitz, J.I. Zink, *J. Am. Chem. Soc.,* **2017,** *19*, 6663–6668.

[117] a) E. Climent, R. Martínez–Máñez, F. Sancenón, M. D. Marcos, J. Soto, A. Maquieira, P. Amorós, *Angew. Chem. Int. Ed*., **2010***, 49*, 7281–7283; *Angew. Chem*., **2010**, *122*, 7439–7441; b) M. Oroval, M. Coronado-Puchau, J. Langer, M.N. Sanz-Ortiz, Á. Ribes, E. Aznar, C. Coll M.D, Marcos, F. Sancenón, R. Martínez-Máñez, *Chem. Eur. J.*, **2016,** *38*, 13488–13495; c) L. Pla, E. Xifré-Pérez, À. Ribes, E. Aznar, M.D.Marcos, L.F. Marsal, R. Martínez–Máñez, F. Sancenón, *ChemPlusChem*, **2017**, *3*, 337–341.

[118] a) Q. Zhang, E. Uchaker, S.L. Candelaria G. Cao, *Chem. Soc. Rev*., **2013**, *42*, 3127−3171; b) N. Linares, A. M. Silvestre–Albero, E. Serrano, J. Silvestre–Albero, J. García–Martínez, *Chem. Soc. Rev*., **2014**, *43*, 7681−7717; c) T. Wagner, S. Haffer, C. Weinberger, D. Klaus, M. Tiemann, *Chem. Soc. Rev*., **2013**, *42*, 4036−4053; d) C. Perego, R. Millini, *Chem. Soc. Rev*., **2013**, *42*, 3956−3976; e) A.E. Garcia–Bennett Synthesis, *Nanomedicine,* **2011**, *6*, 867−877; f) V. Valtchev, L. Tosheva, *Chem. Rev*. **2013**, *113*, 6734−6760; g) A. Stein, *Adv. Mater*., **2003**, *15*, 763−775; j) G.J.A.A. Soler–Illia, O. Azzaroni, *Chem. Soc. Rev*., **2011**, *40*, 1107−1150.

the group of Martínez–Máñez in 2006. The system consisted of an SMS loaded with $Ru(bipy)_3^{2+}$ dye as the reporter and functionalized on the external surface with 3-[2-(2-aminoethylamino)ethylamino]-propyl trimethoxysilane and it is based on the on–off behavior shown in Figure 15A. At a neutral pH, in which the experiments were carried out, the gate was open, and delivery of the ruthenium complex was detected chromo-fluorogenically. However, presence of adenosine triphosphate (ATP), and of adenosine diphosphate (ADP) to a lesser extent, allowed the selective inhibition of indicator delivery by the formation of strong complexes between tethered polyamines and ATP anions through hydrogen bonding and electrostatic interactions (Figure 16). The system presented good selectivity for ATP in the presence of other anions, such as chloride, sulfate, or guanosine monophosphate (GMP), which were either too small or formed complexes that were too weak to effectively cap pores.[106a]

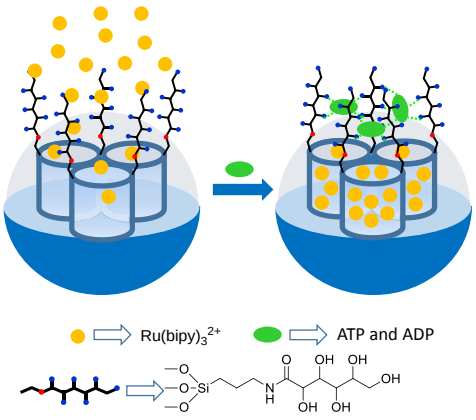

Figure 16. Mesoporous support functionalized with polyamines for the detection of ATP.

As mentioned above the second approach, on-off behavior, (Figure 15B) is the most common used. For this type of systems it is normally necessary to use large molecules to allow to pre pare capped materials, which could be opened in the presence of target analytes. One method to achieve this goal used aptamers. An example of detection of anions using this protocol was reported in 2011, by Özalp

and co-workers, who paid attention to the use of aptamers to develop an ATP-responsive gated material (Figure 17).[107a] In their work, they used an amino-terminated oligonucleotide sequence (5'-CAC CTG GGG GAG TAT TGC GGA GGA AGG TTC CAG GTG-NH2-3'), which contained the well-known ATP aptamer (5'-CAC TG GGG GAG TAT TGC GGA GGA AGG TT-3'), and a short extra fragment (5'-CCA GGT G-NH_2-3') to induce a hairpin-like structure that blocked pores. An SMS in the form of nanoparticles, loaded with fluorescein and functionalized on the external surface with sulfhydryl groups, was prepared and the amino functionalized aptamer was covalently attached using sulfo-N-succinimidyl 4-maleimidobutyrate as a crosslinker. These authors observed that the hairpin aptamer blocked pores, while presence of ATP triggered the delivery of the entrapped fluorescein dye. This was explained by ATP binding, which induced a conformational change from a duplex to a single-stranded DNA near the aptamer region, which was close to the SMS surface and resulted in fluorescein release. These authors also found that nanoparticles capped with a mutated hairpin did not respond to ATP, and that guanosine 5'-triphosphate (GTP) was also unable to trigger fluorescein release. They also confirmed that cargo delivery was dependent on ATP concentration.

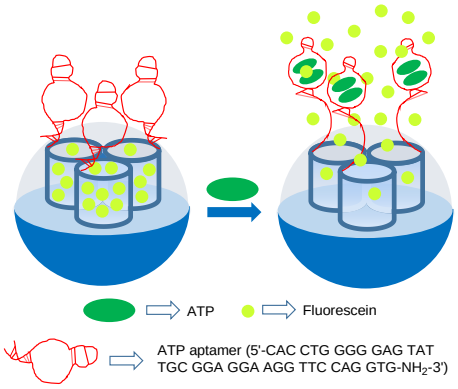

Figure 17. MSNs support loaded with fluorescein and capped with ATP aptamers for the detection of ATP.

✓ Sensing of cations

The examples for the detection of small cations by using gated materials are scarce compared with anions.

As far as we know, the first example reported was designed to sense the presence of cation CH_3Hg^+.[108a] This work is also the first example which used an off-on approach (Figure 15B). The gated material consisted of a mesoporous support loaded with dye safranin O and capped with 2,4-bis-(4-dialkylaminophenyl)-3-hydroxy-4-alkylsulfanylcyclobut- 2-one (APC) groups. APC moieties were readily formed by the reaction of a squaraine dye and thiol units, which were previously anchored to the external surface of the mesoporous support. When CH_3Hg^+ was added to the acetonitrile: toluene 4:1 v/v suspension of the APC-capped support, safranin O release was observed. This uncapping process derived from the reaction of methylmercury with the thiol group on APC moieties, which resulted in the coordination of the cation to thiols and, in both, the release of the bulky squaraine chromophore and the delivery of the entrapped safranin O reporter (Figure 18). Experiments were done in acetonitrile:toluene 4:1 v/v mixtures to achieve discrimination from Hg^{2+} given its low solubility in this medium. This procedure was successfully tested to optically determine methylmercury in fish samples by a simple extraction procedure with toluene and CH_3Hg^+ detection with the APC-capped solid. These real fish samples were also spiked with cations Na^+, K^+, Ca^{2+}, Mg^{2+}, Cu^{2+}, Ni^{2+}, Zn^{2+}, Ag^+, Pd^{2+}, Cd^{2+}, Au^{3+}, and Tl^+ and various organic species, for example, sodium lauryl sulfate, cysteine, histamine, ethanol, heptylamine, and hexanethiol. However, none of these species affected the response of the capped material to CH_3Hg^+.

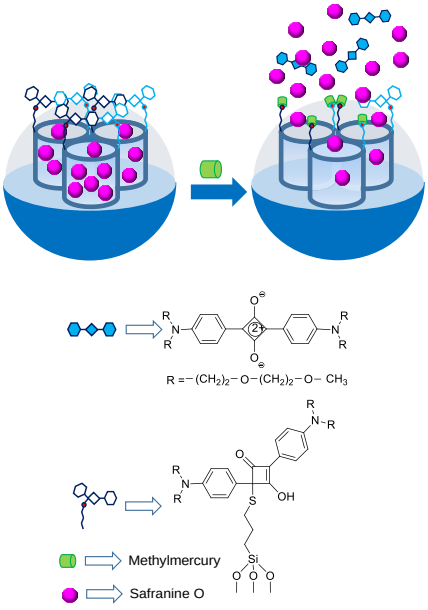

Figure 18. MSNs support loaded with safranine and capped with 2,4-bis-(4-dialkylaminophenyl)-3-hydroxy-4-alkylsulfanylcyclobut-2-one (APC) groups for the detection of methylmercury.

Choi et al. reported the design of capped silica mesoporous nanoparticles capable of being opened in the presence of K^+ using macrocycles. These authors used a SMS in the form of nanoparticles, which was loaded with curcumin dye and anchored a 18-crown-6 derivative to the external surface. Nanopar ticles were finally capped upon the addition of the Cs^+ cation, which formed sandwich complexes with the grafted 18-crown-6 moieties. The systems showed a zero release until the K^+ cation was added, which induced the release of the entrapped curcumin. The uncapping protocol was due to the Cs^+ exchange, owing to the formation of 1:1 macrocycle-K^+ complexes with a higher stability constant (see Figure 19). However the authors did not specifically use this system to sense applications, and no opening studies of macrocycle-capped nanoparticles with other metal cations were carried out.[109]

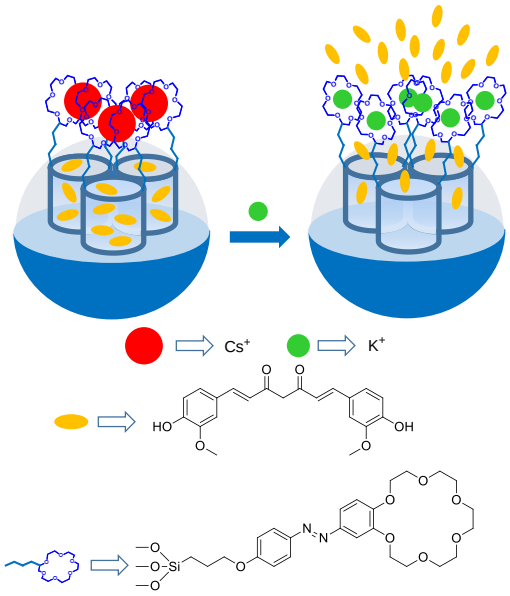

Figure 19. MSNs support loaded with curcumin and capped with Cs^+-18-crown-6 complexes for the detection of K^+ cations.

✓ Sensing Neutral Molecules

Several gated materials have been developed to sense glucose. One of these systems was described by Lu and co-workers. Mesoporous silica nanoparticles were selected as the inorganic scaffold, and their external surface was functionalized with prop-2-yn-1-yl(3-(triethoxyxilyl)propyl)carbamate. Following this functionalization, inhibitor D-(+)-glucosamine was grafted by a click chemistry reaction. Then pores were loaded with rhodamine B and capped by the addition of the glucose oxidase enzyme (GOx) through the formation of a complex with the grafted inhibitor (see Figure 20). PBS suspensions of the capped material showed negligible rhodamine B release, whereas the addition of glucose induced marked dye release. The observed release, which was proportional to the amount of glucose added, was the result of a displacement reaction of GOx from the pore outlets due to the formation of the corresponding glucose–GOx complex. The

uncapping protocol was highly selective and the authors confirmed that other tested monosaccharides.[119]

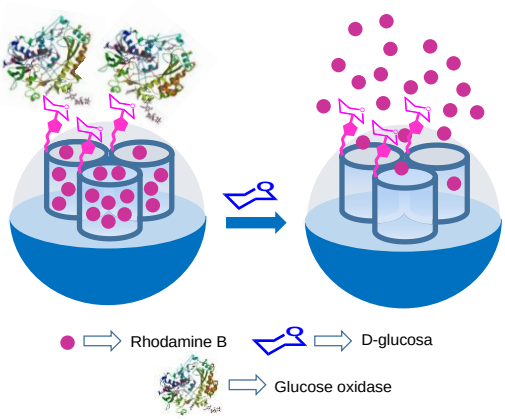

Figure 20. MSNs support loaded with rhodamine B and capped with glucose oxidase enzyme (GOx) for the detection of d-glucose.

Villalonga and co-workers developed a new gated SMS in which an enzyme also acted as a cap. However in this case, the uncapping process was triggered by the product obtained by the enzyme's activity on glucose.[113] In their work, porter $Ru(bipy)_3^{2+}$ and functionalized the external surface with 3-iodopropyltrimethoxysilane, which was transformed into 1- propyl-1-H-benzimidazole moieties via a nucleophilic substitution reaction using benzimidazole. Mesopores were then capped with active cyclodextrin-modified glucose oxidase (CD-GOx) through the formation of an inclusion complex between the cyclodextrins and the propylbenzymidazole groups anchored to the solid support. In their study, these authors confirmed that dye delivery was induced when glucose was present in the solution due to the displacement of CD-GOx as a result of the CD-GOx-induced oxidation of glucose to gluconic acid, which induced the subsequent protonation of the benzimidazole groups. The capped material

[119] M. Chen, C. Huang, C. He, W. Zhu, Y. Xu, Y. Lu, *Chem. Commun*. **2012**, *48*, 9522–9524.

was also tested in the presence of others saccharides, such as mannose, fructose, galactose, maltose, and saccharose however, no cargo delivery was observed.

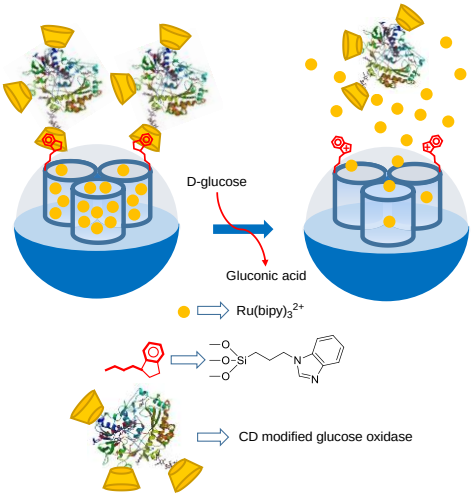

Figure 21. Nanometric silica mesoporous support loaded with $Ru(bipy)_3^{2+}$ and capped with cyclodextrin-modified glucose oxidase (CD-GOx) for the detection of d-glucose.

✓ Sensing of biomolecules

One of the first examples of gated materials to the detection of biomolecules, in particular a certain oligonucleotide, was reported by the group of Martínez-Máñez. The system was based on an SMS in the form of nanoparticles loaded with fluorescein and functionalized with (3-aminopropyl) triethoxysilane on the outer surface. Oligonucleotide 5'-AAT GCT AGC TAA TCA ATC GGG-3' was used to cap pores via electrostatic interactions with the anchored amines partially protonated in water at a neutral pH. These authors demonstrated that delivery of dye from the solid at pH 7.5 was selectively triggered in the presence of the complementary single strand of the capping oligonucleotide due to the hybridization of both single oligonucleotide

sequences with the concomitant cargo release. They also tested dye delivery in the presence of other oligonucleotides with a single or two-base mismatch sequence(s), but delivery was poor in these cases.[117a]

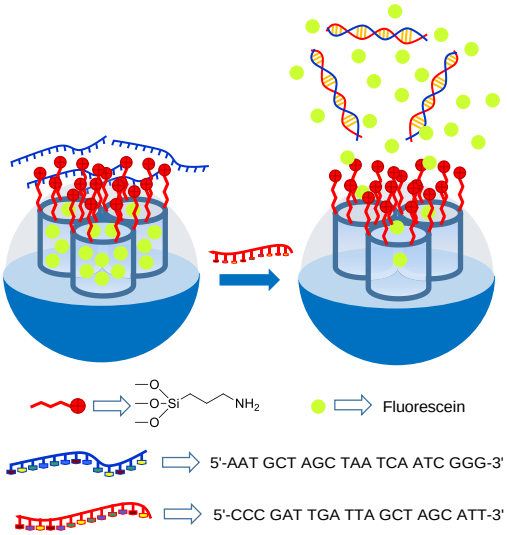

Figure 22. MSNs loaded with fluorescein and capped with oligonucleotide for the detection of the complementary strand.

Encouraged by the obtained result, the same authors designed a system able to detect genomic DNA.[120] For this purpose, an SMS, also in the form of nanoparticles, was loaded with rhodamine B and functionalized with (3-aminopropyl)triethoxysilane on the external surface. As the capping oligonucleotide, a highly conserved sequence in the *Mycoplasma* genome, which corresponds to a fragment of the 16S ribosomal RNA subunit, was used (e.g. 5'-GGG AGC AAA CAG GAT TAG ATA CCC T-3'). The system remained closed until the genomic DNA of Mycoplasma fermentans was added, which had been previously dehybridized by thermal treatment. The capped SMS was unable to deliver the

[120] E. Climent, L. Mondragón, R. Martínez–Máñez, F. Sancenón, M.D. Marcos, J.R. Murguía, P. Amorós, K. Rurack, E. Pérez–Payá, *Angew. Chem. Int. Ed*., **2013**, *52*, 8938–8942; *Angew. Chem*., **2013**, *125*, 9106–9110.

cargo in the presence of genomic DNA from other bacteria, such as *Candida albicans* or *Legionella pneumophilla*. (Figure 23A)

In a more recent work, the same authors developed a similar system to detect genomic DNA. In this case, they used nanoparticles loaded with rhodamine B and capped with covalently attached DNA (Figure 23B).[121] Two single-stranded oligonucleotides were selected for the gating mechanism: 1) a short DNA sequence (NH_2-$(CH_2)_6$-5'-GAC TAC GAC GGT ATC-3'), which was covalently anchored to the SMS via the formation of urea bonds and 2) a single-stranded oligonucleotide selective for *Mycoplasma* (e.g. 5'-AAG CGT GGG GAG CAA ACA GGA TTA GAT ACC CTG GTA GTC-3'). The authors also found that *Candida albicans* and *Legionella pneumophilla* genomic DNA were unable to induce dye release.

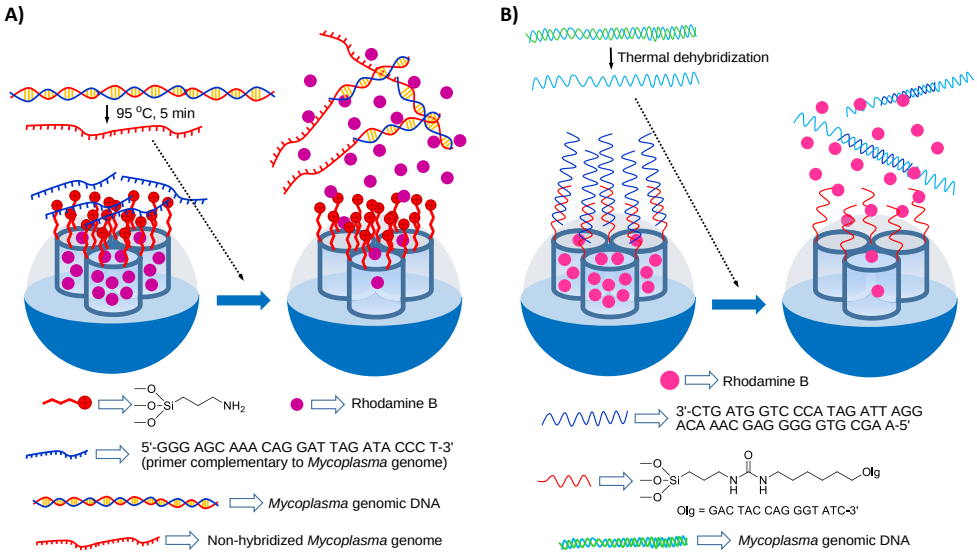

Figure 23. MSNs support loaded with rhodamine B and capped with a single-stranded oligonucleotide for the detection *Mycoplasma fermentans* genomic DNA, (A) electrostatically, and (B) covalently.

[121] L. Pascual, I. Baroja, E. Aznar, F. Sancenón, M.D. Marcos, J.R. Murguía, P. Amorós, K. Rurack, R. Martínez–Máñez, *Chem. Commun*., **2015**, *51*, 1414–1416.

Following all the previously described concepts, in this thesis new sensing systems based in gated materials are developed. Using different gating ensembles implemented in different supports new functional material have been developed. In particular, five differents systems to detect an addictive-stimulant drug, toxins and biomolecules have been designed, synthetized and evaluated. This new concept of sensing is very versatile and could be used to prepare other systems to detect a large variety of species in very different areas such as diagnosis, or quality

2. Objectives

Taking into account the concepts and examples detailed above, in this thesis we considered the possibility of designing different systems for the fluorogenic detection of target analytes of biomedical or environmental interest. It is expected the systems prepared in this thesis represent an advance in the fields of recognition and diagnose since they are fast and have high sensibility and selectivity.

The general objectives of the present PhD thesis are to design, prepare and evaluate different hybrid materials based on silica and alumina mesoporous supports, loaded with a reporter (dye) and capped with biomolecules as possible systems to detect target species. These objectives can be summarized in five general goals:

- To develop a new system based on aptamer-capped mesoporous silica nanoparticles to detect Bisphenol A with high accuracy and fast response.
- To design, prepare and evaluate two new methods to detect Ochratoxin A based on aptamer-capped mesoporous silica nanoparticles for the recognition of this species in real environments.
- To design, synthetize and evaluate a new method to detect cocaine, based on nanoporous anodic alumina supports capped with aptamers with a high selectivity and sensitivity.
- To develop a new sensing method for the detection of genomic DNA of *Candida albicans*, based on oligonucleotide-capped nanoporous anodic alumina and its use to discriminate between healthy patients and those infected with *Candida*.
- To design and prepare a new system to detect miRNA, using mesoporous silica nanoparticles capped with different oligonucleotides as a new procedure to detect specific biomarkers found at low levels in biofluids such as plasma.

3. Fluorogenic sensing of carcinogenic Bisphenol A using aptamer-capped mesoporous silica nanoparticles

Fluorogenic sensing of carcinogenic bisphenol A using aptamer-capped mesoporous silica nanoparticles

Àngela Ribes,[a,b] Elena Aznar,[b,a] Andrea Bernardos,[a,b] María D. Marcos, [a,b,d] Pedro Amorós,[c] Ramón Martínez-Máñez[a,b,d] and Felix Sancenon[a,b,d]

[a] Instituto Interuniversitario de Investigación de Reconocimiento Molecular y Desarrollo Tecnológico (IDM). Universitat Politècnica de València, Universitat de València, Departamento de Química, Universitat Politècnica de València, Camino de Vera s/n, 46022, Valencia, Spain.

[b] CIBER de Bioingeniería, Biomateriales y Nanomedicina (CIBER-BBN).

[c] Institut de Ciència dels Materials (ICMUV), Universitat de València, P.O. Box 22085, E-46071, Valencia (Spain).

[d] Departamento de química, Universitat Politècnica de València, Camí de Vera s/N, 46022, Valencia (Spain).

Received: *6th March 2017*

First published on the web: *5th June 2017*

Chemistry European Jounal, ***2017****, 23, 1-5*

Mesoporous silica nanoparticles loaded with rhodamine B and capped with a bisphenol A aptamer were used for the selective and sensitive detection of this lethal chemical. The pores of the nanoparticles are selectively opened in the presence of bisphenol A (through its selective coordination with the grafted aptamer) with subsequent rhodamine B delivery. With this capped material a limit of detection as low as 3.5 μM of bisphenol A was measured.

Bisphenol A (BPA) is a small toxic and carcinogenic organic molecule,[1] which has been reported to be particularly harmful to the fetus, infants and young children.[2] Moreover, BPA is an additive used in the production of epoxy resins and polycarbonate plastics, with multiple industrial applications, such as the production of lacquers, the inner coating of food cans and the coating of thermal paper.[3] Besides, BPA is the main component of some food containers, such as non-returnable bottles, feeding bottles, etc.[4] According to the European Commission's Scientific Committee on Food, the exposure estimate for BPA is 0.48-1.6 μg kg^{-1} body weight/day. Moreover, it has been reported that concentrations as low as 20 ppm in tap water are enough to produce genetic modifications.[5] In addition, several toxicological and biochemical studies suggested that BPA is a potent endocrine disrupting chemical.[6] High pressure liquid chromatography (HPLC), gas chromatography (GC), immunochemistry and electrochemical techniques have been used as traditional methods for BPA detection.[7] While these methods can correctly measure BPA, most of them require expensive equipment, sophisticated sample pre-treatments and complicated operator training.[8] In this scenario, the design of simple, yet selective and sensitive, probes for BPA detection is of interest.

Nanomaterials for sensing applications have been played in the last years a great role due to their capacity to provide rapid, simple and sensitive responses to target analytes.[9] Moreover, among nanomaterials used in sensing protocols, mesoporous silica nanoparticles (MSNs) have been widely employed due some of their remarkable properties such as large load capacity, biocompatibility, high inner surface area and the possibility to easily modify their surface.[10] Moreover, MSNs can be functionalized with a wide range of different (bio)molecules than act

as “molecular gates”, to obtain hybrid organic-inorganic supports for the design of stimuli-responsive systems, able to release an entrapped cargo upon the application of specific stimuli.[11] These capped materials have been used recently in sensing protocols and in the preparation of smart nanoparticles for drug delivery.[9c,11] For the former application, gated MSNs are loaded with a reporter, which is selectively delivered in the presence of a target analyte.

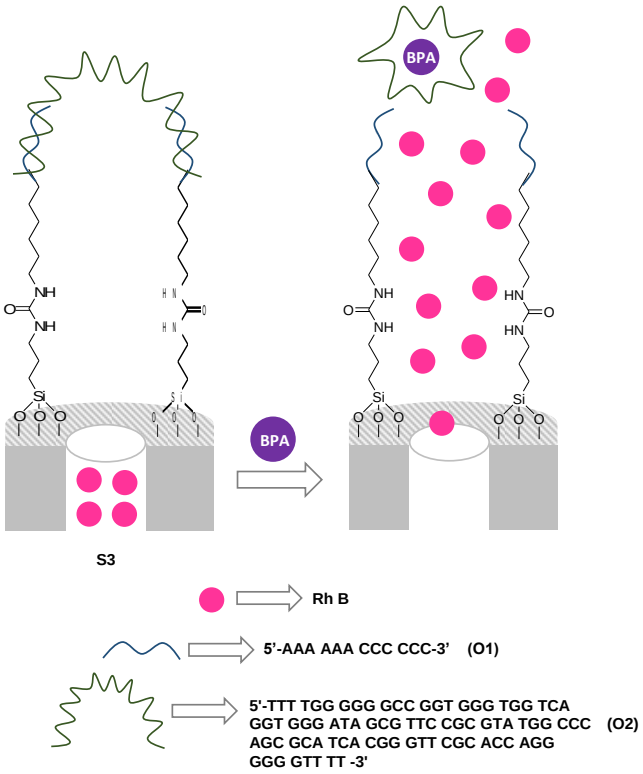

Scheme 1. Representation of the gated material **S3** capped with oligonucleotide **O2**. Delivery of the entrapped dye (rhodamine B) was selectively observed in the presence of BPA via coordination of **O2** with the BPA molecule.

From another point of view, the development of sensing materials using aptamers as potential systems able to detect trace amounts of target substances has recently attracted great attention.[12] Aptamers are stable DNA sequences with high affinity and selectivity for target biomolecules, small neutral molecules or

ions and their use in the design of several sensors and probes has resulted in the development of highly sensitive systems for different analytes. Recently, some aptasensors to determine BPA have been described.[13] However, as far as we know, the use of aptamer-based gated materials for the fluorogenic detection of BPA has not yet been reported.

In this scenario, we report herein the preparation of a new gated material based on MSNs loaded with a fluorophore and capped with an aptamer selective to BPA. The MSNs remained blocked until there is a selective uncapping in the presence of the BPA, which leads to the release of the entrapped cargo. Scheme 1 shows the proposed sensing paradigm. MCM-41-type mesoporous silica nanoparticles of a diameter of ca. 100 nm, were selected as inorganic scaffolds and were obtained according to reported procedures.[14] The nanoparticles were first loaded with the fluorophore rhodamine B in acetonitrile and then an excess of (3-isocyanatopropyl) triethoxysilane was added to the suspension (solid **S1**). A short DNA sequence functionalized with an aminohexyl moiety at the 5'-end position (NH_2-$(CH_2)_6$-5'-AAA AAA CCC CCC-3', **O1**) was covalently attached to **S1** via the formation of urea bonds (solid **S2**). Finally, a second single stranded oligonucleotide (i.e. 5'- TTT TGG GGG GCC GGT GGG TGG TCA GGT GGG ATA GCG TTC CGC GTA TGG CCC AGC GCA TCA CGG GTT CGC ACC AGG GGG GTT TT -3', **O2**) which contains the specific sequence of the BPA aptamer, was hybridized with **O1** to yield solid **S3** (see Supporting Information for details). Hybridization of **O1** with **O2** on the pore outlets of the MSNs blocked the pores and inhibits payload delivery from **S3**. Moreover, as stated above, the presence of the target analyte (i.e. BPA) was expected to selectively displace the aptamer, resulting in pore opening and dye release.

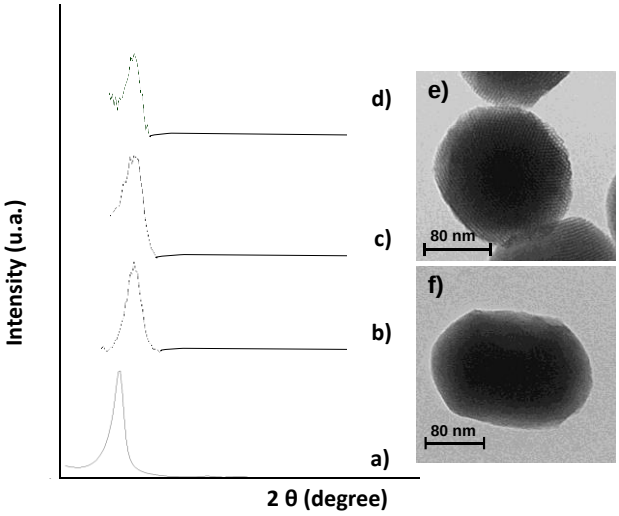

Figure 1. Powder X-ray patterns of (a) MSNs as synthesized, (b) calcined MSNs, (c) **S1**, and (d) **S2.** Inset: TEM images of (e) calcined MSNs and (f) **S3**.

The starting MSNs and the synthetized materials were characterized by standard procedures (see Supporting Information for further details). PXRD and TEM carried out on calcined MSNs clearly showed the presence of a mesoporous structure that persisted in solids **S1**, **S2** and **S3** regardless of the loading process with rhodamine B and further functionalization with (3-isocyanatopropyl) triethoxysilane, **O1** and **O2** (see Figure 1). BET specific surface area, pore volume and pore size were calculated from the N_2 adsorption-desorption measurements.[15] For the starting MSNs a value of BET specific surface of 1027.5 m^2g^{-1} was obtained, while for **S1** a decrease in the same value was observed (465.5 m^2 g^{-1}) in agreement with presence of the rhodamine B dye inside the pores and surface functionalization. Moreover, the size of starting MCM-41, **S1**, **S2** and **S3** was determined by dynamic light scattering (DLS) studies (see Supporting Information). Additionally, the presence of the DNA in the prepared nanoparticles was confirmed by FTIR spectroscopy (see also Supporting Information).

Besides, the organic content of the different prepared solids was calculated from thermogravimetric and elemental analysis (see Table 1). For instance, amounts of 1.46 % wt of rhodamine B, 0.61 % wt of **O1** and 0.37 % wt of **O2** were determined for the final sensing material **S3**.

Table 1. Contents (in % wt) of rhodamine B, (3-isocyanatopropyl), **O1** and **O2** in the different hybrid supports.

	Rhodamine B	3-(isocyanatopropyl)	O1	O2
S1	6.24	0.23	-	-
S2	1.48	0.23	0.61	-
S3	1.46	0.23	0.61	0.37

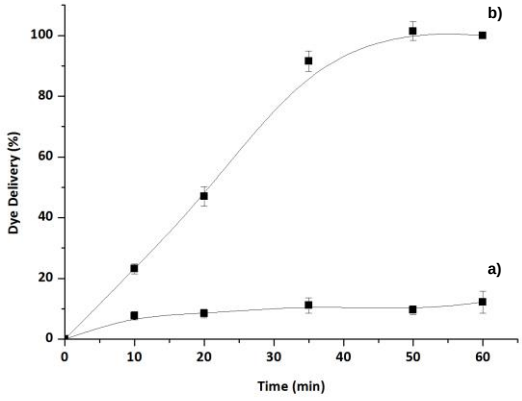

Figure 2. Release profile of rhodamine B from solid **S3** in the absence (a) and the presence (b) of BPA in Tris-HCl buffer at pH 7.5

The response of **S3** was tested in the presence of BPA. In a typical experiment 0.1 mg of **S3** were suspended in hybridization buffer (20 mM Tris-HCl, 37.5 $MgCl_2$, pH 7.5) and separated in 2 aliquots. BPA was added to one of the aliquots, whereas water was added to the other. Both samples were filled to a final volume of 1000 µL of hybridization buffer. The suspensions were maintained at 25°C and, at programed times, fractions were taken and centrifuged to eliminate the solid. Cargo release to the solution was then measured by the rhodamine B fluorescence at 585 nm (λ_{exc} = 555 nm). Figure 2 shows the delivery kinetic profiles of rhodamine B from solid **S3** in the presence and in the absence of BPA. In the absence of the analyte (curve a), a poor rhodamine B delivery was observed, indicating tight pore closure. In contrast, a clear cargo release was observed in the

presence of BPA, which reached nearly 90 % of the maximum dye delivered after ca. 35 min.

In a further step, the sensitivity of **S3** solid towards BPA was evaluated. In this experiment cargo released after 30 min from **S3** in the presence of different amounts of BPA was studied. Rhodamine B was released proportionally to the BPA concentrations (see Figure 3), which is in agreement with the uncapping protocol detailed above involving preferential binding of the **O2** oligonucleotide with BPA, which resulted in uncapping of the pores and payload delivery. From these studies a limit of detection (LOD) of 3.5 μM for the detection of BPA was obtained (see Figure 3). This LOD obtained for probe **S3** fells within the range of other methods reported for BPA detection using aptamers as recognition subunit[13] and it is enough to detect concentration as low as 20 ppm (87.6 mM) of BPA in water (20 ppm concentrations have been reported to produce genetic modifications, *vide ante*).[5]

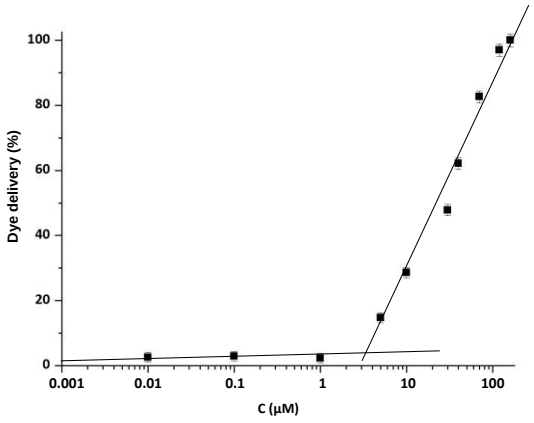

Figure 3. Release of rhodamine B from solid **S3** at different concentrations of BPA.

Moreover, one advantage of gated materials for sensing applications is the possible observation of amplification features. In **S3** the recognition protocol (in our case, BPA–**O2** pair formation) is separated from the signaling event (dye delivery from the pores), which means that sensing is independent of the stoichiometry of the formed host–guest complex. In terms of signal amplification, in our particular case, it was found that one molecule of BPA was able to deliver

ca. 10 molecules of rhodamine B at low BPA concentrations (ca. 10 mM), which results in an order of magnitude amplification (see Supporting Information for more details).

Additionally, the selectivity of **S3** to BPA was confirmed. With this aim, cargo release from **S3** was tested in water containing 10 mM of BPA, bisphenol C (BPC) and bisphenol E (BPE). As shown in Figure 4, BPA is the only molecule able to induce a notable dye delivery, whereas BPC and BPE induced negligible pore opening and poor payload release. This observation corroborates the selective BPA-aptamer interaction as mechanism of the observed optical response.

Motivated by the sensing behaviour displayed by **S3**, we took a step forward and tested the performance of the capped material for the determination of BPA in a more realistic context. In particular the addition standard method and **S3** was used to determine the BPA content in tap water spiked with BPA (262 µM). In a typical experiment four different amount of BPA standard solution were added to four aliquots of **S3** in tap water spiked with BPA. After 30 min at 25°C the emission of the rhodamine B released from solid **S3** in the different aliquots was measured and a calibration curve was obtained. From the intercept of the curve with the x-axis a concentration of BPA in the spiked sample of 255 µM was determined (97 % recovery).

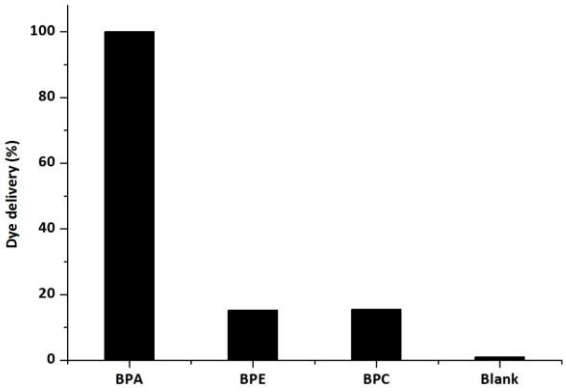

Figure 4. Release of rhodamine B (from right to left) in the absence and in the presence of BPC, BPE and BPA.

In summary, we have developed a new fluorogenic probe for the detection of BPA by using MSNs loaded with a dye and capped with BPA-selective aptamer. The response of the probe is related with the interaction between the capping aptamer and BPA that induced a displacement of the aptamer, pore opening and dye release. A LOD as low as 3.5 μM for BPA was calculated. Moreover, the probe displayed an amplification of the signal and it was found that a unique molecule of BPA was able to induce the delivery of ca. 10 molecules of the dye. In addition, the capped nanomaterial allowed accurate BPA determination in tap water samples. As far as we know, this is the first time that aptamer-capped mesoporous supports have been used for the detection of BPA.

Acknowledgements

We thank the Spanish Government (projects MAT2015-64139-C4-1-R and AGL2015-70235-C2-2-R (MINECO/FEDER)) and the Generalitat Valenciana (project PROMETEOII/2014/047) for support. A.R. thanks UPV for her predoctoral fellowship. A.B. thanks the Spanish Government for the finantial support “Juan de la Cierva-Incorporación” (IJCI-2014-21534). The authors also thank the Electron Microscopy Service at the UPV for support.

Keywords

Mesoporous silica nanoparticles • bisphenol A aptamer • gated nanomaterials • bisphenol A • fluorogenic sensing

References

1. a) R. A. Keri, S.M. Ho, P.A. Hunt, K. E. Knudsen, A. M. Soto, G. S. Prins, *Reprod. Toxicol.*, **2007**, *24*, 240-252; b) L.N. Vandenberg, R. Hauser, M. Marcus, N. Olea, W.V. Welshons, *Reprod. Toxicol.*, **2007**, *24*, 139-177.
2. A.K. Pandey, S.B. Deshpande, *Neuroscience*, **2015**, *289*, 349-357.

3. a) A. Guart, F. Bono-Blay, A. Borrell, S. Lacorte, *Food Addit. Contam.*, **2011**, *28*, 1–10; b) W.F. Smith, Foundations of Materials Science and Engineering, fourth Ed., McGraw-Hill, New York, **2005**; c) A. Ballesteros-Gómez, F.J. Ruiz, S. Rubio, D. Pérez-Bendito, *Anal. Chim. Acta*, **2007**, *603*, 51–59.
4. a) C. Lambert, M. Larroque, *J. Chromatogr. Sci.*, **1997** *35*, 57-62; b) N. Olea, R. Pulgar, P. Perez, F. Olea-Serrano, A. Rivas, A. Novillo-Fertell, V. Pedraza, A. M. Soto, C. Sonnenschein, *Environ. Health Perspect.*, **1996**, *104*, 298-305; c) M. Larroque, L. Vian, A. Blaise, S. Brun, *J. Chromatogr. A*, **1988**, *445*, 107-117; d) H. W. Kuo, W. H. Ding, *J. Chromatogr. A*, **2004**, *1027*, 67-74; e) C. A. Staples, P. B. Dorn, G. M. Klecka, S. O'Block, L. R. Harris, *Chemosphere*, **1998**, *36*, 2149-2173; f) H. Yamasaki, Y. Nagake, H. Makino, *Nephron.*, **2001** *88*, 376-378.
5. a) EU, Commision of the European Communities 90/128/EU, Off. J. Eur. Community, **1990**, L75, 19; b) I. Rykowska, A. Szymański, W. Wasiak, *Chem. Papers*, **2004**, *58*, 382-385.
6. a) F.S. von Saal, B.T. Akingbemi, S.M. Belcher, L.S. Birnbaum, D.A. Crain, M. Eriksen, et al, *Reprod. Toxicol.*, **2007**, *24*, 131-138; b) M. J. Hemmer, B.L. Hemmer, C.J. Bowman, K.J. Kroll, L. C. Folmar, D. Marcovich, M.D. Hoglund, N.D. Denslow, *Environ. Toxicol. Chem.*, **2001**, *20*, 336-343; c) H.B. Patisaul, H.B. Adewale, *Front Behav. Neurosci.*, **2009**, *3*, 1-18; d) K. Moriyama, T. Tagami, T. Akamizu, *J. Clin. Endocrinol. Metab.*, **2002**, *87*, 5185-5190; e) G.R. Boyd, H. Reemtsma, D.A. Grimm, S. Mira, *Sci. Total Environ.*, **2003**, *311*, 135-149.
7. a) Y. Watabe, T. Kondo, M. Morita, N. Tanaka, J. Haginaka, K. Hosoya, *J. Chromatogr. A*, **2004**, *1032*, 45-49; b) Y. Watabe, T. Kondo, H. Imai, N. Tanaka, J. Haginaka, K. Hosoya, *Anal. Sci.*, **2004**, *20*, 133-137; c) S. Rodriquez-Mozaz, M.J. Lopez de Alda, D. Barcelo, *J. Chromatogr. A*, **2004**, *1045*, 85-92; d) P. Paseiro Losada, C. Pérez Lamela, M.F. López Fabal, P. Sanmartín Fenollera, J. Simal Lozano, *J. Agric. Food Chem.*, **1997**, *45*, 3493−3500; e) M. Moeder, S. Schrader, M. Winkler, P. Popp, *J. Chromatogr. A*, **2000**, *873*, 95-106; f) F. Yang, L. Xu, L. Zhu, Y. Zhang, W. Meng, R. Liu, *Environ. Sci. Pollut. Res.*, **2016**, *23*, 10714-10721; g) K.K. Reza, M.A. Ali, S. Srivastava, V.V. Agrawal, A.M. Biradar, *Biosens. Bioelectron.*, **2015**, *74*, 644-651; h) K.S. Kim, .J. Jang, W.S. Choe, P.J. Yoo, *Biosens. Bioelectron.*, **2015**, *71*, 214-221.
8. K.V. Ragavan, N.K. Rastogi, M.S. Thakur, *Trends Anal. Chem.*, **2013**, *52*, 248-260
9. a) R. Wang, L. Xu, Y. Li, *Biosen. Bioelectron.*, **2015**, *67*, 400-407; b) I. Willner, B. Shlyahovsky, M. Zayats, B. Willner, *Chem. Soc. Rev.*, **2008**, *37*, 1153-1165; c) F. Sancenón, Ll. Pascual, M. Oroval, E. Aznar, R. Martínez- Máñez, *ChemOpen*, **2015**, *4*, 418-437.
10. a) J.L. Vivero-Escoto, I.I. Slowing, B.G. Trewyn, V.S.Y. Lin, *Small*, **2010**, *6*, 1952-1967; b) F. Tang, L. Li, D. Chen, *Adv. Mater.*, **2012**, *24*, 1504-1534; c) M. Liong, S. Angelos, E. Choi, K. Patel, J. F. Stoddart, J.I. Zink, *J. Mater. Chem.*, **2009**, *19*, 6251-6257; d) J.E. Lee, N. Lee, H. Kim, J. Kim, S.H. Choi, J.H. Kim, T.Kim, I.C. Song, S.P. Park, W.K. Moon, T. Hyeon, *J. Am. Chem. Soc.*, **2010**, *132*, 552-557; e) H. Song, R. M. Rioux, J. D. Hoefelmeyer, R. Komor, K. Niesz, M. Grass, P. Yang, G. A. Somorjai, *J. Am. Chem. Soc.*, **2006**, *128*, 3027-3037; f) A. Dandapat, D. Jana, G. De, *ACS Appl. Mater. Interfaces*, **2009**, *1*, 833-840.

11. E. Aznar, M. Oroval, Ll. Pascual, J.R. Murguía, R. Martínez-Máñez, F. Sancenón, *Chem. Rev.*, **2016**, *116*, 561-718.
12. a) Ll. Pascual, I. Baroja, E. Aznar, F. Sancenón, M.D. Marcos, J.R. Murguía, P. Amorós, K. Rurack, R. Martínez-Máñez, *Chem. Commun.*, **2015**, *51*, 1414-1416; b) C.H. Lu, B. Willner, I. Willner, *ACS Nano*, **2013**, *7*, 8320-8332; c) E. Climent, R. Martínez-Máñez, F. Sancenón, M.D. Marcos, J. Soto, A. Maquieira, P. Amorós, *Angew. Chem. Int. Ed.*, **2010**, *122*, 7439-7441; d) M. Oroval, E. Climent, C. Coll, R. Eritja, A. Aviñó, M.D. Marcos, F. Sancenón, R. Martínez-Máñez, P. Amorós, *Chem. Commun.*, **2013**, *49*, 5480-5482; e) W. Wang, T. Yan, S. Cui, J. Wan, *Chem. Commun.*, **2012**, *48*, 10228-10230; f) V.C. Özalp, A. Pinto , E. Nikulina, A. Chuvilin, T. Schäfer, *Part. Part. Syst. Charact.*, **2014**, *31*, 161-167.
13. a) F. Xue, J. Wu, H. Chu, Z. Mei, Y. Ye, J. Liu, R. Zhang, C. Peng, L. Zheng, W. Chen, *Microchim. Acta*, **2013**, *180*, 109–115; b) K.V. Ragavan, L.S. Selvakumar, M.S. Thakur, *Chem. Commun.*, **2013**, *49*, 5960-5962; c) Z. Mei, H. Chu, W. Chen, F. Xu, J. Liu, H. Xu, R. Zhang, L. Zheng, *Biosens. Bioelect.*, **2013**, *39*, 26-30; d) D. Zhang, J. Yang, J. Ye, L. Xu, H. Xu, S. Zhan, B. Xia, L. Wang, *Anal. Biochem.*, **2016**, *499*, 51-56; e) J. Xu, Y. Li, J. Bie, W. Jiang, J. Guo, Y. Luo, F. Shen, C. Sun, *Microchim. Acta*, **2015**, *182*, 2131–2138.
14. E. Aznar, C. Coll, M.D. Marcos, R. Martínez-Máñez, F. Sancenón, J. Soto, P. Amorós, J. Cano, E. Ruiz, *Chem. Eur. J.*, **2009**, *15*, 6877-6888.
15. a) S. Brunauer, P.H. Emmett, E. Teller, *J. Am. Chem. Soc.*, **1938**, *60*, 309–319; b) E.P. Barrett, L. G. Joyner, P.P. Halenda, *J. Am. Chem. Soc.*, **1951**, *73*, 373–380.

Chem. Eur. J. 2017, 23,1–5

SUPPORTING INFORMATION

Fluorogenic sensing of carcinogenic bisphenol A using aptamer-capped mesoporous silica nanoparticles

Àngela Ribes, Elena Aznar, Andrea Bernardos, María D. Marcos, Pedro Amorós, Ramón Martínez-Máñez,* and Felix Sancenón

General techniques. Powder X-ray diffraction (PXRD), transmission electron microscopy (TEM), N_2 adsorption-desorption, dynamic light scattering (DLS), Fourier transform infrared spectroscopy (FTIR)**,** thermogravimetric analysis (TGA) and fluorescence spectroscopy were employed to characterize the synthesized materials. PXRD measurements were performed on a D8 Advance diffractometer using Cu Kα radiation (Philips, Amsterdam, The Netherlands). Thermogravimetric analyses were carried out on a TGA/SDTA 851e balance (Mettler Toledo, Columbus, OH, USA), using an oxidizing atmosphere (air, 80 mL min^{-1}) with a heating program: gradient of 393-1273 K at 10°C min^{-1}, followed by an isothermal heating step at 1273°C for 30 min. TEM images were obtained with a 100 kV CM10 microscope (Philips). N_2 adsorption-desorption isotherms were recorded with an ASAP2010 automated adsorption analyser (Micromeritics, Norcross, GA, USA). The samples were degassed at 120°C in vacuum overnight. The specific surface areas were calculated from the adsorption data in the low pressure range using the Brunauer, Emmett and Teller (BET) model.[1] Pore size was determined following the Barret, Joyner and Halenda (BJH) method.[2] Dynamic light scattering was used to obtain the particle size distribution of the different solids, using a Malvern Mastersizer 2000 (Malvern Instruments, Malvern, UK). For the measurements, samples were dispersed in distilled water. Data analysis was based on the Mie theory using refractive indices of 1.33 and 1.45 for the dispersant and mesoporous silica nanoparticles, respectively. An adsorption value of 0.001 was used for all samples. Variation of this adsorption value did not significantly alter the obtained distributions. Measurements were performed in triplicate. FTIR spectra were acquired with a Bruker tensor II Platinum ATR spectrometer. Fluorescence spectroscopy measurements were carried out on a Felix 32 Analysis version 1.2 (Build 56, Photon Technology International, Birmingham, NJ, USA).

Chemicals. The chemicals tetraethylorthosilicate (TEOS), n-cetyltrimethylammonium bromide (CTABr), sodium hydroxide (NaOH), rhodamine B, (3-isocyanatopropyl)triethoxysilane, tris(hydroxymethyl)aminomethane (TRIS),

Bisphenol A (BPA), Bisphenol E (BPE) and Bisphenol C (BPC) were purchased from Sigma-Aldrich Química (Madrid, Spain) and oligonucleotides **O1** (NH_2-$(CH_2)_6$-5'-AAA AAA CCC CCC-3') and **O2** (5'- TTT TGG GGG GCC GGT GGG TGG TCA GGT GGG ATA GCG TTC CGC GTA TGG CCC AGC GCA TCA CGG GTT CGC ACC AGG GGG GTT TT -3') were purchased from Isogen-Lifesciences (Barcelona, Spain). Analytical-grade solvents were from Scharlab (Barcelona, Spain). All products were used as received.

Buffer solutions. Hybridization buffer consisting in 20 mM Tris-HCl, 37.5 mM $MgCl_2$ (pH 7.5) was used for controlled release experiences.

Synthesis of mesoporous silica nanoparticles (MSNs). n-cetyltrimethylammoniumbromide (CTABr, 1.00 g, 2.74 mmol) was first dissolved in 480 mL of deionized water. Then a 3.5 mL of NaOH 2.00 M in deionized water was added to the CTABr solution, followed by adjusting the solution temperature to 80°C. TEOS (5 mL, 25.7 mmol) was then added dropwise to the surfactant solution. The mixture was allowed stirred for 2 h to give a white precipitate. Finally, the solid was centrifuged, washed with deionized water and dried at 60°C (MSNs as-synthesized). To prepare the final mesoporous material, the as-synthesized solid was calcined at 550°C using oxidant atmosphere for 5 h in order to remove the template phase.

Synthesis of S1. In a typical synthesis, calcined MSNs (200 mg) and rhodamine B (766.40 mg, 0.16 mmol) were suspended in CH_3CN (10 mL). The suspension was stirred at room temperature for 24 h. Then an excess of (3-isocyanatopropyl)triethoxysilane (247.60 µl , 1.00 mmol) was added to the suspension and the final mixture was stirred at room temperature during 5.5 h. The resulting solid (**S1**) was isolated by filtration, washed with CH_3CN (5 mL) and dried at 38°C for 18 h.

Synthesis of S2. 100 µL of oligonucleotide **O1** (10 µM) were added to a suspension containing of 1 mg of solid **S1**, 700 µL of CH_3CN and rhodamine B (1

mM). The resulting material was isolated by filtration, washed with hybridization buffer to eliminate residual dye and free oligonucleotide and dried at vacuum.

Synthesis of S3. 100 μg of solid **S2** were suspended in 190 μL of hybridization buffer and 5 μL of **O2** (100 μM) was added to the reaction. The mixture was stirred 2 h at room temperature. The resulting material was isolated by filtration, washed with hybridization buffer to eliminate residual dye and free oligonucleotide and dried at vacuum.

Characterization of the prepared materials. The MSNs and **S1**, **S2** and **S3** were characterized following standard techniques including: PXRD, TEM, N_2 adsorption-desorption analysis, DLS, FTIR and TGA. PXRD pattern of as synthesized MSNs (Fig. 1, curve a) showed four low-angle reflections typical of a hexagonal array, indexed as (100), (110), (200), and (210) Bragg peaks. A significant displacement of 3Å of the (100) peak in the PXRD pattern of the calcined MSNs was evident in curve b, and related to further condensation of silanol groups during the calcination step. Curve c corresponds to the **S1** XRD pattern. A decrease in intensity of the (100) peak and a broadening of the (110) and (200) reflections was observed and related to a loss of contrast due to the filling of the pore voids with the rhodamine B dye. The XRD pattern to the final solid **S2** is shown in curve d. Mesoporosity is observed in the powder X-Ray pattern of **S1** where the mesoporous characteristic (100) peak diffraction was present, indicating that the loading process with dye and the further functionalization with (3-isocyanatopropyl)triethoxysilane did not damage the mesoporous scaffolding. Moreover mesoporosity was neither affected in solids **S2** and **S3**.

The N_2 adsorption–desorption isotherms of the calcined MSNs type nanoparticles show an adsorption step at an intermediate P/P_0 value (0.1–0.5) typical of this type of solid (see Fig. S1 a). This step can be related to the nitrogen condensation inside the mesoporous by capillarity. The absence of a hysteresis loop in this interval and the narrow BJH pore suggested the existence of uniform cylindrical mesopores with a total pore volume of 0.84 $cm^3\ g^{-1}$ calculated by using the BJH model on the adsorption branch of the isotherm. The application of the

BET model resulted in a value for the total specific surface of 1027.54 $m^2 g^{-1}$. From the XRD, porosimetry, and TEM studies a pore diameter of 2.69 nm was determined. In addition to this adsorption step associated to the micelle generated mesopores, a second feature appeared in the isotherm at a high relative pressure (P/P_0>0.8). This adsorption corresponds to the filling of the large voids among the particles, presents a volume of 0.26 $cm^3 g^{-1}$ and a main pore diameter of 43.57 (calculated by using BJH model) and must be considered as a textural-like porosity. In this case, the curves show a characteristic H1 hysteresis loop and a wide pore size distribution.

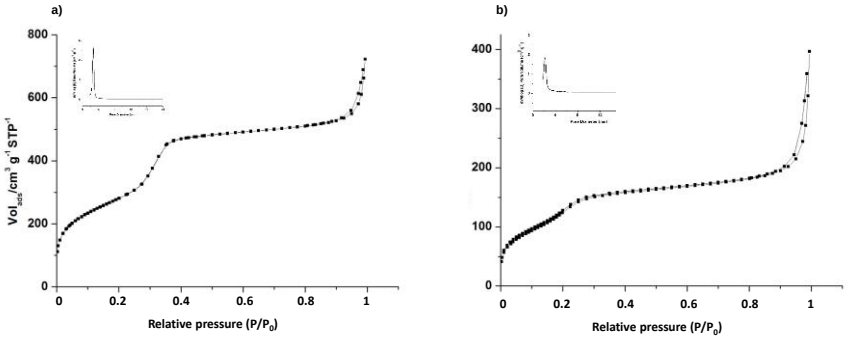

Figure S1. Nitrogen adsorption-desorption isotherms for (a) MSNs type nanoparticles and (b) **S1**. Inset: (a) pore size distribution of MSNs and (b) **S1**.

The N_2 adsorption–desorption isotherm of **S1** (see Fig. S1 b) was typical of mesoporous systems with filled mesopores, and a significant decrease in the N_2 volume adsorbed (0.31 $cm^3 g^{-1}$) and surface area (465.5 $m^2 g^{-1}$) were observed. The most relevant feature was the decrease of a sharp step at low-medium relative pressure ($0.1 < P/P_0 < 0.4$). In addition to this adsorption step associated to the micelle generated mesopores, a second feature appeared in the isotherm at a high relative pressure ($P/P_0 > 0.8$). This adsorption corresponds to the filling of the large voids among the particles, presents a volume of 0.24 $cm^3 g^{-1}$ and a main pore diameter of 44.61 (calculated by using BJH model). Parameters calculated from N_2 adsorption-desorption isotherms of calcined MSNs and solid **S1** are listed in Table S1.

Table S1. BJH specific surface values, pore volumes and pores sizes calculated from N2 adsorption-desorption isotherms for calcined MSN and S1.

	S_{BET} ($m^2\ g^{-1}$)	Pore volume ($P/P_0<0.8$)[a] ($cm^3\ g^{-1}$)	BJH pore size ($P/P_0<0.8$)[b] (nm)	Pore volume ($P/P_0>0.8$)[c] ($cm^3\ g^{-1}$)	BJH pore size ($P/P_0>0.8$)[d] (nm)
MSNs	1027.54	0.84	2.69	0.26	43.57
S1	465.55	0.31	2.43	0.24	44.61

[a]Pore size estimated by using the BJH model applied on the adsorption branch of the isotherm, for P/P0 < 0.8, which can be associated with the surfactant generated mesopores. [b]Pore size estimated by using the BJH model applied on the adsorption branch of the isotherm, for P/P0 < 0.8, which can be associated with the textural porosity. [c]Pore volume for P/P0 > 0.8, which can be associated with the surfactant generated mesopores. [d]Pore volume for P/P0 > 0.8, which can be associated with the textural porosity.

Moreover, the size of calcined MSNs, **S1, S2** and **S3** was measured by dynamic light scattering (DLS) (see Fig. S2 and Table S2). This technique was used to compare the size of the different solids and how the presence of DNA strands affected to the size of the nanoparticles. An increase in particle size from 106±3 nm for MCM-41 to 190±3 nm for **S3** was observed (values of 142±1 and 164±2 nm were found for **S1** and **S2**, respectively) due to the functionalization with the capping oligonucleotides.

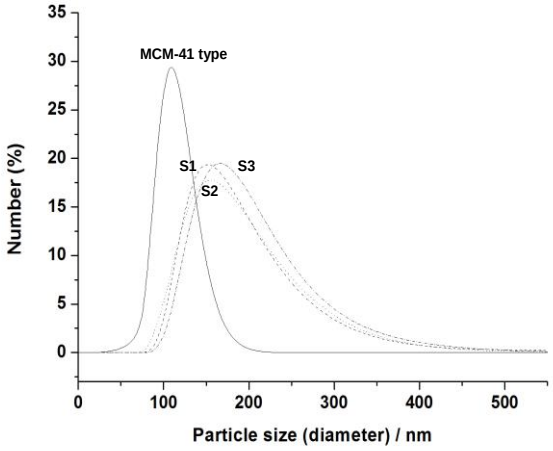

Figure S2. Size distribution by number of particles obtained by DLS studies for calcined MCM-41, **S1**, **S2** and **S3**.

Table S2. Diameter of calcined MSNs, **S1**, **S2** and **S3** measured by DLS.

	Particle diameter (nm)
MCM-41 type	106±3
S1	142±1
S2	153±2
S3	164±3

The presence of the DNA onto the surface nanoparticles was confirmed by FTIR spectroscopy. Fig. S3 and table S3 show the characteristic peaks of the synthesized materials. The appearance of a peak around 1560 cm^{-1}, which is characteristic of acylamide vibration, was found in solid **S3**. Besides peaks at 740 cm^{-1}, attributed to stretching vibrations of N=H in the thymine base, and at 1492, ≈1300 and 1294 cm^{-1} corresponding to C=N bond stretching and in plane vibration from guanine and cytosine groups,[4] were also observed in **S3**.

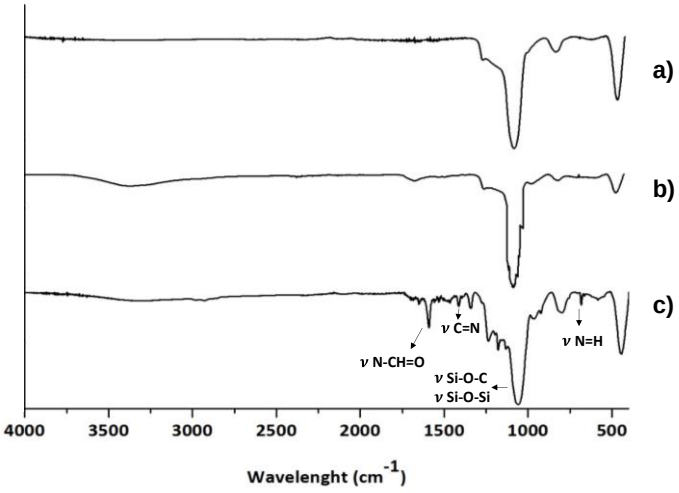

Figure S3. FTIR spectra of the (a) calcined MSNS, (b) **S1** and (c) **S3**.

Table S3. Characteristic peaks of the synthesized solids.

Assignment	**Frequencies (wavelength in cm^{-1})**	**Comment**
Acylamide group	1560	N-CH=O vibration
Thymine	740	N=H vibration
Guanine and Cytosine	1492, ≈1300, 1294	C=N bond stretching and plane vibration

Release experiments of solid S3. 100 µg of **S3** were suspended in 400 µL of the hybridization buffer and separated in 2 aliquots of 200 µL. Both samples were filled to a volume of 995 µL with hybridization buffer. Then, 5 µL of the BPA solution in milliQ water (2 mM) was added to one of the **S3** suspensions. Simultaneously, 5 µL of water (milliQ grade) were added to the remaining aliquot. Both suspensions were stirred at 25°C for 60 min. Aliquots of 120 µL were taken at scheduled times and centrifuged 2 min at 12000 rpm (in order to remove the solid) and the fluorescence of the rhodamine B released measured at 575 nm (λ_{exc} = 555 nm).

Sensitivity of S3 solid with BPA. 1 mg of solid **S3** was suspended with 1 mL of hybridization buffer and separated in 10 aliquots of 100 µL. Different amounts of BPA standard solution were added to each aliquots and filled to final volume of 1000 µL with the hybridization buffer. All samples were stirred at 25°C for 30 min, and then centrifuged 2 min at 12000 rpm in order to remove the solid. The fluorescence of the released rhodamine B was then measured at 575 nm (λ_{exc} = 555 nm). A limit of detection (LOD) of 3.5 µM was calculated based in the intersection point of the two slopes (see Fig. 3).

Amplification study. To study signal amplification features of probe **S3**, 100 µg of **S3** were suspended in 400 µL of the hybridization buffer and separated in 2 aliquots of 200 µL. Both samples were filled to a volume of 995 µL with hybridization buffer. Then, 5 µL of the BPA solution (2 mM) was added to one of the **S3** suspensions. Simultaneously 5 µL of water (milliQ grade) were added to the remaining aliquot. Both suspensions were stirred at 25°C for 30 min and an aliquot was taken and centrifuged 2 min at 12000 rpm (in order to remove the solid) and the fluorescence of the rhodamine B released measured at 575 nm (λ_{exc} = 555 nm). Calibration curve of rhodamine B as a function of fluorescence was obtained (see Fig. S4). The signal amplification was evident from a comparison between BPA concentration added and rhodamine B concentration calculated.

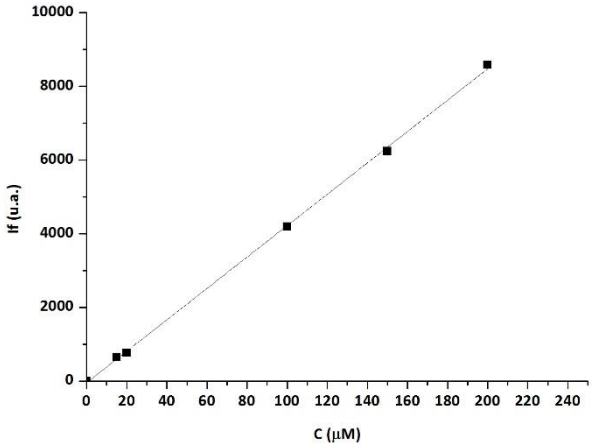

Figure S4. Calibration curve of rhodamine B.

Selectivity studies with S3. 200 μg of **S3** were suspended in 400 μL of hybridization buffer and separated in 4 aliquots of 100 μL each one. The **S3** suspensions were spiked with 2 mM solutions of BPA (5 μL), BPC (5 μL) and BPE (5 μL). One fraction was treated as control to which 5 μL of water were added. In all cases volume was completed to 1 mL with hybridization buffer. All samples were stirred at 25°C for 30 min, and after that, samples were centrifuged 2 min at 12000 rpm in order to remove the solid. The fluorescence of the released rhodamine B was then measured at 575 nm (λ_{exc} = 555 nm).

Real sample determination. A standard addition method was followed to minimize possible matrix effects present in real samples.[5] In order to evaluate the possible use of our material for detection in realistic environments, solid **S3** was added to different aliquots containing 100 μL of tap water spiked with BPA (262 μM). Then, different known amounts of BPA were added (the volume was completed to 1 mL with hybridization buffer) to obtain final additional BPA concentrations of 0, 6.55, 13.1, 65.5 and 131 μM. After 30 min at 25°C, the emission of the rhodamine B released from solid **S3** in the different aliquots was

measured and a curve that follows the linear equation $y = 8x10^6 x + 204460$ was obtained (see Fig. S5). From the intercept of the curve with the x-axis a concentration of BPA in the spiked sample of 255 µM was determined (97 % recovery).

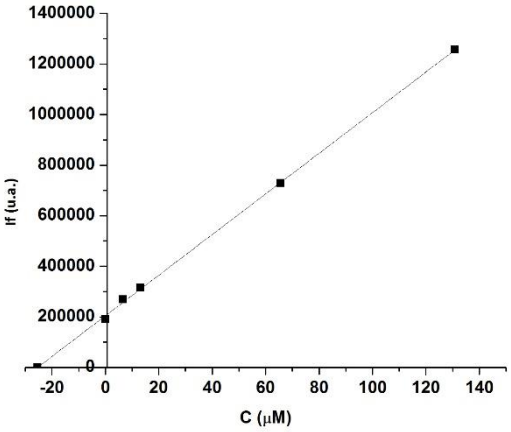

Figure S5. Release of rhodamine B from solid **S3** at different concentrations of BPA by addition standard method.

References

1. E.P. Barrett, L.G. Joyner, P.P. Halenda, *J. Am. Chem. Soc*., **1951**, *73*, 373–380.
2. S. Brunauer, P.H. Emmett, E. Teller, *J. Am. Chem. Soc.,* **1938**, *60*, 309–319.
3. C. Chen, F. Pu, Z. Huang, Z. Liu, J. Ren and X. Qu, *Nucleic Acids Res*., **2011**, *39*, 1638-1644.
4. M.L.S. Mello and B.C. Vidal, *Plos One*, **2012**, *7*, e43169.
5. J.V. Ros-Lis, B. García, D. Jiménez, R. Martínez-Máñez, F. Sancenón, J. Soto, F. Gonzalvo and M.C. Valldecabres, *J.Am.Chem. Soc.*, **2004**, *126*, 4064-4066.

4. Two new fluorogenic aptasensors to detect Ochratoxin A based on capped mesoporous silica nanoparticles

Two new fluorogenic aptasensors to detect Ochratoxin A based on capped mesoporous silica nanoparticles

Àngela Ribes,[a,b,c] Sara Santiago-Felipe,[b,a,c] Andrea Bernardos,[a,b,d] M. Dolores Marcos,[a,b,c,d] Teresa Pardo, [a,b,c,d] Félix Sancenón,[a,b,c,d] Ramón Martínez-Máñez,, [a,b,c,d] and Elena Aznar [b,a,c,d]*

[a] *Instituto Interuniversitario de Investigación de Reconocimiento Molecular y Desarrollo Tecnológico,*
Universitat Politècnica de València, Universitat de València,
Camino de Vera s/n, 46022 Valencia, Spain
E-mail: rmaez@qim.upv.es

[b] *CIBER de Bioingeniería, Biomateriales y Nanomedicina (CIBER-BBN).*

[c] *Unidad Mixta de Investigación en Nanomedicina y Sensores.*
Universitat Politècnica de València, Instituto de Investigación Sanitaria La Fe

[d] *Unidad Mixta UPV-CIPF de Investigación en Mecanismos de Enfermedades y Nanomedicina,*
Universitat Politècnica de València, Centro de Investigación Príncipe Felipe
Valencia, Spain.

Received: May 29, 2017
First published on the web: August 2, 2017

ChemistryOpen, **2017**, *6*, 653–659

Abstract

Aptamers have been used as recognition elements for several molecules due to their great affinity and selectivity. On the other hand, mesoporous nanomaterials have demonstrated great potential for sensing applications. Based in these concepts, we report herein the use of two aptamer-capped mesoporous silica materials for the selective detection of Ochratoxin A (OTA). A specific aptamer for OTA was used to block the pores of rhodamine B-loaded mesoporous silica nanoparticles. Two solids were prepared in which the aptamer capped the porous scaffolds using a covalent or electrostatic approach. Whereas the prepared materials remained capped in water, dye delivery was selectively observed in the presence of OTA. The protocol showed excellent analytical performance in terms of sensitivity (LOD: 0.5-0.05 nM), reproducibility and selectivity. Moreover, the aptasensors were tested for OTA detection in commercially foodstuff matrices, demonstrating their potential applicability in real samples.

Introduction

Mycotoxines are metabolites produced by fungi species that are capable of causing disease and death in both humans and animals. They appear when food and feedstuff are stored or processed under favorable environmental conditions for fungi proliferation. Most common mycotoxins are, ochratoxins, aflatoxins, fumonisins, trichothecenes and zearalenone (Scheme 1).[1] Among them, Ochratoxin A (OTA), produced by Aspergillus and Penecillium strains, has been labeled as a carcinogen and nephrotoxin agent, and is the most predominant contaminant in a wide variety of food commodities such as cereals,[2,3] beverages and dried fruits.[4] The European Commission's Scientific Committee on Food has stablished the maximum permitted contents of OTA in 5 μg/kg for raw cereal grains, 3 μg/kg for all cereal-derived products and 10 μg/kg for soluble coffee.[5] A number of different techniques have been developed in the last years for the detection of OTA, most of them based on gas chromatography/mass spectrometry (GC/MS)[6] and liquid chromatography (HPLC).[7,8] However, while these methods can correctly determine the presence of OTA, they require

expensive equipment and complicated operator training.[9-11] In this scenario, the design of simple, yet selective and sensitive probes for the detection of this carcinogen agent is a field of interest.

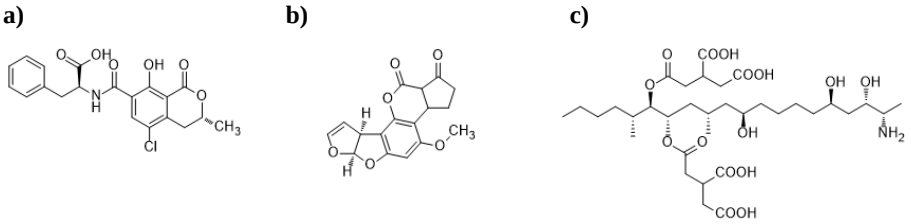

Scheme 1. Chemical structures of the most common micotoxines a) Ochratoxin A, b) Aflatoxin B1, c) Fumonisin B.

From another point of view, nanomaterials for sensing applications have played a great role in the last years due to their capacity to provide rapid, simple and sensitive responses to target analytes.[12-15] Moreover, among nanomaterials used in sensing protocols, mesoporous silica nanoparticles (MSNs) have been widely employed due to some of their remarkable properties such as large load capacity and the possibility to easily modify their surface by means of several groups due to the presence of silanol groups (Si-OH) which have an excellent reactivity.[16-24] Moreover, MSNs can be functionalized with different (bio)molecules than can act as "molecular gates", to obtain hybrid gated organic-inorganic capped supports for the design of systems able to release an entrapped payload upon the application of specific stimuli.[25] These gated supports have been widely used in the design of drug delivery carriers and to a lesser extent in sensing protocols.[26-30]

Additionally, the development of sensing materials using aptamers as potential systems able to detect trace amounts of target substances has also attracted attention of research community.[31-36] Aptamers are stable DNA sequences with high affinity and selectivity for target biomolecules, small neutral molecules or ions, and their use in the design of several sensors and probes has resulted in the development of highly sensitive systems for different analytes.[37-40] Recently, some aptasensors to determine OTA have been described.[41] However, as far as we

know, the use of aptamer-based gated materials using MSNs for the fluorogenic detection of OTA has not yet been reported.

Based in these ideas we report herein the development of two new gated materials based on MSNs loaded with a fluorophore (rhodamine B) and capped with an aptamer selective to OTA. It was also in our aim to study different modes in which the aptamer can be used as cap and its effect on the performance of the aptasensors. The materials were fully characterized and used for the selective and sensitive detection of OTA in spiked wheat samples.

Results and Discussion

Preparation and characterization of the sensing support. For the preparation of the sensing materials two different approaches have been followed involving two different methods to cap the pores with the OTA aptamer (**Scheme 2**). In both cases MSNs of ca. 100 nm were selected as inorganic scaffolds and pores were loaded with a fluorophore (rhodamine B).

In the first approach (hereinafter referred to as covalent approach) (Scheme 2A), the external surface of the MSNs was functionalized with (3-isocyanatopropyl)triethoxysilane yielding solid **S1**. In a subsequent step, a short DNA sequence, functionalized with an aminohexyl moiety at the 5'-end position (i.e. NH_2-$(CH_2)_6$-5'-AAA AAA CCC CCC-3', **O1**) was covalently attached to **S1** via the formation of urea bonds resulting in solid **S2**. Then, a single stranded oligonucleotide (i.e. 5'- TTT TGG GGG GGC ATC TGA TCG GGT GTG GGT GGC GTA AAG GGG GGG GTT TT-3', **O2**) which contains the specific sequence of the OTA aptamer was hybridized to the attached **O1**, obtaining the final capped solid **S3**. In the second approach (hereinafter referred to as electrostatic approach) (Scheme 2B) MSNs were functionalized with (3-aminopropyl)triethoxysilane to yield solid **S4**. Aminopropyl moieties are partially charged at a neutral pH and are known to display electrostatic interactions with the negatively charged aptamers. Based on this, addition of **O2** to suspensions of solid **S4** yielded the gated probe **S5**.

Starting MSNs, **S1**, **S2**, **S3**, **S4** and **S5** were characterized following standard techniques, including powder X-ray diffraction (PXRD), transmission electron

microscopy (TEM), N_2 adsorption–desorption isotherms, thermogravimetric analysis (TGA), dynamic light scattering (DLS) and Fourier transform infrared spectroscopy (FTIR).

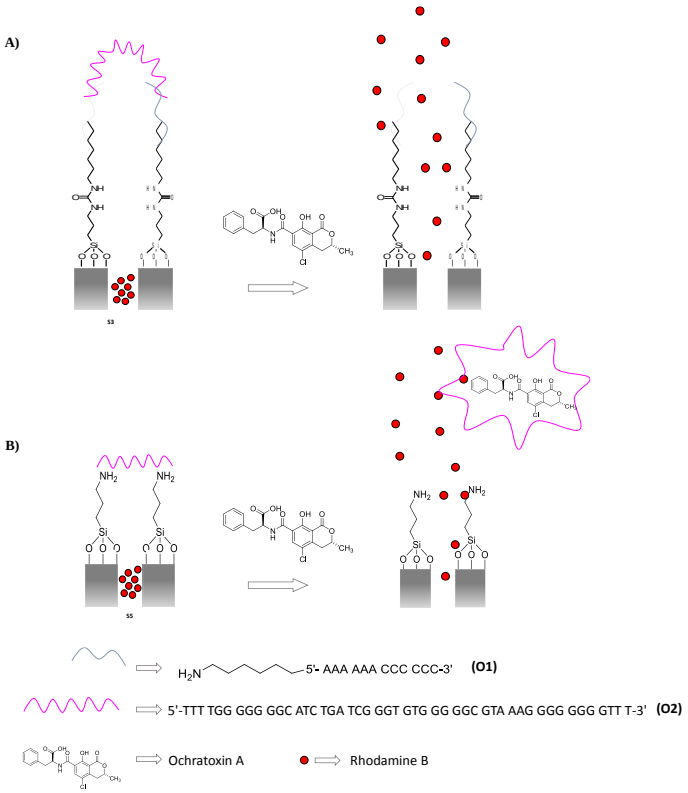

Scheme 2. Performance of gated materials A) **S3** capped with an aptamer in covalent approach and B) **S5** capped with an aptamer in electrostatic approach. Dye (rhodamine B) delivery entrapped in **S3** and **S5** is selectively accomplished in the presence of OTA.

PXRD pattern of the as-synthesised MSNs (**Figure 1,** curve a) showed four low-angle reflections typical of a hexagonal array, indexed as (100), (110), (200), and (210) Bragg peaks. A significant displacement of the (100) peak in the PXRD pattern of the calcined MSNs was evident in curve b, related to a cell contraction (5Å) due to the condensation of silanol groups during calcination. Curves c-f correspond to the XRD pattern of **S1**, **S3**, **S4** and **S5**. A decrease in the intensity of the (100) peak and a broadening of the (110) and (200) reflections was observed,

related to a loss of contrast due to both filling the solid with the dye and capping of the pores. Moreover, the presence of the mesoporous structure in calcined MSNs and final functionalized solids was confirmed by TEM analysis, in which the typical channels of a mesoporous silica matrix were clearly visualized (**Figure 1h** and **1i**).

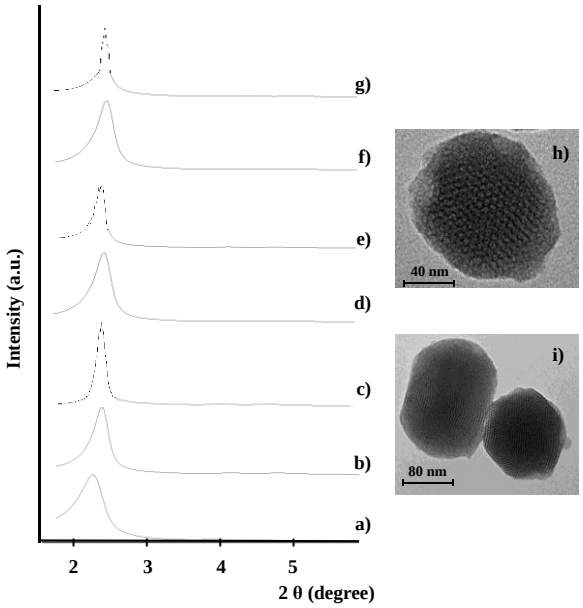

Figure 1. Powder X-ray diffraction patterns of the (a) as made MSNs, (b) calcined MSNs, (c) solid **S1** (d) solid **S2**, (e) solid **S3**, (f) solid **S4** and (g) solid **S5.** Inset: TEM images of (h) calcined MSNs and (i) **S3**.

In addition, mesoporosity was analyzed by N_2 adsorption–desorption isotherms. For the starting calcined MSNs a value of BET specific surface of 908.6 $m^2\ g^{-1}$ was obtained, while for **S1** and **S4** a decrease of the specific surface was observed and BET values of 112.7 $m^2\ g^{-1}$ and 414.7 $m^2\ g^{-1}$ for **S1** and **S4** were found, respectively (see Figure S1 and Table S1 in the Supporting Information). This is in agreement with the presence of the rhodamine B dye inside the pores and surface functionalization. Moreover, the content of 3-isocyanatopropyl and 3-aminopropyl moieties, rhodamine B, **O1** and **O2** in the different prepared solids

was calculated from thermogravimetric data (Table 1). Taking into account that the typical external surface of MSNs is 70 m^2/g an estimate capping density of 0.0029 mmol **O2**/m^2 and 0.0014 mmol **O2**/m^2 was calculated for solids **S3** and **S5**, respectively. The size of the nanoparticles was determined by dynamic light scattering (DLS) studies. Diameters of 152, 162, 194, 379, 164 and 190 nm were found for starting calcined MSNs, **S1**, **S2**, **S3**, **S4** and **S5**, respectively (see Figure S2 and Table S2 in the Supporting Information). Moreover, the presence of the DNA in the prepared nanoparticles was confirmed by FTIR spectroscopy (see Figure S3 and Table S3).

Table 1. Contents (in mmol mg^{-1}) of 3-isocyanatopropyl, 3-aminopropyl, rhodamine B, **O1** and **O2** in the different prepared solids

	Rhodamine B	3-isocyanatopropyl	3-aminopropyl	**O1**	**O2**
S1	0.024	0.024	-	-	-
S2	0.011	0.024	-	0.00009	-
S3	0.003	0.024	-	0.00009	0.0002
S4	0.003	-	0.020	-	-
S5	0.0008	-	0.020		0.0001

Release experiments. **Figure 2A** shows the delivery kinetics profile of the dye from solid **S3** (covalent approach). In the absence of OTA (curve a), a poor rhodamine B release was observed, indicating tight pore closure, however payload delivery was clearly found when OTA was added to the solution (curve b). Dye delivery was attributed to the displacement of the aptamer **O2** induced when OTA was present in the solution due to aptamer-OTA binding (Scheme 2). A similar selective delivery in the presence of OTA was observed for solid **S5** (electrostatic approach). As depicted in **Figure 2**, dye delivery from solid **S3** reached 80% of the total amount of dye delivered at 10 minutes (Figure 2A), whereas at the same time a payload delivery of ca. 60% was found from solid **S5** (Figure 2B). This difference in release rate should be ascribed to the different method used to cap solids **S3** and **S5** (*vide ante*).

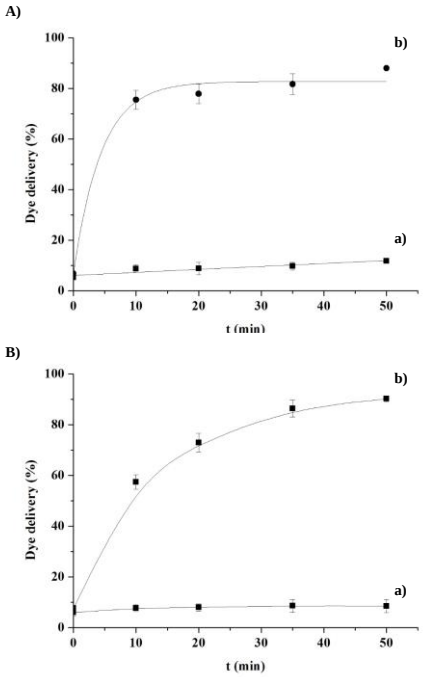

Figure 2. Release profile of rhodamine B from solid **S3** (A) and solid **S5** (B) in the absence (a) and in the presence (b) of OTA (5 μM) in hybridization buffer.

Sensitivity and selectivity studies. To assess the sensitivity of the method, the response of **S3** and **S5** to different concentrations of OTA was studied. It was found that delivered rhodamine B was proportional to OTA concentration, which is in agreement with the uncapping protocol detailed above. A limit of detection (LOD) of 0.5 nM was determined for **S3** (see Figure S4A), whereas for solid **S5**, a LOD as low as 0.05 nM was found (see Figure S4B). This difference in LOD is tentatively attributed to a weaker interaction of the aptamer **O2** to the silica surface in the electrostatic approach (solid **S5**) when compared to the covalent approach (solid **S3**). This weaker attachment of the aptamer to the surface favors the aptamer-OTA interaction, the displacement of the aptamer and cargo delivery. Nevertheless, both LOD comply with those established by the legislation

and are similar or better than most published techniques for the detection of OTA (see Table S4).[45-57]

Additionally, the selectivity of **S3** (Figure 3 in black) and **S5** (Figure 3 in grey) to OTA was also studied. With this aim, cargo release from **S3** and **S5** was tested in presence of OTA, Fumonisin B1 and Aflatoxin B1. As shown in **Figure 3**, OTA was the only mycotoxin able to induce a notable dye delivery, whereas Fumonisin B1 and Aflatoxin induced negligible pore opening and poor payload release. This observation corroborates the selective OTA-aptamer interaction as mechanism of the observed optical response.

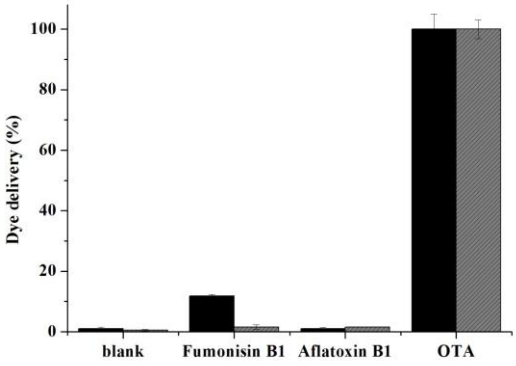

Figure 3. Release of rhodamine B from solid **S3** (in black) and **S5** (in grey) in the presence of OTA, Aflatoxin B1 and Fumonisin B1.

OTA detection in realistic samples. Encouraged by these results, the potential use of **S3** to detect OTA in more competitive realistic samples was studied. With this aim, the detection of OTA in wheat samples was evaluated, using an addition standard method. After OTA extraction, aliquots of 100 µL were spiked with different known amounts of a standard OTA solution (0, 10, 15, 20, 30, 50, 75 nM). In a following step 100 µg of solid **S3** were added to each fraction and completed to a final volume of 1000 µL with hybridization buffer. After 30 min at 25°C, the emission of the rhodamine B released from solid **S3** in the different

aliquots was measured and a curve that follows the linear equation y = 81.791x + 24870 was obtained (see Figure S5A). From the intercept of the curve with the x-axis a concentration of OTA in the spiked sample of 372 nM was determined (93.05 % recovery). A similar procedure was followed using solid **S5**. In this case a recovery of 96.28 % was calculated (see Figure S5B). Utilization of the proposed aptasensor for quantitative determination of OTA may provide a simple approach in food safety applications through the use of this simple, rapid and sensitive assay. Moreover, as a preliminary study towards possible simple in situ application, we have confirmed that **S3** and **S5** materials can be stored for weeks and then used without changing their sensing features.

Conclusions

In summary, we have developed two new fluorogenic aptasensors for the detection of OTA by using MSNs loaded with a dye and capped with an OTA-selective aptamer. Two approaches, based on an electrostatic or covalent protocol, were used to cap the pores. The response of both probes is related with the interaction between the capping aptamer and OTA, which induced a displacement of the aptamer from the solid, pore opening and dye release. Although solid **S3** displayed dye delivery in a shorter time than **S5**, a lower LOD was observed for the latter. Specifically, a LOD as low as 0.5 nM for **S3** and 0.05 for **S5** were calculated. In addition, the capped nanomaterial allowed an accurate determination of OTA in realistic wheat samples. As far as we know, this is the first time that aptamer-capped mesoporous supports have been developed for the detection of OTA mycotoxine. Moreover, the method is simple, portable, can be easily tunable via the use of different reporting molecules (e.g. dyes, fluorophores or electroactive species) and may allow the development of simple test for the detection of OTA in food samples.

Experimental Section

General Techniques. Powder X-ray diffraction (PXRD), transmission electron microscopy (TEM), N_2 adsorption-desorption, thermogravimetric analysis (TGA), dynamic light scattering (DLS), Fourier transform infrared spectroscopy (FTIR) and fluorescence spectroscopy were employed to characterize the synthesized materials. PXRD measurements were performed on a D8 Advance diffractometer using Cu Kα radiation (Philips, Amsterdam, The Netherlands). Thermogravimetric analyses were carried out on a TGA/SDTA 851e balance (Mettler Toledo, Columbus, OH, USA), using a oxidizing atmosphere (air, 80 mL min^{-1}) with a heating program, which consist of a gradient of 393-1273 K at 10°C min^{-1}, followed by an isothermal heating step at 1273°C for 30 min. TEM images were obtained with a 100 kV CM10 microscope (Philips). N_2 adsorption-desorption isotherms were recorded with an ASAP2010 automated adsorption analyzer (Micromeritics, Norcross, GA, USA). The samples were degassed at 120°C in vacuum overnight. The specific surface areas were calculated from the adsorption data in the low pressure range using the Brunauer, Emmett and Teller (BET) model.[42] Pore size was determined following the Barret, Joyner and Halenda (BJH) method.[43] Dynamic light scattering was used to obtain the particle size distribution of the different solids, using a Zetasizer Nano (Malvern Instruments, Malvern, UK). For the measurements, samples were dispersed in distilled water. Data analysis was based on the Mie theory using refractive indexes of 1.33 and 1.45 for the dispersant and mesoporous silica nanoparticles, respectively. An adsorption value of 0.001 was used for all samples. Variation of this adsorption value did not significantly alter the obtained distributions. Measurements were performed in triplicate. FTIR spectra were acquired with a Bruker tensor II Platinum ATR spectrometer. Fluorescence spectroscopy measurements were carried out on a Felix 32 Analysis version 1.2 (Build 56, Photon Technology International, Birmingham, NJ, USA)

Compounds. Tetraethylorthosilicate (TEOS), n-cetyltrimethylammonium bromide (CTABr), sodium hydroxide (NaOH), triethylamine (TEA), (3-isocyanatopropyl)triethoxysilane, (3-aminopropyl)triethoxysilane, rhodamine B,

tris(hydroxymethyl)aminomethane (TRIS), hydrochloric acid, Ochratoxin A, Fumonisin B1 and Aflatoxin B1 were purchased from Sigma-Aldrich Química (Madrid, Spain). Oligonucleotides **O1** (NH_2-$(CH_2)_6$-5'-AAA AAA CCC CCC-3') and **O2** (5'- TTT TGG GGG GGC ATC TGA TCG GGT GTG GGT GGC GTA AAG GGG GGG GTT TT-3') were purchased from Isogen-Lifesciences (Barcelona, Spain). All products were used as received.

Synthesis of mesoporous silica nanoparticles (MSNs). CTABr (1.00 g, 2.74 mmol) was first dissolved in 480 mL of deionized water. Then, 3.5 mL of NaOH 2.00 M in deionized water was added, followed by adjusting the solution temperature to 80°C. TEOS (5 mL, 25.7 mmol) was then added dropwise to the CTABr solution. The mixture was stirred for 2 h to give a white precipitate. Finally the solid product was centrifuged, washed with deionized water and dried at 60°C (as-synthesized MSNs). To prepare the final starting material the as-synthesized solid was calcined at 550°C using an oxidant atmosphere for 5 h in order to remove the template phase (calcined MSNs).

Synthesis of S1. Calcined MSNs (200 mg) and rhodamine B (766.4 mg, 0.16 mmol) were suspended in CH_3CN (10 mL). The suspension was stirred at room temperature for 24 h. Then (3-isocyanatopropyl)triethoxysilane (247.6 µL, 1.0 mmol) was added, and the final mixture was stirred at room temperature for 5.5 h. The resulting pink solid (S1) was isolated by filtration, washed with CH_3CN (5 mL) and dried at 38°C for 18 h.

Synthesis of S2. 100 µL of oligonucleotide **O1** (10 µM) were added to a suspension containing 1 mg of solid **S1**, 700 µL of CH_3CN with rhodamine B (1 mM) and 2 µL of TEA. The mixture was stirred for 3 h. The resulting material was isolated by centrifugation, washed with hybridization buffer to eliminate residual dye and free oligonucleotide, and dried at vacuum.

Synthesis of S3. 100 µg of solid **S2** were suspended in 297.5 µL of hybridization buffer and 2.5 µL of **O2** (100 µM) was added to the reaction. The mixture was

stirred 2 h at room temperature. The resulting material was isolated by centrifugation, washed with hybridization buffer and dried at vacuum.

Synthesis of S4. Calcined MSNs (200 mg) and rhodamine B (766.4 mg, 0.16 mmol) were suspended in CH_3CN (10 mL). The suspension was stirred at room temperature for 24 h. Then an excess of (3-aminopropyl)triethoxysilane (292.5 µL, 1 mmol) was added, and the final mixture was stirred at room temperature for 5.5 h. The resulting pink solid (**S4**) was isolated by filtration, washed with CH_3CN (5 mL) and dried at 38°C for 18 h.

***Synthesis of S5*.** 500 µg of solid **S4** were suspended in 495 µL of hybridization buffer and 5 µL of **O2** (100 µM) was added to the reaction. The mixture was stirred 30 minutes at 37°C. The resulting material was isolated by centrifugation, washed with hybridization buffer and dried at vacuum.

Assay protocol. The response of solids **S3** and **S5** was tested in the presence of OTA by measuring the emission of rhodamine B delivered from the capped materials. For solid **S3**: 100 µg of the material were suspended with 400 µL of hybridization buffer (20 mM Tris-HCl, 37.5 $MgCl_2$, pH 7.5) and separated in 2 aliquots of 200 µL. Then, 10 µL of an aqueous solution of OTA 500 µM was added to one of the aliquots whereas 10 µL of water were added to the other. In both cases, volume was completed to 1000 µL with hybridization buffer. Suspensions were maintained at 25°C and at certain times fractions were taken and centrifuged to separate the solid. For solid **S5**, 500 µg of the material were suspended with 1000 µL of hybridization buffer and separated in 2 aliquots of 500 µL. Next steps were the same as solid **S3** described above, but maintaining the suspensions at 37°C. Cargo release from the solids was measured by the rhodamine B fluorescence in the supernatants at 585 nm (λ_{exc} = 555 nm).

Calibration curve. For solid **S3**: 1 mg of the material was suspended in 1000 µL of hybridization buffer and separated into 10 aliquots of 100 µL. Different amounts of OTA standard solution were added to each aliquot and the volume

was completed to 1000 µL with hybridization buffer. All samples were stirred at 25°C for 30 min, and then centrifuged 2 min at 12000 rpm to separate the solid. Finally, fluorescence of the released rhodamine B was measured in the supernatants at 575 nm (λ_{exc} 555 nm). For solid **S5**: 500 µg of the material were suspended in 1000 µL of hybridization buffer and separated into 10 aliquots of 100 µL. Different amounts of OTA standard solution were added to each aliquot and the volume was completed to 1000 µL with hybridization buffer. All samples were stirred at 37°C for 30 min and centrifuged 2 min at 12000 rpm to remove the solid. Finally, fluorescence of the released rhodamine B was measured in the supernatants at 575 nm (λ_{exc} = 555 nm).

Selectivity studies with S3 and S5. In order to carry out these experiments, 400 µg of **S3** were suspended in 400 µL of hybridization buffer and separated in 4 aliquots of 100 µL each one. The **S3** suspensions were spiked to reach a final concentration of 100 nM of OTA, Fumonisin B1 and Aflatoxin B1. In all cases, the volume was completed to 1000 µL with hybridization buffer. All samples were stirred at 25°C for 30 min and centrifuged 2 min at 12000 rpm to separate the solid. The fluorescence of the released rhodamine B was then measured in the supernatants at 575 nm (λ_{exc} = 555 nm). The same protocol was carried out for solid **S5**, however in this case samples were stirred at 37°C.

OTA detection in realistic samples. For these experiments, 1000 µL of OTA solution (10000 nM) were added to 0.05 g of wheat. The mixture was homogenized using a vortex, 5 mL of MeOH:H_2O (6:4/v:v) were added and stirred 30 minutes. Then solid was separated by centrifugation and the liquid phase was completely evaporated. The expected mycotoxine concentration (400 nM), was then determined by the standard addition method[43] using solids S3 and S5.

Acknowledgment

We thank the Spanish Government (projects MAT2015-64139-C4-1-R and AGL2015-70235-C2-2-R (MINECO/FEDER)) and the Generalitat Valenciana (project PROMETEOII/2014/047) for support. A.R. thanks UPV for her predoctoral fellowship. S.S. thanks the Instituto de Salud Carlos III and the European Social Fund for the financial support "Sara Borrell" (CD16/000237). A.B. thanks the Spanish Government for the financial support "Juan de la Cierva-Incorporación" (IJCI-2014-21534). The authors also thank the Electron Microscopy Service at the UPV for support.

Keywords.

Ochratoxin A functional nanomaterials · sensing · silica mesoporous nanoparticles · aptamers.

References

1. J. Chen, Z. Fang, J. Liu, L. Zeng, *Food Control,* **2012**, *25*, 555-560.
2. L. Kupski, E. Badiale-Furlong, *Food Chem*., **2015**, *177,* 354-360.
3. G. Deng, K. Xu, Y. Sun, Y. Chen, T. Zheng, J. Li, *Anal. Chem*., **2013**, *85*, 2833-2840.
4. C. Wang, J. Qian, K. Wang, K. Wang, Q. Liu, X. Dong, C. Wang, X. Huang, *Biosens. Bioelectron*., **2015**, *68*, 783-790.
5. Commission Regulation, [EC] No 1881/2006 of 19 December 2006 setting maximum levels for certain contaminants in foodstuffs. Off. *J. Eur. Communities: Legis*., **2006**, *364*, 5-24.
6. T. Tanaka, A. Yoneda, S. Inoue, Y. Sugiura, Y. Ueno, *J. Chromatogr*. A, **2000**, *882*, 23-28.
7. R. Ghali, I. Belouaer, S. Hdiri, H. Ghorbel, K. Maaroufi, A. Hedilli, J. *Food Compos. Anal*., **2009**, *22*, 751-755.
8. F. Al-Taher, J. Cappozzo, J. Zweigenbaum, H.J. Lee, L. Jackson, D. Ryu, *Food Control,* **2017**, *72*, 27-35.
9. C. N. Rossi, C. R. Takabayaski, M. A. Ono, G. H. Saito, E. N. Itano, O. Kawamura, E. Y. Hirooka, E. Y. S. Ono, *Food Chem*., **2012**, *132*, 2211-2216.
10. A. Sun, Y. Z. Zhang, G. P. Sun, X. N. Wang, D. Tang, *Biosens. Biolectron*., **2017**, *89*, 659-665.
11. K. E. Sapsford. C. R. Taitt, S. Fertig, M. H. Moore, M. E. Lassman, C. M. Maragos, L. C. Shriver-Lake, *Biosens. Biolectron*., **2006**, *21*, 2298-2305.
12. R. Wang, L. Xu, Y. Li, *Biosen. Bioelectron*., **2015**, *67*, 400-407.
13. I. Willner, B. Shlyahovsky, M. Zayats, B. Willner, *Chem. Soc. Rev*., **2008**, *37*, 1153-1165.

14. F. Sancenón, Ll. Pascual, M. Oroval, E. Aznar, R. Martínez-Máñez, *Chemistry Open,* **2015**, *4*, 418-437.
15. E. Aznar, M. Oroval, Ll. Pascual, J. R. Murguía, R. Martínez-Máñez, F. Sancenón, *Chem. Rev*., **2016**, *116*, 561-718.
16. J. L. V. Escoto, I. I. Slowing, B. G. Trewyn, V. S. Y. Lin, *Small,* **2010**, *6*, 1952-1967.
17. F. Tang, L. Li, D. Chen, *Adv. Mater*., **2012**, *24*, 1504-1534.
18. H. Song, R. M. Rioux, J. D. Hoefelmeyer, R. Komor, K. Niesz, M. Grass, P. Yang, G. A. Somorjai, *J. Am. Chem. Soc*. **2006**, 128, 3027-3037.
19. A. Dandapat, D. Jana, G. De, *ACS Appl. Mater. Interfaces,* **2009**, *1*, 833-840.
20. M. H. Lim, C. F. Blanford, A. Stein, *J. Am. Chem. Soc*., **1997**, *119*, 4090-4091.
21. M. H. Lim, C. F. Blanford, A. Stein, *Chem. Mater*., **1998**, *10*, 467-470.
22. S. L. Burkett, S. D. Sims, S. Mann, *Chem. Commun*., **1996**,*11*, 1367-1368.
23. C. E. Fowler, S. L. Burkett, S. Mann, *Chem. Commun*., **1997**,*18*, 1769-1770.
24. B. H. Wouters, T. Chen, M. Dewilde, P. J. Grobet, *Micropor. Mesopor. Mat*., **2001**, *44*, 453-457.
25. F. Zhang, J. Cheng, R. Zhou, J. Cao, J. Li, C. Burda, Q. Min, J. Zhu, *Angew. Chem. Int. Ed*. **2014**, *53*, 2371-2375; *Angew. Chem*., **2014**, *126*, 2403-2407.
26. S. Alberti, G.J.A.A. Soler-Illia, O. Azzaroni, *Chem. Commun*., **2015**, *28*, 6050-5075.
27. C. H. Lu, B. Willner, I. Willner, *ACS Nano,* **2013**, *7*, 8320-8332.
28. R. Villalonga, P. Díez, A. Sánchez, E. Aznar, R. Martínez-Máñez, J. M. Pingarrón, *Chem. Eur. J*., **2013**, *19*, 7889-7894.
29. Ll. Pascual, I. Baroja, E. Aznar, F. Sancenón, M. D. Marcos, J. R. Murguía, P. Amorós, K Rurack, R. Martínez-Máñez, *Chem. Commun*., **2015**, *51*, 1414-1416.
30. A. Ribes, E. Xifré-Perez. E. Aznar, F. Sancenón, T. Pardo, Ll. F. Marsal, R. Martínez-Máñez, *Sci. Rep*., **2016**, 6, 38649-38658.
31. M. Oroval, C. Coll, A. Bernardos, M. D. Marcos, R. Martinez-Mañez, D. G. Shchukin, F. Sancenón, *ACS Appl. Mater. Interfaces,* **2017**, *9*, 11332-11336.
32. M. Oroval, E. Climent, C. Coll, R. Eritja, A. Aviñó, M. D. Marcos, F. Sancenón, R. Martínez-Máñez, P. Amorós, Chem. Commun., **2013**, 49, 5480-5482.
33. W. Wang, T. Yan, S. Cui, J. A. Wan, *Chem. Commun*., **2012**, *48*, 10228-10230
34. V. C. Özalp, A. Pinto, E. Nikulina, A. Chuvilin. T. Schäfer, *Part. Syst. Charact*. **2014**, *31*, 161-167.
35. M. McKeague, M. C. DeRosa, *J. Nucleic Acids,* **2012**, 78-98.
36. M. McKeague, E. M. McConnell, J. Cruz-Toledo, E. D. Bernard, A. Pach, E. Mastronardi, X. Zhang, M. Beking, T. Francis, A. Giamberardino, A. Cabecinha, A. Ruscito, R. Aranda-Rodriguez, M. Dumontier, M. C. DeRosa, *J. Mol. Evol*., **2015**, *81*,150-161.
37. A. D. Ellington, J. W. Szostak, *Nature,* **1992**, *356*, 850-852.
38. C. Tuerk, L. *Gold, Science,* **1990**, *249*, 505-510.
39. J. Xue, H. Wu, Z. Chu, Y. Mei, J. Ye, R: Liu, C. Zhang, L. Peng, W. Zheng, F. Chen, *Microchim. Acta,* **2013**, *180*, 109-115.
40. K. V. Ragavan, L. S. Selvakumar, *Chem. Commun*., **2013**, *49*, 5960-5962.

41. Z. Mei, H. Chu, W. Chen, F. Xu, J. Liu, H. Xu, R. Zhang, L. Zheng, *Biosens. Bioelect*., **2013**, *39*, 26-30.
42. L. Lv, D. Li, R. Liu, C. Cui, Z. Guo, *Sens. Actuators, B*, **2017**, *246*, 647-652.S. Brunauer, P.H. Emmett, E. Teller, *J. Am. Chem. Soc*., **1938**, *60*, 309-319.
43. S. Hu, W. Ouyang, L. Guo, Z. Lin, X. Jiang, B. Qiu, G. Chen, *Biosens. Bioelect*, **2017**, *92*, 718-723.
44. M. A. Andrade, F. M. Lanças, *J. Chromatogr. A*, **2017**, *1493*, 41-48.
45. S. Joshi, R. M. Annida, H. Zuilhof, T. A. van Beek, M. W. Nielen, *J. Agric. Food Chem.*, **2016**, *64*, 8263-8271.
46. M. Mahdi, B. Mansour, M. Afshin, *Microchim. Acta*, **2016**, *183*, 3093-3099.
47. V. Pagkali, P. S. Petrou, A. Salapatas, E. Makarona, J. Peters, W. Haasnoot, G. Jobs, A. Economou, K. Misiakos, I. Rapti, S. E. Kakabakos, *J. Hazard. Mater.* , **2017**, *323*, 75-83.
48. P. Novo, G. Moulas, D. M. F. Prazeres, V. Chu, J. P. Conde, *Sens. Actuators, B*, **2013**, *176*, 232-240.
49. A. Karczmarczyk, K. Haupt, K. H. Feller, *Talanta*, **2017**, *166*, 193-197.
50. A. Karczmarczyk, C. Reiner-Rozman, S. Hageneder, M. Dubiak-Szepietowska, J. Dostálek, K. H. Feller, *Anal. Chim. Acta*, **2016**, *937*, 143-150.
51. C. Zhang, J. Tang, L. Huang, Y. Li, D. Tang, *Microchim. Acta*, **2017**, 1-9.
52. Y. Ji, Q. He, Y. Xu, Z. Tu, H. Yang, Y. Qiu, X. Wang, Y. Liu, *Anal. Methods*, **2016** *8*, 7824-7831.
53. H. Jiang, X. Li, Y. Xiong, K. Pei, L. Nie, Y. Xiong, Y. *Toxins*, **2017**, *9*, 83-94.
54. J. Xu, W. Li, R. Liu, Y. Yang, Q. Lin, J. Xu, P. Shen, Q. Zheng, Y. Zhang, Z. Han, J. Li, T. Zheng, *Sens. Actuators, B*, **2016**, *232*, 577-584.
55. J. V. Ros-Lis, B. García, D. Jiménez, R. Martínez-Máñez, F: Sancenón, J. Soto, F. Gonzalvo, M. C. Valldecabres, *J. Am. Chem. Soc.* **2004**, *126*, 4064-4066.
56. E. P. Barrett, L. G. Joyner, P. P. Halenda, *J. Am. Chem. Soc.* **1951**, *73*, 373-380.
57. S. Brunauer, P.H. Emmett, E. Teller, *J. Am. Chem. Soc.* **1938**, *60*, 309-319.

ChemistryOpen, 2017, 6, 653–659

SUPPORTING INFORMATION

Two new fluorogenic aptasensors to detect Ochratoxin A based on capped mesoporous silica nanoparticles

Àngela Ribes, Sara Santiago-Felipe, Andrea Bernardos, M. Dolores Marcos, Teresa Pardo, Félix Sancenón, Ramón Martínez-Máñez, and Elena Aznar

Preparation and performance of gated materials

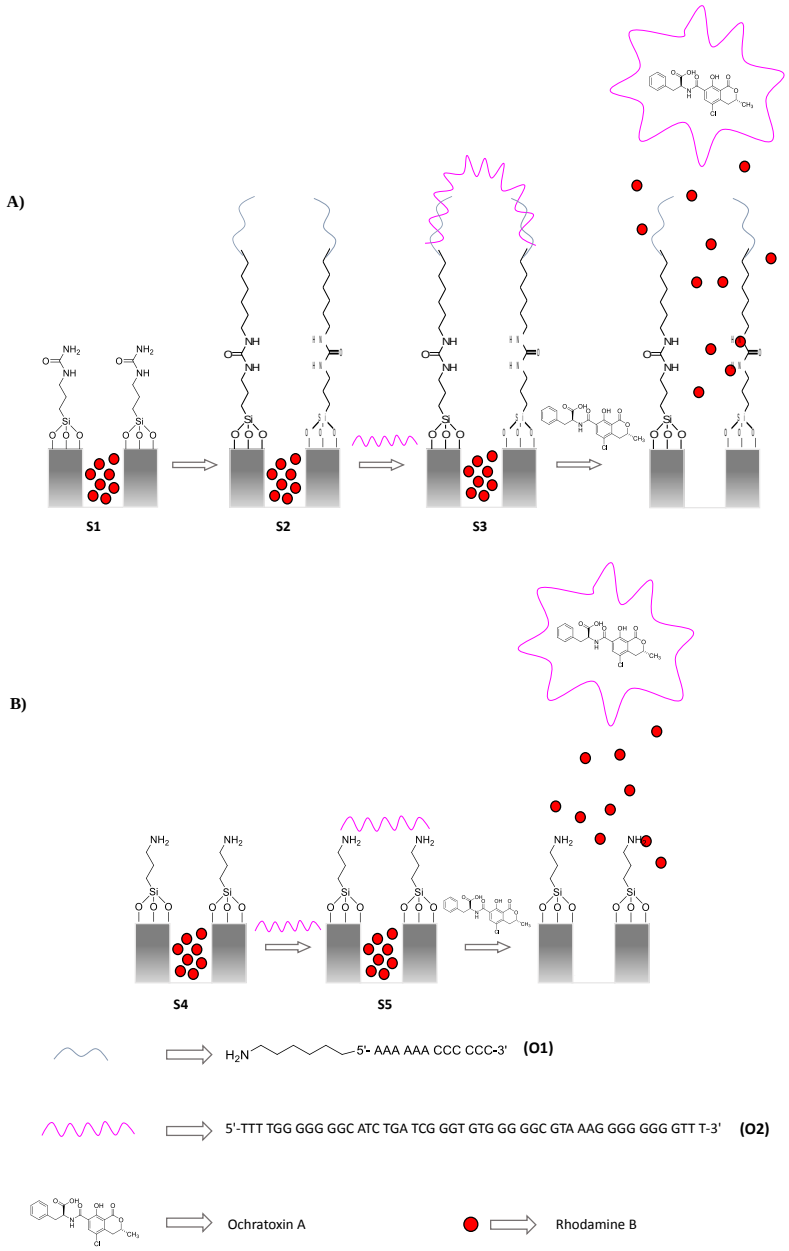

Scheme S1. Preparation and performance of gated materials A) **S3** capped with an aptamer in covalent approach and B) **S5** capped with an aptamer in electrostatic approach. Dye (rhodamine B) delivery entrapped in **S3** and **S5** is selectively accomplished in the presence of OTA.

N_2 adsorption–desorption characterization. Mesoporosity was analysed by N_2 adsorption–desorption isotherms. Calcined MSNs showed an adsorption step at an intermediate P/P_0 value (0.1–0.5) typical of this type of solid (see **Figure S1**). This step can be related to the nitrogen condensation inside the mesoporous by capillarity. The absence of a hysteresis loop in this interval and the narrow BJH pore suggest the existence of uniform cylindrical mesopores with a total pore volume of 0.31 $cm^3\ g^{-1}$ calculated by using the BJH model on the adsorption branch of the isotherm. The application of the BET model resulted in a value for the total specific surface of 908.6 $m^2\ g^{-1}$. From the XRD, porosimetry and TEM studies, a pore diameter of 2.43 nm was determined. In addition to this adsorption step associated to the micelle generated mesopores, a second feature appeared in the isotherm at a high relative pressure (P/P0 > 0.7). This corresponded to the filling of the large voids among the particles and presented a volume of 0.24 $cm^3\ g^{-1}$ (calculated by using BJH model), which must be considered as a textural-like porosity. In this case, the curves showed a characteristic H1 hysteresis loop and a wide pore size distribution.The N_2 adsorption–desorption isotherm of **S1** and **S4** (see **Figure S1**) is typical of mesoporous systems with filled mesoporores, and a decrease in the N_2 volume adsorbed (0.08 $cm^3\ g^{-1}$ and 0.25 $cm^3\ g^{-1}$, for **S1** and **S4**, respectively) and surface area (112.7 $m^2\ g^{-1}$ and 414.7 $m^2\ g^{-1}$, for **S1** and **S4**, respectively) were observed. The most relevant feature in the N_2 adsorption–desorption isotherm of these solids is the absence of a sharp step at low-medium relative pressure ($0.1 < P/P_0 < 0.4$). In fact, this solid showed flat curves when compared (at the same scale) to those of the starting MSNs parent material, this indicates a significant pore blocking and the subsequent absence of appreciable mesoporosity

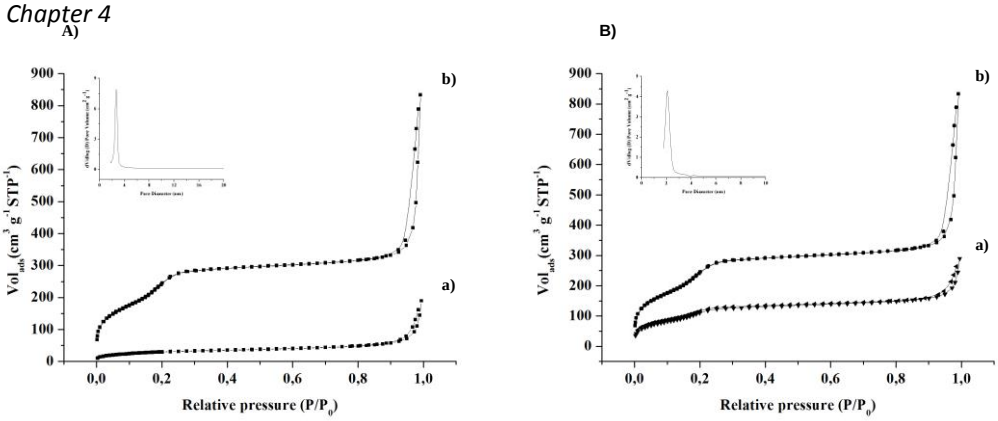

Figure S1. Nitrogen adsorption-desorption isotherms for A: (a) calcined MSNs (b) solid **S1** and B: (a) calcined MSNs, (b) solid **S4**. Inset: Pore size distribution of calcined MSNs

Table S1. BET Specific Surface Values, Pore Volumes, and Pore Sizes Calculated from the N_2 Adsorption−Desorption Isotherms for Selected Materials

	S_{BET} ($m^2\ g^{-1}$)	Pore volume (P/P_0<0.8)[a] ($cm^3\ g^{-1}$)	BJH pore size (P/P_0<0.8)[b] (nm)	Pore volume (P/P_0>0.8)[c] ($cm^3\ g^{-1}$)	BJH pore size (P/P_0>0.8)[d] (nm)
Calcined MSNs	908.6	2.43	0.31	54.02	0.24
S1	112.7	-	0.08	41.22	0.17
S4	414.7	2.37	0.25	39.53	0.17

[a]Pore size estimated by using the BJH model applied on the adsorption branch of the isotherm, for $P/P_0 < 0.7$, which can be associated with the surfactant generated mesopores. [b]Pore volume estimated by using the BJH model applied on the adsorption branch of the isotherm, for $P/P_0 < 0.7$, which can be associated with the the surfactant generated mesopores. [c]Pore size for $P/P_0 > 0.7$, which can be associated with the textural porosity. [d]Pore volume for $P/P_0 > 0.7$, which can be associated with the textural porosity.

Dynamic Light scattering characterization. **Figure S2** shows the progressive diameter increase in each functionalization step from calcined MSNs to final solids **S3** and **S5**. **Table S2**, summarizes the diameter size values for all solids

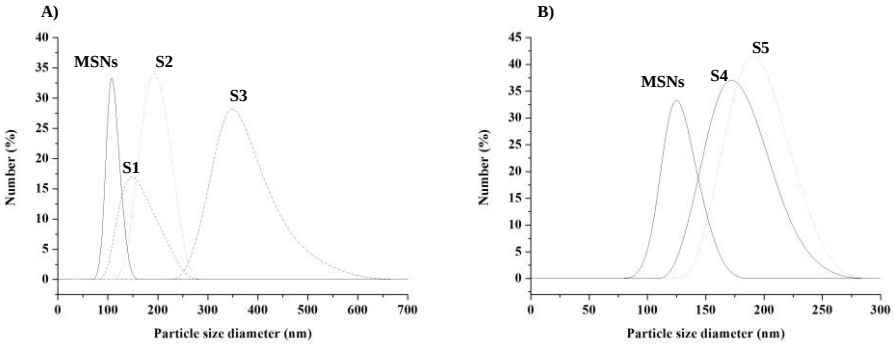

Figure S2. Size distribution obtained by DLS studies for calcined MSNs, **S1**, **S2**, **S3**, **S4** and **S5** solids.

Table S2. Diameter values for calcined MSNs, **S1**, **S2**, **S3**, **S4** and **S5** determined by DLS

	Particle diameter (nm)
MCM-41 type	152
S1	162
S2	194
S3	379
S4	164
S5	190

Infrared spectra.Infrared spectra were recorded to confirm the presence of DNA on the surface of solids **S3** (Figure S3). Results for solid **S5** were omitted for similarity to **S3**. In Table S2, summarizes characteristics peaks

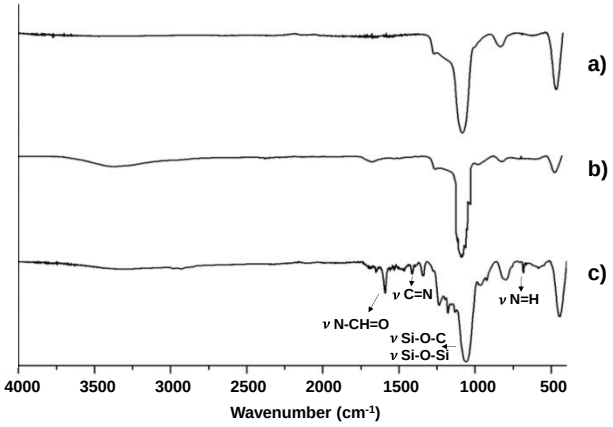

Figure S3. FTIR spectra of the (a) calcined MSNS, (b) **S1** and (c) **S3**.

Table S3. Characteristic peaks of the synthesized solids.

Assignment	**Frequencies (wavelength in cm^{-1})**	**Comment**
Acylamide group	1560	N-CH=O vibration
Thymine	740	N=H vibration
Guanine and Cytosine	1492, ≈1300, 1294	C=N bond stretching and plane vibration

Limit of detection

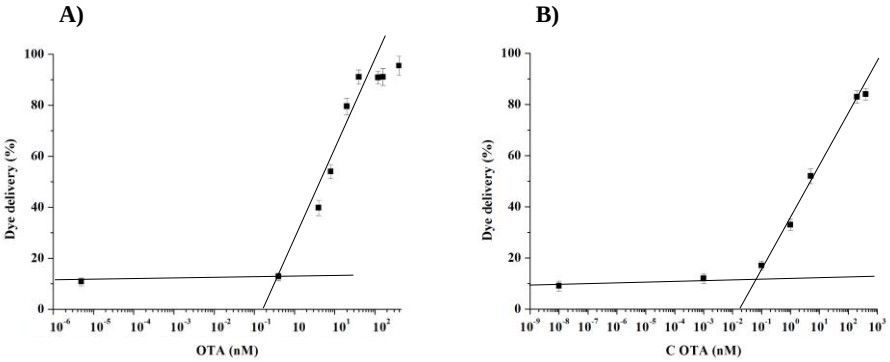

Figure S4. Release of rhodamine B from solid **S3** (A) and **S5** (B) in the presence of different concentrations of OTA in hybridization buffer (pH7.5).

Detection of OTA in wheat samples

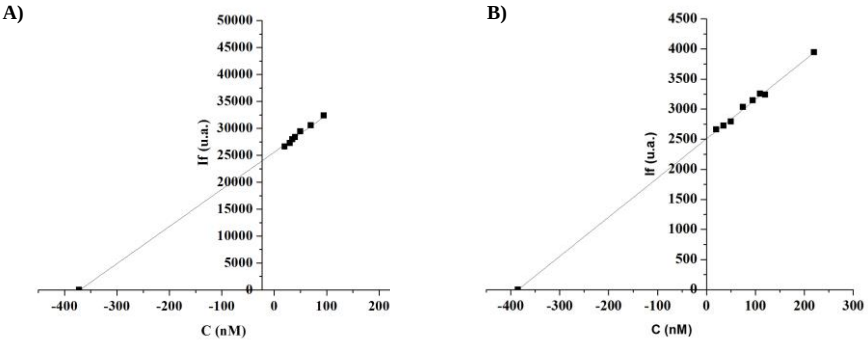

Figure S5. Standard addition method used for the detection of OTA in spiked wheat samples and using **S3** and b) **S5** as probes.

Table S4. Selection of reported methods to detect OTA

Sensory system	Detection	LOD (nM)	Reference
Biosensor based on a structure-switching aptamer	Fluorescence	1.98	1
Acid extraction and HPTLC and HPLC	Fluorescence	0.62-0.74	2
Magnetic-fluorescent-targeting multifunctional aptasensor using CdTe quantum dots as label	Fluorescence	0.01	4
Liquid chromatography	Mass spectrometry	0.25	8
Aptamer–graphene oxide nanosheets and DNase I-based target recycling reaction	Electrochemical	0.014	10
Aptasensors employing SYBR gold and exonuclease I	Fluorescence	1.65	44
Aptasensor based on Fe_3O_4/g-C_3N_4/HKUST-1 composites	Fluorescence	6.19	45
In-tube solid phase microextraction followed by HPLC	Mass spectrometry	20	46
Competitive immunoassay using 3-dimensional carboxymethylated dextran as immobilizer	Surface plasmon resonance	17.33	47
Competitive immunoassay using quantum dot-labeled antibody to rhodamine-coated magnetic silica nanoparticles	Fluorescence resonance energy transfer (FRET)	0.002	48
Competitive immunoassay on an array of ten Mach-Zehnder interferometers	Interferometry	4.95	49
Indirect competitive immunoassay using thin film hydrogenated amorphous silicon photodiode arrays	Chemiluminescence	69.33	50
Immunoassay whith quartz crystal microbalance	Piezoelectric	0.4	51
Competitive inhibition immunoassay using gold-nanoparticles	Surface plasmon resonance	0.044	52
Competitive immunoassay using platinum-enclosed gold cores	Voltammetry	1.8×10^{-4}	53
Competititve immunoassay using anti-idiotypic nanobodies	Colorimetry	0.01	54

Competititve immunoassay using silver nanoparticles	Fluorescence	60	55
Enzyme immunoassay using silica-hydrogel photonic crystal microsphere	Chemiluminescence	0.001	56
Aptasensor using silica nanoparticles	Fluorescence	0.5 (**S3**) 0.05 (**S5**)	This paper

5. Molecular gated nanoporous anodic alumina for the detection of cocaine.

Molecular gated nanoporous anodic alumina for the detection of cocaine

Àngela Ribes[1,2], Elisabet Xifré-Pérez[3], Elena Aznar[1,2], Félix Sancenón[1,2], Teresa Pardo[1,2], Lluís F. Marsal[3,], and Ramón Martínez-Máñez[1,2,*]*

[1] Instituto Interuniversitario de Investigación de Reconocimiento Molecular y Desarrollo Tecnológico (IDM). Universitat Politècnica de València, Universitat de València, Departamento de Química, Universitat Politècnica de València, Camino de Vera s/n, 46022, Valencia, Spain.

[2] CIBER de Bioingeniería, Biomateriales y Nanomedicina (CIBER-BBN), Spain.

[3] Departamento de Ingeniería Electrónica, Eléctrica y Automática, Universidad Rovira i Virgili, Avda. Països Catalans 26, 43007, Tarragona, Spain.

Received: August 9, 2016

Available online: December 7, 2016

Scientific Reports, **2016**, *6*, 38649–38658

Abstract

We present herein the use of nanoporous anodic alumina (NAA) as a suitable support to implement “molecular gates” for sensing applications. In our design, a NAA support is loaded with a fluorescent reporter (rhodamine B) and functionalized with a short single-stranded DNA. Then pores are blocked by the subsequent hybridisation of a specific cocaine aptamer. The response of the gated material was studied in aqueous solution. In a typical experiment, the support was immersed in hybridisation buffer solution in the absence or presence of cocaine. At certain times, the release of rhodamine B from pore voids was measured by fluorescence spectroscopy. The capped NAA support showed poor cargo delivery, but presence of cocaine in the solution selectively induced rhodamine B release. By this simple procedure a limit of detection as low as 5×10^{-7} M was calculated for cocaine. The gated NAA was successfully applied to detect cocaine in saliva samples and the possible re-use of the nanostructures was assessed. Based on these results, we believe that NAA could be a suitable support to prepare optical gated probes with a synergic combination of the favourable features of selected gated sensing systems and NAA.

Introduction

The combination of different inorganic solids with organic compounds has resulted in the preparation of an almost unlimited number of new supports with a wide range of new functionalities. In this field, interesting materials are gated nano-devices that can deliver an entrapped cargo in the presence of certain external stimuli.[1-4] In most cases gated materials are based on a suitable inorganic support and a switchable ensemble capable of being “opened” or “closed” on command. In fact gated nanochemistry is a highly topical and rapidly developing tool that is demonstrating the possibility of achieving new advanced pre-designed functions by means of mass transport control. In fact in the last few years, nano-containers that bear gated scaffoldings have proved excellent candidates for the design of controlled-release “nanomachines” at different levels. Gated materials have been used mainly in drug delivery, although some examples have also been reported for sensing applications.[5-8] For the latter, the approach involves loading

the porous support with a reporter and using a capping mechanism in such a way that cargo delivery is triggered by the presence of the target analyte. According to this principle, gated systems able to respond to anions,[9,10] cations,[11,12,13] neutral molecules[14,15,16,17] or biomolecules[18,19,20] have been recently developed. Most of these sensing materials are based on the use of mesoporous silica nanoparticles thanks to their well-known properties, such as large load capacity, biocompatibility and functionalization ease. However, the use of nanoparticulated supports for sensing has some drawbacks. In particular, nanoparticles are not easy to handle, can be harmful if breathed in or deposited on skin, and can sometimes not form uniform suspensions to obtain highly reproducible sensing systems. Despite these problems, the implementation of gated ensembles for sensing applications on other nanostructured supports has not yet been fully developed.

From a different point of view, nanoporous anodic alumina (NAA) has emerged as a competitive support in nanotechnology for a significant number of applications.[21-23] Moreover, preparation of NAA is easy, cost-effective and easily up-scalable by well-known production techniques.[24] Nanotechnological applications of this material can be found in a wide variety of fields, such as energy, nanofabrication or biotechnology.[25-28] One interesting advantage of NAA over other systems for cargo release is that their structure is stable and does not degrade or erode in aqueous solutions, which may contribute to the development of robust reproducible devices, most of them for biosensing applications.[29-31] NAA is also biocompatible, and can be calcined and reused several times, which prolongs the support's lifespan.

In this context we were interested in studying the possible use of NAA as support to design gated materials for sensing applications. To develop our idea, we selected an aptamer-based gating mechanism. Aptamers have been widely recognised as versatile signal-transducing elements for sensing platforms.[32,33,34] Aptamers are DNA sequences with high selectivity and affinity for certain target proteins, small molecules or ions.[35,36,37,38] Their production is based on an in vitro selection method called SELEX (systematic evolution of ligands by exponential enrichment)[39-41] and their use has revolutionised the sensing field as ultrasensitive systems have been obtained to detect a number of different analytes.[42,43] In the

particular field of gated materials, Özalp and co-workers described the first aptamer-based gating mechanism capable of selectively releasing fluorescein in the presence of ATP.[44] Based on this first example, some other reports based on aptamers and gated materials have been reported for ATP,[45] potassium,[46] adenosine[47] and thrombin,[48] which indicate the high potential of aptamers as capping systems to prepare highly selective and sensitive probes.

We herein selected cocaine as the target analyte, which is a powerful addictive stimulant drug isolated from coca plant leaves. Its consumption causes a short-lived intense high, which is immediately followed by the opposite, e.g., intense depression, edginess and dependence. It is one of the commonest illegal drugs consumed worldwide and the design of easy-to-use detection systems for cocaine is very important. For this reason, many researchers have been involved in developing new methods to detect cocaine.[49] Immunoassay techniques are the first option for the rapid screening of illicit drugs.[50] However, these methodologies are sometimes not very selective and require positive confirmation by other procedures. Liquid or gas chromatography coupled with a mass spectrometry detector is the most widely used procedure to identify cocaine.[51] Although the limit of detection (LOD) of this method is very low, this technique is not widely accessible, is not portable, is time-consuming and requires trained personnel. Hence aptamers have also been used to develop cocaine-sensing systems. For instance, Soh et al.[52] developed a method based on the use of target-specific DNA aptamers which generates an electrochemical signal in response to cocaine coupled with a microfluidic detection system. Cai et al.[53] fabricated a sandwich biosensor by using fragments of the cocaine aptamer immobilised in a gold electrode and on the surface of tris(2,2′-bipyridyl)ruthenium(II)-doped silica nanoparticles, which gave an electroluminescent signal if cocaine was present. Liu et al. designed a simple colorimetric method[54] with an aptamer attached to the surface of gold nanoparticles, which aggregated when cocaine was present. Finally, Yu et al.[55] designed a label-free method in which cocaine selectively induced the polymerisation of an oligonucleotide that detached from a graphene oxide (GO) platform and brought about a change in the support's fluorescence.

Given the background of these fields (i.e. gated materials, optical sensors design, aptamers and NAA supports), we became interested in combining the use of NAA and gating concepts to prepare a new cocaine-sensing system. The design of the probe is depicted in Figure 1. The NAA support was loaded with a fluorescent reporter (rhodamine B) and functionalized with a short single-stranded DNA. Then pores were capped by the subsequent hybridisation of a specific cocaine aptamer. The capping DNA sequence was expected to be bulky enough to block pores and to inhibit dye delivery. Presence of the target analyte (i.e. cocaine) in the medium was expected to selectively displace the aptamer, resulting in pore opening and dye release.

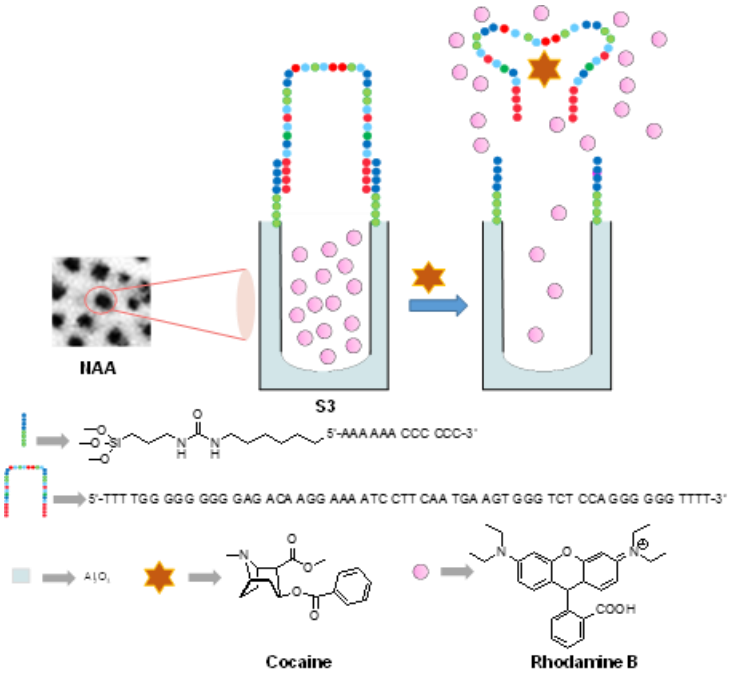

Figure 1. Scheme of the gated NAA support **S3** capped with the selected aptamer. Delivery of the entrapped dye (rhodamine B) is selectively accomplished in the presence of cocaine.

Results and discussion

***Preparation and characterization of the sensing support*.** The NAA support was obtained according to reported procedures.[56] Firstly, high purity aluminium sheets were electropolished in a mixture of ethanol and perchloric acid. Then the electropolished aluminium sheets were anodised by a two-step anodisation process with sulphuric acid. During this process, the second anodisation time was crucial to acquire a specific thickness on the aluminium layer (8 μm). To implement the gating mechanism, NAA supports were loaded with rhodamine B dye. Then the external surface was functionalized with (3-isocyanatopropyl)triethoxysilane to yield support **S1**. In another step, the short DNA sequence NH_2-$(CH_2)_6$-5'-AAA AAA CCC CCC-3' (**O1**), specifically designed to hybridise with a 3'-TTT TGG GGG G-5' sequence was covalently attached to **S1** by the formation of urea bonds to give support **S2**. Finally, the single-stranded oligonucleotide 5'-TTT TGG GGG GGG GAG ACA AGG AAA ATC CTT CAA TGA AGT GGG TCT CCA GGG GGG TTTT-3' (**O2**), which contained the specific sequence of the cocaine aptamer with dissociation constant K_D ~20μM,[45] was used to cap pores by hybridisation with **O1** to yield the final sensing capped support **S3**.

The starting NAA support was characterised by field emission scanning electron microscopy (FESEM), powder X-ray diffraction and thermogravimetric analyses. All the functionalized supports were also characterised by the same techniques. The nanostructure of the starting NAA support was assessed by FESEM. Representative images showed disordered pores with an average diameter of 8 nm (see Figure 2a). This disordered structure was confirmed by powder X-ray diffraction (See the Supplementary Information), where only a very strong peak at 2θ = 38º, which corresponded to crystalline aluminium, and a weak and broad peak, which corresponded to amorphous alumina oxide, were found. No more peaks were recorded, which indicated that the support did not present an ordered pore distribution. Supports **S1**, **S2** and **S3** showed a similar powder X-ray diffraction pattern to the initial support. The FESEM images of the **S3** support clearly showed the presence of an organic layer that covered most pores. The presence of this organic layer evidenced the suitable consecutive loading, functionalization and capping steps, while the visualisation of the porous

framework in certain areas (see the arrow in Figure 2b) confirmed the preservation of the nanoporous structure in **S3**.

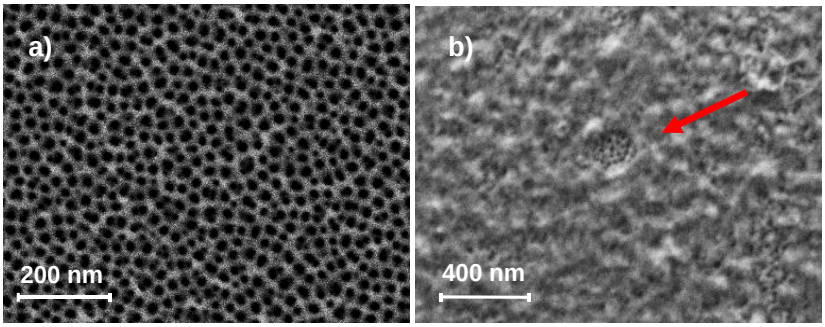

Figure 2. FESEM images of a) parent NAA support and b) support **S3**. Arrow indicates a certain area where the porous framework can be seen below the organic layer.

The functionalization of the NAA support was followed by EDX. As expected, the EDX analysis on the starting NAA gave peaks for aluminium and oxygen, whereas EDX on **S3** also clearly showed the presence of silicon, carbon, nitrogen and phosphorous from the anchored isocyanate moieties and oligonucleotides. The organic content of the different prepared materials was also calculated from the thermogravimetric analysis (see Table 1). An amount of 0.24 mmol/gSiO_2 of rhodamine B, 0.10 mmol/gSiO_2 of **O1** and 0.11 mmol/gSiO_2 of **O2** was determined for **S3**. The high content of the (3-isocyanato)propyl organosilane derivative incorporated into **S1** indicated that functionalization was not only restricted to the aluminol groups on the external surface, which suggested that incorporation of (3-isocyanato)propyl organosilane groups into mesopore entrances and/or external polymerization cannot be ruled out. From these data contents, the molecular ratio of **O1** compared to the (3-isocyanato)propyl moieties in **S3** was 35.4%, while the ratio between **O2** and **O1** was 48.6%, which indicated a good coverage of NAA with the aptamer.

Table 1. Contents (in mmol/gSiO_2) of (3-isocyanatopropyl), rhodamine B, **O1** and **O2** in the different hybrid supports.

	3-(isocyanate-propyl)	Rhoda-mine B	O1	O2	O3
S1	0.01	0.67			
S2	0.01	0.25	0.10		
S3	0.01	0.24	0.10	0.11	
S4	0.01	0.22	0.10		0.16

Sensing support performance. The response of support **S3** to the presence of cocaine was studied in aqueous solution. In a typical experimental, two **S3** supports were immersed in 2.5 mL of hybridization buffer (Tris-HCl 20 mM, $MgCl_2$ 37.5 mM, pH 7.5) each. Then 2.5 mL of an aqueous solution of cocaine (1 mM) were added to one of the supports, whereas 2.5 mL of water were added to the second support. Both systems were maintained at 25°C and aliquots of the supernatant solution were taken at certain times. Cargo release was measured by rhodamine B emission at 585 nm (λ_{exc} = 555 nm). Figure 3 shows the delivery profile of rhodamine B from support **S3** in the presence and absence of cocaine. In the absence of the target analyte (Figure 3, curve a), poor rhodamine B delivery took place, which is indicative of remarkable pore closure. In contrast when cocaine was present, clear dye delivery to the solution was detected (Figure 3, curve b). A simple calculation allowed us to determine that the ratio between the cargo released by leakage and that released upon cocaine recognition at a concentration of 0.01 mM after 20 minutes was 8-fold.

In order to assess the specificity of the sequence chosen in our work (**O2**), a NAA support loaded with rhodamine B and capped with a scrambled sequence (**O3**) was prepared (support **S4**) by a similar procedure to that used for **S3**. Our intention on preparing **S4** (that was capped by a DNA sequence that does not present any cocaine affinity) was to demonstrate that the cocaine selective opening of **S3** solid was induced by the aptamer used to cap the pores. In **S3**, selective coordination of cocaine with the aptamer induced selective pore opening and dye release, whereas it was expected that addition of cocaine to **S4** would not result in payload delivery. In fact, as depicted in Figure 3, the release of rhodamine B from **S4** in the absence (Figure 3, curve c) and presence of cocaine (Figure 3, curve d) was the same as that obtained for support **S3** in the absence of the analyte. This result confirmed the requirement of using a specific cocaine-aptamer to cap the NAA support pores to prepare selective probe **S3**.

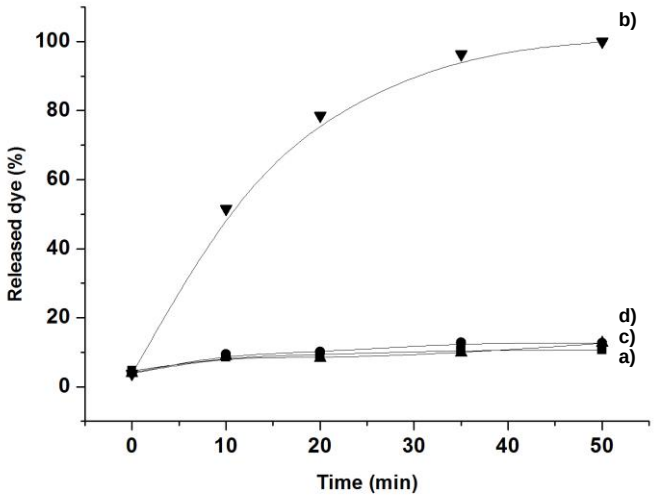

Figure 3. Release of rhodamine B from support **S3** a) in the absence and b) presence of cocaine (1 mM). Release of rhodamine B from support S4 c) in the absence and d) presence of cocaine (1 mM).

In another step, the response of **S3** to different concentrations of cocaine was studied. Following a procedure similar to that described above, the solutions with a different cocaine concentration were added to **S3**. After 20 min, the rhodamine

B released from the pore voids of the support was measured by fluorescence spectroscopy. As seen in Figure 4, the amount of rhodamine B delivered was proportional to the cocaine concentration in the solution. From this figure, a limit of detection (LOD) of ca. 5 x 10^{-7} M was determined. Both the LOD and analysis time for probe S3 fell within the ranges of other methods reported for cocaine detection (see Table 2).

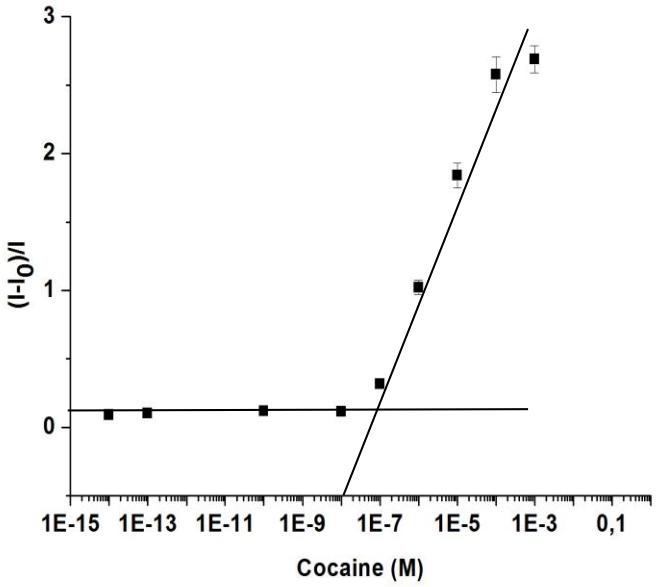

Figure 4. Release of rhodamine B from support **S3** according to the cocaine concentration in Tris-HCl buffer

Table 2. Comparison of the LOD and analysis time of other methods reported to detect cocaine.

Sensory system	Detection	LOD (M)	Time (min)	Reference
Gas chromatography	Mass spectrometry	1.65 x 10^{-11}	20	51
Cozart® RapiScan	Colorimetry	9.89 x 10^{-8}	3	57,58
Germanium strip waveguide on a silicon substrate integrated with a microfluidic	Infrared	1.65 x 10^{-3}	10	59

chip				
Immunochromatographic paper-based strip coupled with an OLED	Fluorescence	$1.64\ 10^{-8}$	Not reported	60
Microfluidic Electrochemical Aptamer-based Sensor	Voltammetry	10×10^{-6}	20	52
Gold electrode functionalized with an aptamer	Electrochemi luminescence	3.7×10^{-12}	120	53
Aptamer with gold nanoparticles	Colorimetry	100×10^{-6}	Not reported	54
Isothermal circular strand-displacement amplification and graphene oxide absorption	Fluorescence	190×10^{-9}	10	61
NAA loaded with rhodamine B and capped with cocaine aptamer	Fluorescence	5×10^{-7}	20	This paper

The selectivity in the detection of cocaine of support **S3** was investigated by carrying out similar delivery experiments in the presence of other drugs (Figure 5). As seen, poor cargo delivery from **S3** was observed with the 0.01 mM concentration of heroin and morphine compared with the response obtained for cocaine.

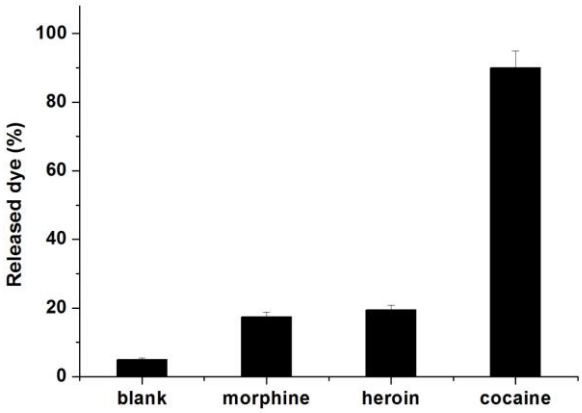

Figure 5. Release of rhodamine B from support **S3** in the presence of morphine, cocaine and heroin at 0.01 mM in Tris-HCl buffer.

The rapid cocaine detection in oral fluids is crucial in in situ drug abuse controls.[62] Encouraged by our results, we studied the potential use of **S3** to detect cocaine in more competitive real samples. Thus the possibility of detecting cocaine in oral fluids, such as human saliva, was studied (vide infra). The typical cocaine concentration in saliva in real-life samples is highly variable because its concentration is related with the degree of abuse of this drug by consumers. Nevertheless, on the market there are several kits to detect cocaine drug consumption. The most widely used test employed by trained police is the Cozart® RapiScan (CRS) test, which is not specifically selective for cocaine, but for a family of opiates. This test has a cut-off point of 30 ng/mL (9.89×10^{-8} M)[55,56] which is comparable with our LOD, and suggests that our method could be used for the selective detection of cocaine in saliva samples at typical concentration levels. In order to evaluate the possible use of our material for detection in realistic environments solids **S3** were submerged into different aliquots containing 100 µL of saliva spiked with cocaine (63 µM). Then, different known amounts of cocaine were added to each aliquot until final concentrations of 0.05, 0.1, 0.15

and 0.20 mM were reached. After 20 min, the emission of the rhodamine B released from solid S3 in the different aliquots was measured and a calibration curve was obtained (see Figure S2 in the Supporting Information) that responds to the linear equation y = 4010212x + 227496. From the intercept of the curve with the x-axis a concentration of cocaine in the spiked sample of 56 μM was determined. Taking into account that the initial saliva sample had a cocaine concentration of 63 μM a 90% recovery was achieved.

Finally, we also tested the possible re-use of the NAA support. In this respect, an already used **S3** support was calcined to remove organic matter and was then functionalized following a similar procedure to that described above. Cargo release from recycled gated supports **S3-R** was very similar to **S3** (Figure S3). Moreover, calibration curve of solid **S3-R** was also very similar to that found for **S3** in terms of linear range and limit of detection (Figure S4). This recycled procedure via calcination was repeated 3 times with similar results (Figure S4). Both experiments demonstrated that the supports could be reused after cocaine detection.

In summary, we demonstrated that the combination of nanoporous anodic alumina supports and selected aptamers can be used to prepare gated probes to detect specific molecules. In particular, we loaded NAA with rhodamine B and capped the support using a specific oligonucleotide sequence capable of recognizing cocaine. The studies demonstrated that the functional support was able to retain the cargo in an aqueous buffered solution, yet a clear delivery of the entrapped dye was selectively observed in the presence of cocaine. The response of the gated support to different cocaine concentrations was evaluated and a LOD of 5 x 10^{-7} M was determined. Furthermore, the selectivity of the system was assessed, which demonstrated that heroin and morphine drugs were unable to induce remarkable dye delivery. In addition, the real applicability of capped support **S3** was confirmed by the detection of cocaine in a competitive matrix, such as saliva. As a final point, we also demonstrated that it was possible re-use the NAA support. Our procedure, based on measuring an easy-to-detect fluorescent molecule that is delivered when cocaine is present, avoids analyte

pre-treatment steps, such as extraction or derivatization. Therefore, it is appropriate for rapid analyses by non-specialized personnel. We demonstrate that NAA is a suitable support to prepare optical gated probes with a synergic combination of the favorable features of selected gated sensing systems and NAA, which is easy to prepare and handle, and can be easily recovered.

Methods

General techniques. PXRD measurements were taken by a D8 Advance diffractometer using Cu Kα radiation (Philips, Amsterdam, The Netherlands). A Field Emission Scanning Electron Microscopy (FESEM) analysis was performed under a ZEISS Ultra 55 microscope. Fluorescence spectroscopy was carried out in a Felix 32 Analysis, version 1.2 (Build 56), PTI (Photon Technology International) instrument. Thermogravimetric analyses were carried out on a TGA/SDTA 851e balance (Mettler Toledo, Columbus, OH, USA), using an oxidising atmosphere (air, 80 mL min^{-1}) with a heating program: gradient of 393-1,273 K at 10°C min^{-1}, followed by an isothermal heating step at 1,273°C for 30 min.

Chemicals. (3-isocyanatopropyl)triethoxysilane, rhodamine B, tris(hydroxymethyl)aminomethane (TRIS), hydrochloric acid were purchased from Sigma-Aldrich Química (Madrid, Spain) and oligonucleotides **O1** (NH_2-$(CH_2)_6$-5'-AAA AAA CCC CCC-3'), **O2** (TTT TGG GGG GGG GAG ACA AGG AAA ATC CTT CAA TGA AGT GGG TCT CCA GGG GGG TTTT-3') and **O3** (TTT TGG GGG GAC CAC AAG ACA TGC ATC CCG GGG GGG TTTT) were acquired from Isogen-Lifesciences (Barcelona, Spain). All the products were used as received. All the drugs were provided by the Agencia Española del Medicamento y Productos Sanitarios (AEMPS; Spanish Agency of Medication and Health Products).

***Fabrication of the nanoporous anodic alumina (NAA) support*.** Porous alumina substrates were produced by electrochemical anodisation of high purity aluminium sheets (99.99% purity). The used electrolyte was sulphuric acid 0.3 M. Before anodisation, the aluminium sheets were electropolished in a mixture of ethanol and perchloric acid 4:1 (v:v) at 20 V for 4 min to reduce their surface

roughness. Then sheets were cleaned with abundant water and ethanol, and air-dried to avoid any acid residue. The electropolished aluminium sheets were then anodised in the H_2SO_4 electrolyte by a two-step anodisation process. The first anodisation step was performed for 24 h at 10 V. The electrolyte temperature was 2°C. This porous alumina layer was dissolved by wet chemical etching in a mixture of phosphoric acid 0.4 M and chromic acid 0.2 M at 70°C for 3 h to obtain a pre-patterned aluminium surface. Subsequently, the second anodisation step was performed under the same anodisation conditions as the first step. The anodisation time for this second step, which determines layer thickness, was adjusted to produce a porous alumina layer with a thickness of 8 µm.

***Synthesis of support S1*.** For a typical synthesis, NAA was immersed in 8 mL of a mixture of rhodamine B (18.6 mg, 0.04 mmol) in CH3CN (30 mL). The suspension was stirred at room temperature for 24 h. Then excess (3-isocyanatopropyl)triethoxysilane (328 µl, 1.32 mmol) was added, and the final mixture was stirred at room temperature for 24 h. The resulting pink support (**S1**) was washed slightly with acetonitrile and dried at 37°C for 2 h.

Synthesis of support S2. Support **S1** was immersed in 700 µL of a solution of rhodamine B in CH3CN (1 mM). Then 100 µL of oligonucleotide **O1** (at 20 µM concentration) and 2 µL of triethylamine were added. Finally, the mixture was stirred 3 h at room temperature

Synthesis of support S2*.* Support **S1** was immersed in 700 µL of a solution of rhodamine B in CH3CN (1 mM). Then 100 µL of oligonucleotide **O1** (at 20 µM concentration) and 2 µL of triethylamine were added. Finally, the mixture was stirred 3 h at room temperature

Synthesis of support S3. Support **S2** was immersed in a solution that contained 780 µL of hybridisation buffer (20 mM Tris-HCl, 37.5 mM $MgCl_2$, pH 7.5) and 41.05 µL of **O2** (100 µM). The mixture was stirred for 2 h at room temperature.

The resulting material was thoroughly washed with hybridisation buffer (20 mM Tris-HCl, 37.5 mM $MgCl_2$, pH 7.5) to eliminate the unbounded oligonucleotide.

***Synthesis of support S4*.** Support **S2** was immersed in a solution that contained 780 µL of hybridisation buffer (20 mM Tris-HCl, 37.5 mM $MgCl_2$, pH 7.5) and 41.05 µL of **O3** (100 µM). The mixture was stirred for 2 h at room temperature. The resulting material was thoroughly washed with hybridisation buffer (20 mM Tris-HCl, 37.5 mM $MgCl_2$, pH 7.5) to eliminate the unbounded oligonucleotide.

Release experiments of supports S3, S3-R and S3-RL. To investigate the gating properties of **S3**, two fractions of this material were immersed in 2.5 mL of hybridisation buffer (20 mM Tris-HCl, 37.5 $MgCl_2$, pH 7.5). Then 2.5 mL of a cocaine aqueous solution (1 mM) were added to one of the supports, whereas 2.5 mL of water were added to the other support. Both experiments were maintained at 25ºC and fractions were taken at certain times. Cargo release to the solution was measured by the rhodamine B fluorescence at 585 nm (λ_{ex}=555 nm).

***Calcination of S3*.** Calcination of support **S3** was performed in a MC/1300 oven (Gallur) using a heating gradient from 25ºC to 550ºC (3º per min), followed by an isothermal period at 550ºC for 5 h.

Detection of cocaine in saliva samples. For these experiments, 100 µL of a cocaine problem solution were added to 2,000 µL of free saliva until a final concentration of 0.063 mM. Then the drug was determined by the method of standard addition. Rhodamine B fluorescence was monitored after 20 minutes.

Acknowledgements

We thank Projects MAT2015-64139-C4-1-R and TEC2015-71324-R (MINECO/FEDER), the Catalan Government (Project 2014 SGR 1344), the ICREA (ICREA Academia Award) and the Generalitat Valenciana (Project PROMETEOII/2014/047) for support. We also thank to the Agencia Española del Medicamento y Productos Sanitarios for its concessions. A.R. thanks the UPV for

her predoctoral fellowship. The authors also thank the Electron Microscopy Service at UPV for support.

Author contributions statement

L.M, and R.M proposed the idea. A.R and E.X carried out the experiments. E.A, F.S and T.P analysed the results. All authors discussed the results, wrote and reviewed the manuscript.

Additional Information

Competing financial interests: The authors declare no competing financial interests.

References

1. P. Nadrah, O. Planinšek, M. Gaberšček, *J. Mater. Sci.,* **2014***, 49***,** 481–495.
2. A. Baeza, M. Colilla, M. Vallet-Regí,. *Expert Opin. Drug Deliv*., **2015**, *12*, 319–337.
3. M. Karimi, H. Mirshekari, H.; M. Aliakbari, P.S. Zangabad, M. R. Hamblin, Drug Delivery. *Nanotech. Rev*., **2016** *5***,** 195–207.
4. E. Aznar, M. Oroval, Ll. Pascual, L.; J.R. Murguía, R. Martínez-Máñez, F. Sancenón, F., *Chem. Rev*., **2016**, *116*, 561−718.
5. F. Sancenón, Ll. Pascual, M. Oroval, E. Aznar, R. Martínez-Máñez,. *Chemistry Open,* **2015** *4***,** 418-437.
6. C.H. Lu, B. Willner, I. Willner, *ACSNano,* **2013**, *7***,** 8320–8332.
7. R. Klajn, J.F. Stoddart, B.A. Grzybowski, *Chem. Soc. Rev*., **2010**, *39***,** 2203–2237.
8. R. Wei, T.G. Martin, U. Rant, H. Dietz, *Angew. Chem. Int. Ed*., **2012** *51***,** 4864 4867.
9. C.L. Zhu, C.H. Lu, X.Y. Song, H.H. Yang, X.R. Wang X.R., *J. Am. Chem. Soc.,* **2011,** *133***,** 1278-1281.
10. V.C. Özalp, A. Pinto, E. Nikulina, A. Chulivin, T. Schäfer, *Part.Part.Sys. Charact.,* **2014,** *31***,** 161-167.
11. Y.L. Choi, J. Jaworski, M.L. Seo, S.J. Lee, J.H. Jung, *J. Mater. Chem.*, **2011,** *21***,** 7882-7885.
12. Z. Zhang, F. Wang, D. Balogh, I. Willner, *J. Mater. Chem. B,* **2014**, 2**,** 4449-4455.
13. L. Fu, J. Zhuang, W. Lai, X. Que, M. Lu, D. Tang, *J. Mater. Chem. B., **2013***, 1**,** 6123–6128 (2013).
14. P. Díez, et al,. *J. Am. Chem. Soc.,* **2014***,* 136**,** 9116-9123.
15. D. Tang, Y. Lin Q. Zhou, Y. Lin, P. Li, R. Niessner, D. Knopp, *Anal. Chem.,* **2014**, *86***,** 11451-11458.
16. L. Hou, C. Zhu, X. Wu, G. Chen, D. Tang, *Chem. Commun*., **2014**, *50*, 1441–1443.

17. Z. Chen, Y. Tan, K. Xu, L. Zhang, B. Qiu, L. Guo, Z. Lin, G. Chen, *Biosens. Bioelectro*., **2016**, *75*, 8–14.
18. Ll. Pascual, et al. *Chem. Commun*., **2015**, 51, 1414-1416.
19. R. Qian, I. Ding, H. Ju, *J. Am. Chem. Soc.,***2013***, 135,* 13282-13285.
20. K. Ren, J. Wu, Y. Zhang, F. Yan, H. Ju, *Anal. Chem*., **2014**, *86,* 7494–7499.
21. Y. Chen, A. Santos, Y. Wang, C. Wang, D. Losic, *ACS Appl Mater Interface*s., *2015*, *7***,** 19816-19824.
22. M.S. Aw, M. Bariana, D. Losic, *Ed. Losic, D., Santos, A*., **2015**, 319-354 (Springer International Publishing)
23. R. Urteaga, C.L. Berli, *Ed. Losic, D., Santos, A*., **2015**, 249-269 (Springer International Publishing,)
24. L. Vojkuvka, L.F. Marsal, J. Ferré-Borrull, P. Formentin, J. Pallarés, *Superlattices Microstruct.,* **2008***, 44***,** 577**–**582.
25. A. De la Escosura-Muñiz, A. Merkoçi, *ACS Nano.,* **2012***, 6*, 7556**–**7583.
26. T. Kumeria, M.M. Rahman, A. Santos, J. Ferré-Borrull L.F. Marsal, D. Losic, *Appl. Mater. Interfaces,* **2014***, 6,* 12971−12978.
27. A. Santos, T. Kumeria, D. Losic, *Materials.,* **2014***,* 7, 4297-4320.
28. J. Ferré-Borrull, J. Pallarès, G. Macías, L.F. Marsal, *Materials, **2014**, 7***,** 5225-5253.
29. D. Gong, V. Yadavalli, M. Paulose, M. Pishko, C.A. Grimes, *Biomed. Microdevices,* **2003***,* 5, 75-80.
30. S. D. Alvarez, C. P. Li, C.E. Chiang, I.K. Schuller, I. K.; M.J.A. Sailor, *ACSNano,* **2009***, 3,* 3301-3307.
31. F.S.H. Krismastuti, H. Bayat, N.H. Voelcker, H. Schönherr, *Anal. Chem.,* **2015**, *87***,** 3856−3863.
32. D. L. Ma, M. Wang, B. He, C. Yang, W. Wang, C.H.A. Leung, *ACS Appl. Mater. Interfaces,* **2015***, 7,* 19060−19067.
33. P. Kohli, C.C. Harrell, Z. Cao, R. Gasparac, W. Tan, C.R. Martin, *Science,* **2004***, 305*, 984**–**986.
34. A.E. Abelow, O. Schepelina, R.J. White, A. Vallée-Bélisle, K.W. Plaxco, I. Zharov, *Chem. Commun*., **2010**, *46*, 7984**–**7986.
35. D. L. Ma, D.S.H. Chan, C.H. Leung, *Acc. Chem. Res*., **2014**, *47*, 3614**–**3631.
36. G. Wanga, Y. Zhua, L. Chena, X. Zhanga, *Biosens. Bioelectron.,* **2015***, 63,* 552-557.
37. O. Laptenko, I. Shiff, W. Freed-Pastor, A. Zupnick, M. Mattia, E. Freulich, I. Shamir, N. Kadouri, T. Kahan, J. Manfredi, I. Simon, C.Prives, *Molec. Cell*., **2015**, *57,* 1034**–**1046.
38. D. L. Ma, M. Wang, B. Bingyong He, C. Chao Yang, W. Wang, C.H. Leung, *ACS Appl. Mater. Interfaces*, **2015**, *7*, 19060-19067.
39. M. McKeague, M.C. DeRosa, *J. Nucleic Acids,* **2012,** *2012***,** 1-20.
40. M. McKeague et al*., J. Mol. Evol.,* **2015***, 81,* 150**–**161.
41. A. D. Ellington, J.W. Szostak, *Nature,* **1990***, 346*, 818-822.
42. A. Wochner, et al., *Anal Biochem*., **2008**, *373***,** 34-42.
43. K. M. Song, E. Jeong, W. Jeon, M. Cho, C. Ban, *Anal. Bioanal. Chem*., **2012**, *402*, 2153**–**2161.
44. V. C. Özalp, T. Thomas Schäfer, *Chem. Eur. J.,* **2011***, 17*, 9893**–**9896.
45. M. N. Stojanovic, P. dePrada, D.W. Landry, *J. Am. Chem Soc*., **2001**, *123*, 4928-4931.
46. Y. Wen, et al. *Chem. Commun*., **2012**, 48, 8410-8412.

47. L. Chen, Y. Wen, B. Su, J. Di, Y. Song, L. Jiang, *J. Mater. Chem*., **2011**, *21,* 13811–13816.
48. M. Oroval, M. et al. *Chem. Commun*. **2013**, *49***,** 5480-5482.
49. M. Barroso, E. Gallardo, J.A. Queiroz, *Bioanalysis.,* **2009***, 1,* 977–1000.
50. H.M. Phan, K. Yoshizuka, D.J. Murry, P.J. Perry, *Pharmacotherapy.,* **2012***, 32***,** 649–656.
51. D. A. Kidwell, M. A. Blanco, F.P. Smith, *Forensic Sci. Int.,* **1997***, 84,* 75-86.
52. J.S. Swensen, et al., *J. Am. Chem. Soc*., **2009**, *131***,** 4262–4266.
53. Q. Cai, et al. *Anal. Bioanal. Chem*., **2011**, *400,* 289–294.
54. R. Zou, et al., *RSC Adv*., **2012**, *2,* 4636–4638.
55. L. Qiu, H. Zhou, W. Zhu, L. Qiu, J. Jiang, G. Shen, R. Yu,. *New J.Chem*., **2013**, *37,* 3998.
56. L. F. Marsal, L. Vojkuvka, P.Formentin, J. Pallarés, J. Ferré-Borrull, J. *Optical Mater.,***2009***, 31,* 860.
57. E. A. Kolbrich, et al., *J. Anal Toxicol*., **2003**, *27*, 407-411.
58. G. Cooper, L. Wilson, C. Reid, L. Main, C. Hand, *Forensic Sci. Int*., **2005**, *150,* 239-243.
59. Y. H. Chang, et al. *Lab Chip*, **2012**, *12,* 3020–3023.
60. R. Walczak, et al., *Procedia Chem*., **2009**, *1,* 999–1002.
61. L. Qiu, H. Zhou, W. Zhu, L. Qiu, J. Jiang, G. Shena, R. Yu, *New J. Chem*., **2013**, *37,* 3998-4003.
62. W. M. Bosker, M.A. Huestis, *Clinical Chem*., **2009***, 55,* 1910–1931.

Sci. Rep., 2016, 6, 38649–38658

SUPPLEMENTARY INFORMATION

Molecular gated nanoporous anodic alumina for the detection of cocaine

Àngela Ribes, Elisabet Xifré-Pérez, Elena Aznar, Félix Sancenón, Teresa Pardo, Lluís F. Marsal, and Ramón Martínez-Máñez

Powder X-Ray diffration

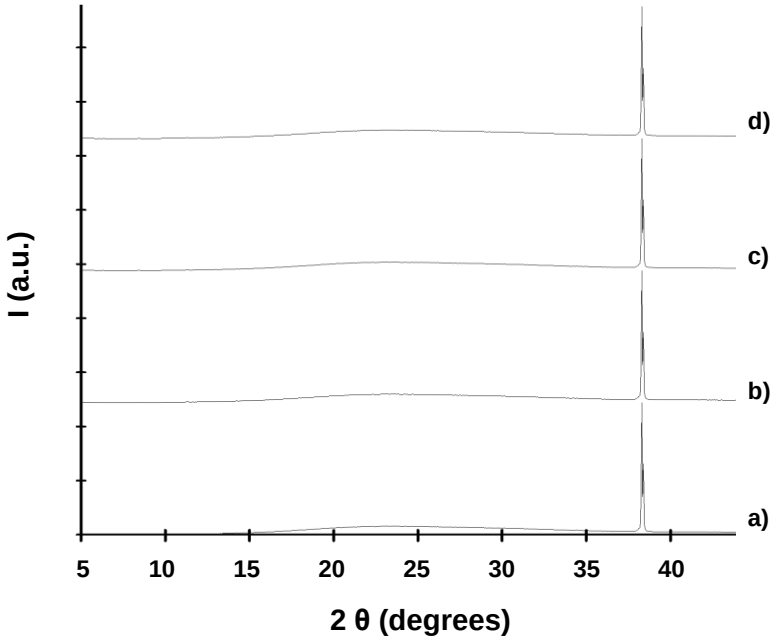

Figure S1. Powder X-ray diffraction pattern for a) as synthesized NAA support, b) **S1**, c) **S2** and d) gated **S3.**

Detection of cocaine in saliva samples

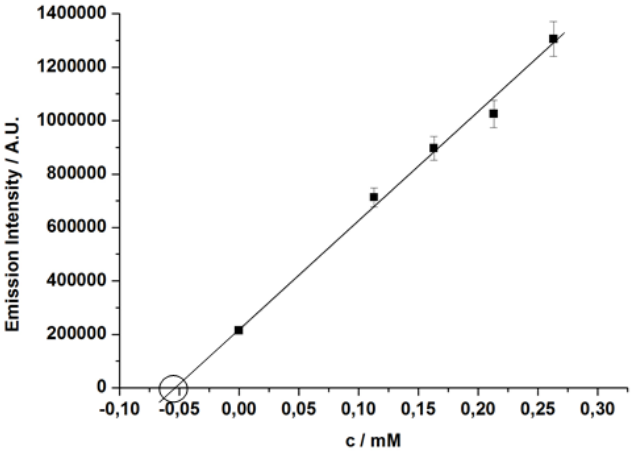

Figure S2. Standard addition method using S3 for the detection of cocaine in a saliva sample spiked with cocaine (63 µM). From the intercept of the curve with the x-axis a concentration of cocaine of 56 µM was determined.

Release experiments of S3-R after calcination

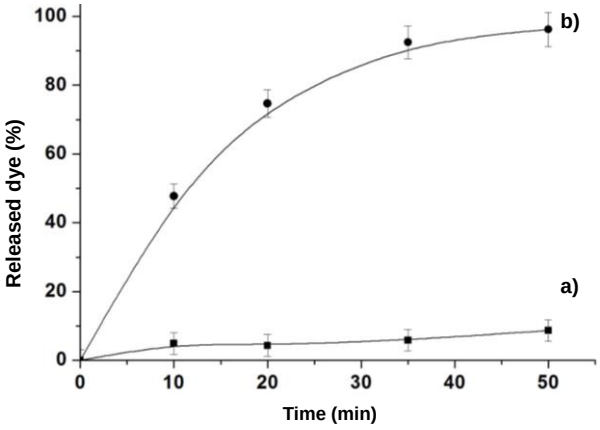

Figure S3. *Release of rhodamine B from support* ***S3-R*** *in the absence (a) and in the presence (b) of cocaine (1 mM).*

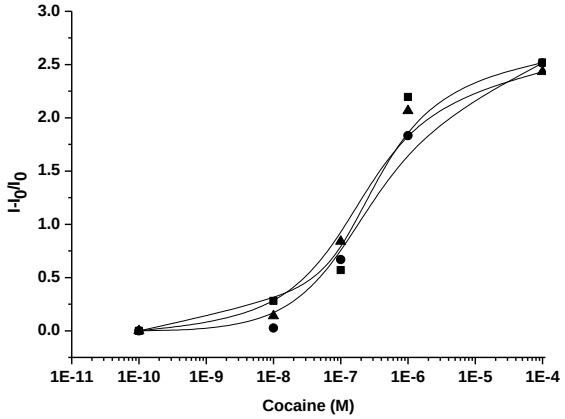

Figure S4. *Release profiles of solid* ***S3-R*** *in the presence of increasing quantities of cocaine for three successive recycling calcination processes.*

6. A rapid, selective and sensitive probe based in oligonucleotide-capped nanoporous alumina for the detection of infection produced by fungi Candida albicans

A rapid, selective and sensitive probe based in oligonucleotide-capped nanoporous alumina for the detection of infection produced by fungi Candida albicans

Àngela Ribes[1,2,3], Elena Aznar[2,1,3,4,], Sara Santiago-Felipe[2,1,3], Elisabet Xifre-Perez[5], Maria Angeles Tormo-Mas[,6],Javier Pemán[7] , Lluis F. Marsal[5,*] and Ramón Martínez-Máñez[1,2,3,4,*]*

[1] Instituto Interuniversitario de Investigación de Reconocimiento Molecular y Desarrollo Tecnológico (IDM). Universitat Politècnica de València, Universitat de València, Departamento de Química, Universitat Politècnica de València, Camino de Vera s/n, 46022, Valencia, Spain.

[2] CIBER de Bioingeniería, Biomateriales y Nanomedicina (CIBER-BBN), Spain.

[3] Unidad Mixta de Investigación en Nanomedicina y Sensores. Universitat Politècnica de València, Instituto de Investigación Sanitaria La Fe, Valencia, Spain

[4] Unidad Mixta UPC-CIPF de Investigación en Mecanismos de Enfermedades y Nanomedicina. Universitat Politècnica de València, Centro de Investigación Príncipe Felipe, Valencia, Spain

[5] Departamento de Ingeniería Electrónica, Eléctrica y Automática, Universidad Rovira i Virgili, Avda. Països Catalans 26, 43007, Tarragona, Spain

[6] Grupo acreditado de investigación Infección Grave, IIS La Fe, Avenida Fernando Abril Martorell, 126, 46026 Valencia, Spain.

[7] Servicio de Microbiología, Hospital Politècnic i Universitari La Fe, Avenida Fernando Abril Martorell, 126, 46026,Valencia, Spain.

Submitted

Abstract

A robust, sensitive and competitive system to detect *Candida albicans* DNA in clinical samples is developed. Nanoporous anodic alumina (NAA) was used as suitable support to implement "molecular gates" for the sensing procedure. In the proposed design, NAA pores are loaded with a fluorescent reporter (rhodamine B) and blocked by an oligonucleotide specific to *C. albicans*. The capped material showed negligible cargo release, whereas dye delivery was selectively observed in the presence of genomic DNA from *C. albicans*. This simple procedure has been successfully applied to discriminate among real samples from healthy patients and those infected with *C. albicans*. The obtained results are promising in terms of sensitivity and selectivity, and agree with those obtained by conventional methods, demonstrating the high potential for diagnosis of the reported design.

Introduction

Invasive candidiasis, with or without associated candidemia, is the most common invasive fungal disease in developed countries. Approximately the 95% of episodes are caused by five Candida species: *Candida albicans*, *Candida glabrata*, *Candida parapsilosis, Candida tropicalis* and *Candida krusei*.[1] They can cause superficial, localized, and/or systemic infection. The most predominant type in intensive care units is intra-abdominal invasive candidiasis, including peritonitis and intra-abdominal abscesses.[2] Intra-abdominal candidiasis occurs in approximately 40% of patients after gastrointestinal surgery, gastrointestinal perforation, or necrotizing pancreatitis, and it is associated with mortality rates around 45–60%.[3]

Early antifungal therapy has a major influence on survival in invasive candidiasis. Rapid identification of the species has importance for the treatment, prediction of the species-specific primary resistance and variable antifungal susceptibility. The long delays associated with traditional methods for the detection and identification of organisms force clinicians to empirically treat patients with unnecessary broad spectrum agents, which in turn increases expenses, may cause adverse side effects, and potentially contributes to the emergence of antifungal resistances.[4] In addition, it is important to differentiate

between C. albicans and other species (non-albicans) due to the different treatments that should be followed for each case. [5]

Regardless of its low sensitivity (50-75%) and long turnaround (10-72 hours), blood culture remains the gold standard technique for invasive candidiasis diagnosis. Alternative procedures based on the detection and quantification of fungal biomarkers and metabolites, like mannan antigen and anti-mannan antibodies, anti-gem tube antibodies or β-1,3-D-glucan, have been developed to improve and anticipate the detection of invasive candidiasis, but these techniques are not accessible to all laboratories due their complexity in the clinical practice.[6] In response to this situation, molecular techniques based on fungal DNA amplification assays are under development and may ultimately replace culture-based tests in the clinical laboratory. However, the clinical usefulness of PCR-based methodologies to detect Candida DNA has not been established due to the inconsistent performance, in terms of sensitivities and specificities, and lack of standardization of these techniques.[7] Thus, it is required to investigate sensitive, easy to perform, and quick new diagnostic tools to guide early antifungal therapy with the most appropriate antifungal drugs.

In response to this situation, nanodevices have played a great role in sensing area in the last years due to its capacity to provide rapid, simple and sensitive responses to target analytes.[8] Specifically, those provided with "molecular gates" have been broadly employed in new recognition and sensing systems based on stimuli-responsive protocols.[9] In these systems, a mesoporous support is loaded with a dye and the capping mechanism is designed so that only a target analyte is able to trigger the delivery of the cargo. [10-12] Among the different biomolecules that could act as caps, nucleic acids have shown excellent performances in sensing applications due to its high degree of specificity.[13-18] However sensing systems based on complementary DNA-DNA hybridization interactions have been scarcely studied until now.[19-21]

Recently, nanoporous anodic alumina (NAA) has emerged as a competitive support in nanotechnology for a significant number of applications in a wide variety of fields such as energy, nanofabrication or biotechnology.[22] The preparation of these scaffold is easy, cost-effective and easily up-scalable by well-

known production techniques, what coupled to its high stability contributes to the development of robust and reproducible sensing devices.[23-26] Moreover NAA has demonstrated some remarkable properties such as the ability of being calcined and reused several times, large load capacity and the possibility to easily modify their surface due to the presence of groups with excellent reactivity (Al-OH).[27-32]

Taking into account these concepts, we have combined the use of NAA supports with oligonucleotides as molecular gates to obtain a new rapid and selectively system, which is able to diagnose infection caused by C. albicans. Beyond a proof of concept, this detection system has been tested in real samples of infected patients, providing fast results that agree with those obtained by other standard techniques.

Material and methods

***General techniques*.** Field emission scanning electron microscopy (FESEM), thermogravimetric analysis (TGA) and fluorescence spectroscopy were employed to characterize the synthesized materials. Field emission scanning electron microscopy analyses were performed under a ZEISS Ultra 55 microscope. Thermogravimetric analyses were carried out on a TGA/SDTA 851e balance (Mettler Toledo, Columbus, OH, USA), using an oxidizing atmosphere (air, 80 mL min−1) with a heating program: gradient of 393–1,273 K at 10 °C min−1, followed by an isothermal heating step at 1,273 °C for 30 min. Fluorescence spectroscopy measurements were carried out on a Synergy H1 microplate reader (BioTek, Winooski, VT, USA). FASTprep FP120 Cell disrupter (Thermo Electron) was used to homogenized cell solutions.

Chemicals. (3-isocyanatopropyl)triethoxysilane, rhodamine B, triethylamine (TEA), tris(hydroxymethyl)aminomethane (TRIS), hydrochloric acid (HCl), sodium chloride (NaCl), potassium chloride (KCl), disodium hydrogen phosphate (Na2HPO4), potassium dihydrogen phosphate (KH2PO4) TRITON, ethylenediaminetetraacetic acid (EDTA), RNAsa enzyme, ammonium acetate (NH4OAc), phenol, chloroform, sodium dodecyl sulfate (SDS), ethanol (EtOH) and isoamyl alcohol were purchased from Sigma-Aldrich Química (Madrid, Spain).

Oligonucleotides O1 (NH2-(CH2)6-5'-AAA AAA CCC CCC-3'), O2 (5'- TTT TGG GGG GTT GAG AAG GAT CTT TCC ATT GAT GGG GGG GTT TT-3'), and complementary DNA (5'-AAC TCT TCC TAG AAA GGT AAC TAC-3') were purchased from Isogen-Lifesciences (Barcelona, Spain). All products were used as received.

Synthesis of nanoporous anodic alumina (NAA) support. Porous alumina substrates were produced by electrochemical anodization of high purity aluminum sheets (99.999% purity). The electrolyte used was sulphuric acid (H_2SO_4) 0.3 M. Before the anodization, the aluminum sheets were electropolished in a mixture of ethanol (EtOH) and perchloric acid ($HClO_4$) 4:1 (v:v) at 20 V for 4 min to reduce their surface roughness. Then the sheets were cleaned with abundant water and ethanol and dried with air to avoid any acid residue. The electropolished aluminum sheets were then anodized in the H_2SO_4 electrolyte using a two-step anodization process. The first anodization step was performed for 24 h at 10 V. The temperature of the electrolyte was 2 °C. The resulting nanostructure is a layer of porous alumina with disordered pores. This porous alumina layer was dissolved by wet chemical etching in a mixture of phosphoric acid (H_3PO_4) 0.4 M and chromic acid (H_2CrO_7) 0.2 M at 70 °C for 3 h, obtaining a pre-patterned aluminum surface. Subsequently, the second anodization step was performed under the same anodization conditions than the first step. The anodization time for this second step, that determines the thickness of the layer, was adjusted to produce a porous alumina layer with thickness 8 µm.

Synthesis of S1. In a typical synthesis, NAA was immersed in 8 mL of rhodamine B (18.6 mg, 0.04 mmol) in CH3CN (30 mL). The mixture was stirred at room temperature for 24 h. Then (3-isocyanatopropyl)triethoxysilane (328 µL, 1.32 mmol) was added, and the final mixture was stirred at room temperature for 24 h. The resulting pink support (**S1**) was slightly washed with acetonitrile and dried at 37°C for 2 h**.**

Synthesis of S2. Solid **S1** was immersed with 700 µL of a solution of rhodamine B in CH_3CN (1 mM), then 100 µL of oligonucleotide O1 (at 10 µM concentration)

and 2 µL of TEA were added. Finally, the mixture was stirred 3 h at room temperature. The resulting material was washed with hybridization buffer dropwised (20 mM Tris-HCl, 37.5 mM $MgCl_2$, pH 7.5) to eliminate the residual dye and unbounded oligonucleotide.

Synthesis of S3. Material S2 was immersed with 1975 µL of hybridization buffer, then 25 µL of O2 (100 µM) was added. The mixture was stirred 2 h at room temperature. The resulting material was washed with hybridization buffer to eliminate the unbounded oligonucleotide.

Organisms and growth conditions. Different species are used in these studies. A total of 3 *C. albicans* strains were used, 2 clinical isolates obtained from patients at La Fe University Hospital and identified at the routine clinic of the Microbiology service as explained below, the third strain of *C. albicans* and the other species used were obtained from the American Type Culture Collection (ATCC) and include the following: *C. albicans* (ATCC 90028), *C. parapsilosis* (ATCC 22019), *C. glabrata* (ATCC 90030), *S. epidemidis* (ATCC 12228), *S. aureus* (ATCC27853), *K. pneumoniae* (ATCC 13883) and *P. aeruginosa* (ATCC 27853). The strains were maintained in BHI agar and were grow in BHI medium at 37 °C.

Extraction protocol. 5 mL of cells grown in agar overnight were centrifuged 10 minutes at 7000 rpm. Supernatant was separated and pellet was suspended in 500 µL of TENTS (0.1M NaCl/25 TRITON/1% SDS with TRIS-EDTA (TE) buffer (Tris-HCl 50mM/ EDTA 1 mM, pH=8)). The suspension was transferred to a Screw cap microtube which contained 0.45 mm of glass beads. Then 500 µL of a mix of phenol/chloroform/ isoamyl alcohol (25:24:1) was added. The mixture was homogenized at 4 °C and left in bath ice for 5 minutes. After centrifugation (15 min, 14000 rpm) the supernatant was transferred to centrifuge tube and 1.5 mL of ethanol was added. The mixture was maintained 1 hour at -20 °C. Afterwards centrifugation (15 min, 14000 rpm), pellet was suspended in 200 µL of TE buffer and 5 µL of RNAse solution (1mg mL^{-1}) was added. Then the mixture was kept at room temperature for 30 minutes. In a following step, 40 µL of NH_4OAc 10M and

500 µL of ethanol were added to the microtube. Mixture was homogenized and left 30 minutes at -20 °C. Then suspension was centrifuged (15 minutes, 14000 rpm) and pellet was washed with 1000 µL of ethanol and centrifuged again. Finally, solid was dried under vacuum and resuspended with 1000 µL of TE. Extracted DNA was quantified using a Nanodrop instrument.

Assay protocol. To study the gating properties of the synthetized material, **S3** was tested in the presence of genomic DNA from *C. albicans* by measuring the emission of rhodamine B delivered from the pores to the solution. For that, two independent solids of **S3** were immersed in 1980 µL of hybridization buffer. Commercial genomic DNA was heated to 95 °C for 5 min in order to dehybridize the double helix structure and then cooled in an ice bath for 3 min. After cooling, 20 µL of a dehybridized commercial genomic solution containing 10.46 µg mL^{-1} was added to one of the solids whereas 20 µL of water were added to the other. Mixtures were maintained at 25°C and fractions were taken at certain times. Cargo release from solids was measured by the rhodamine B fluorescence in the solution at 585 nm (λ_{exc} = 555 nm).

Selectivity studies. In order to carry out selectivity studies, 8 portions of **S3** were suspended with 100 µL of hybridization buffer each. Then, 7 portions were spiked to reach a final concentration of 10^{-4} µg mL^{-1} of extracted genomic DNA from *C. albicans, C. parapsilosis, C. glabrata, Staphylococus epidermidis, Staphylococcus aureus, Klebsiela pneumoniae*, and *Pseudomonas aeruginosa*, respectively. Remaining portion was used as control. Volume of all experiments was completed to 1000 µL with hybridization buffer. Then, all samples were stirred at 25°C for 30 min. Fluorescence of released rhodamine B was measured at 585 nm (λ_{exc} = 555 nm).

Detection of C. albicans. The response of solids **S3** was tested in the presence of *C. albicans* cells. *C. albicans* cells were growth at 37 ºC in BHI agar medium. Then a 0.5 McFarland solution (10^5 cfu mL^{-1}) was prepared in phosphate buffer saline (PBS) and ten-fold dilutions were obtained. Two independent **S3** supports

were immersed in 1980 µL of hybridization buffer and 20 µL of a 10^3 cfu mL^{-1} *C. albicans* aqueous solution were added to one of the suspension, whereas 20 µL of water were added to the other. Suspensions were maintained at 25°C and fractions were taken at certain times. The fluorescence of the released rhodamine B was measured at 585 nm (λ_{exc} = 555 nm).

Quantification curve. The response of solids **S3** was tested in the presence of *C. albicans* cells. For that, *C. albicans* cells were growth at 37 ºC in BHI agar medium. Then a 0.5 McFarland solution (10^5 cfu mL^{-1}) was prepared and ten-fold dilutions were obtained. Ten supports of solid S3 were immersed in 100 µL of hybridization buffer. Then different dilution of C. abicans CFU were added to each aliquot and volume was completed to 1000 µL with hybridization buffer. All samples were stirred at 25ºC for 30 min. Fluorescence of released rhodamine B was then measured at 585 nm (λ_{exc} = 555 nm).

Amplification assay. To study signal amplification, 2 supports of S3 were immersed in 990 µL of hybridization buffer. Genomic DNA from *C. albicans* (10^{-7} µg mL^{-1}) was heated to 95 °C for 5 min in order to dehybridize the double helix structure and then cooled in an ice bath for 3 min. Then 10 µL of commercial genomic DNA were added to one of the suspensions whereas 10 µL of water (milliQ grade) were added to the other. Samples were stirred at 25ºC for 30 min and the amount of released rhodamine B was determined by fluorescence measurements at 585 nm (λ_{exc} = 555 nm).

Assays in real competitive media. The response of solids S3 in the presence of *C. albicans* was tested in different organic body fluids (i.e cerebrospinal fluid, plasma and peritoneal fluid). For that, *C. albic*ans cells were growth at 37 ºC in BHI agar medium. In a typical assay, two independent **S3** supports were immersed in 500 µL of the corresponding medium. To one of them 20 µL of a 10^3 cfu mL^{-1} *C. albicans* aqueous solution were added, whereas 20 µL of water were added to the other. Both samples were filled to a volume of 750 µL with hybridization buffer.

Suspensions were maintained at 25°C and fractions were taken at certain times. Fluorescence of released rhodamine B was measured at 585 nm (λ_{exc} = 555 nm).

Clinical samples characterization. For microbiological diagnosis, clinical samples were processed according to good clinical laboratory practice. Blood cultures were processed by BacT/ALERT® VIRTUOTM automated system (bioMerieux, Marcy l'Etoile, France). Any Candida spp isolated in sterile sample was considered as significative. All Candida isolates were identified by phenotypic and biochemical characteristics, and proteomic profiling technology. Biochemical characteristics were analysed by API ID20C (bioMérieux) and AuxaColorTM 2 (BioRad-Laboratories, Marnes-la-Coquette, France). Proteomic profiles were obtained and evaluated by VITEK MS (bioMérieux) according to the manufacturer's instructions.

Assays with clinical samples. In a typical experiment, **S3** was immersed in 700 µL of hybridization buffer and 300 µL of a sample from a non-infected patient (confirmed by microbiologic culture) was added. In the same way, other solid S3 was immersed in 700 µL of hybridization buffer and 300 µL of a sample from an infected patient (confirmed by microbiologic culture) were added. As control, other S3 portion was immersed in 1000 µL of hybridization buffer. All suspensions were stirred at 25°C for 30 min and the fluorescence of the released rhodamine B was then measured at 585 nm (λ_{exc} = 555 nm). All determinations were carried out by triplicate.

Results and discussion

Preparation and characterization of the sensing support. The NAA support was obtained according to reported procedures.[33,34] To prepare the sensing support, NAA was loaded with rhodamine B dye and then the external surface was functionalized with (3-isocyanatopropyl)triethoxysilane to yield support S1. In a further step, the short DNA sequence NH2-(CH2)6-5'-AAA AAA CCC CCC-3' (**O1**), was covalently attached to **S1** by the formation of urea bonds to give support S2. Finally, the single-stranded oligonucleotide 5'-TTT TGG GGG GTT GAG AAG GAT CTT TCC ATT GAT GGG GGG GTT TT-3' (**O2**) that contains a sequence 5'-TT GAG

AAG GAT CTT TCC ATT GAT G-3' which corresponded to the coding region of the integrin-like alpha Int1p protein (alpha INT1) from *C. albicans*, was used to cap pores by hybridization with **O1**, yielding the final sensing capped support S3 (Scheme 1).[35, 36] In solid S3 the hybridization of **O2** with the genomic DNA from *C. albicans*, is expected to induce pore opening and a selective delivery of the entrapped rhodamine B dye.

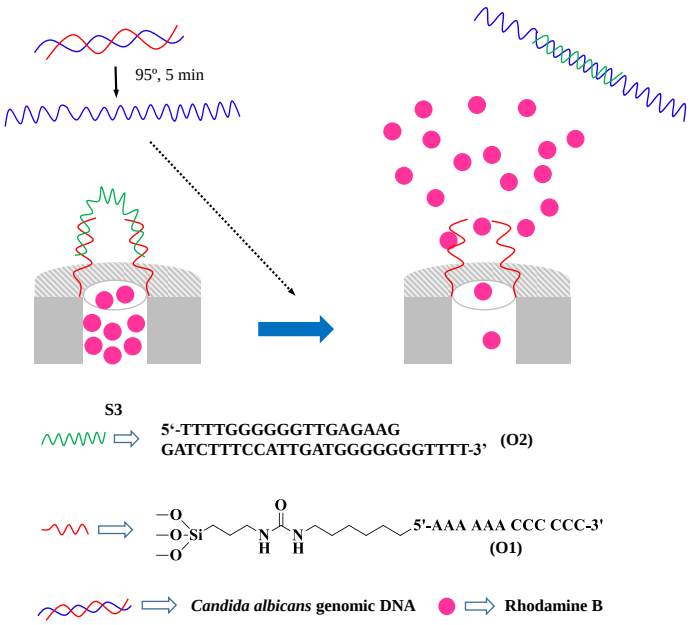

Scheme 1. Representation of the gated material **S3** capped with a single-stranded oligonucleotide (**O2**). Delivery of the entrapped dye is selectively accomplished by the presence of the complementary coding region of the integrin-like alpha Int1p protein (alpha INT1) present in non-hybridized genomic DNA from C. albicans.

Solids **S1**, **S2** and **S3** were characterized by field emission scanning electron microscopy (FESEM) and thermogravimetric analysis. Representative FESEM images for S1 showed the presence of disordered pores with an average diameter of 8 nm (see Figure S1a). FESEM images of the **S3** support clearly showed the

presence of an organic layer due to the presence of the oligonucleotides **O1** and O2 that covered most pores (see Figure S1b). This organic layer evidenced the suitable functionalization and capping of the support, while the visualization of the porous framework in certain areas confirmed the preservation of the nanoporous structure in the final device (see the arrow in Figure S1b). Organic content of the different prepared materials was calculated from thermogravimetric analysis. To obtain the amount of each organic entity, solids **S1**, **S2** and **S3** were analyzed before and after the complete release of rhodamine B (see Supplementary Material for details). Amounts of 0.245 mmol/g of rhodamine B, 0.10 mmol/g of **O1** and 0.11 mmol/g of **O2** were determined for **S3** (see Table 1).

Table 1. Content (in mmol/g) of rhodamine B, 3-isocyanatopropyl, **O1**, and **O2** in the different solids.

	Rhodamine B	3-isocyanatopropyl	O1	O2
S1	0.248	0.013	-	-
S2	0.247	0.013	0.10	-
S3	0.245	0.013	0.10	0.11

Release experiments. Detection of *C. albicans* using probe **S3** is based on the use of a stimuli-responsive uncapping of the gated support that results in selective rhodamine B in the presence of *C. albicans* DNA. This mechanism differs substantially from that used in classic "binding site–signaling subunit" probes. In sensing gated materials, the signaling process (relese of a dye) is disconnected from the host–guest interaction that occurs at the surface of the material. This sensing protocol offers great potential for the preparation of new sensing systems with enhanced features compared with classical signaling probes. The response of **S3** in the presence of *C. albicans* DNA was studied in a first step employing genomic DNA of this yeast. In a typical experiment, two **S3** pieces were immersed in hybridization buffer. 20 µL of a previously dehybridized genomic DNA of *C. albicans* solution was added to one of the pieces, while 20 µL of an aqueous buffered solution was added to the other. At selected times, fractions of the

supernatant solution were taken and studied by fluorescence to quantify the amount of rhodamine B in the aqueous phase. As it can be observed in Figure 1 in the absence of *C. albicans* DNA(curve a), a poor rhodamine B release was observed, indicating tight pore closure. In contrast, payload delivery was clearly found when DNA of *C. albicans* was added to the solution (curve b). After 30 min, approximately 90% of the total rhodamine B released was observed. This dye delivery was attributed to the displacement of the capping oligonucleotide **O2** from the solid to the solution due to the specific **O2**-genomic DNA hybridyzation (Scheme 1).

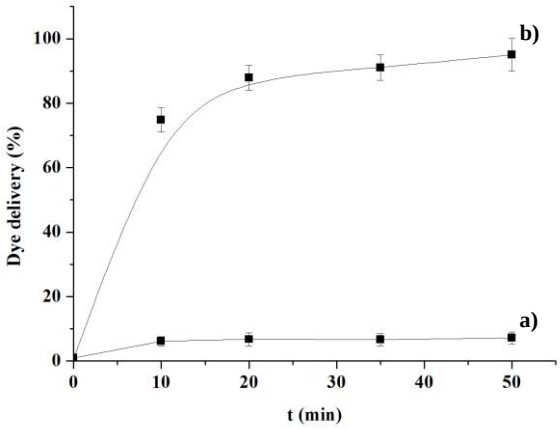

Figure 1. Release profile of rhodamine B from solid **S3** in the absence (a) and in the presence (b) of genomic DNA of *C. albicans* (0.1 μg mL^{-1}) in TRIS-HCl buffer (pH 7.5).

Selectivity studies. To prove the selectivity of the method, similar release experiments from **S3** were carried out in the presence of genomic DNA of *C. albicans, C. parapsilosis, C. glabrata, S. epidermidis, S. aureus, K. pneumoniae*, and *P. aeruginosa* at concentrations of 10^{-8} μg mL^{-1} (Figure 2). As shown in the figure, **S3** is selective to the presence of genomic DNA of *C. albicans*, whereas other species induced negligible cargo delivery.

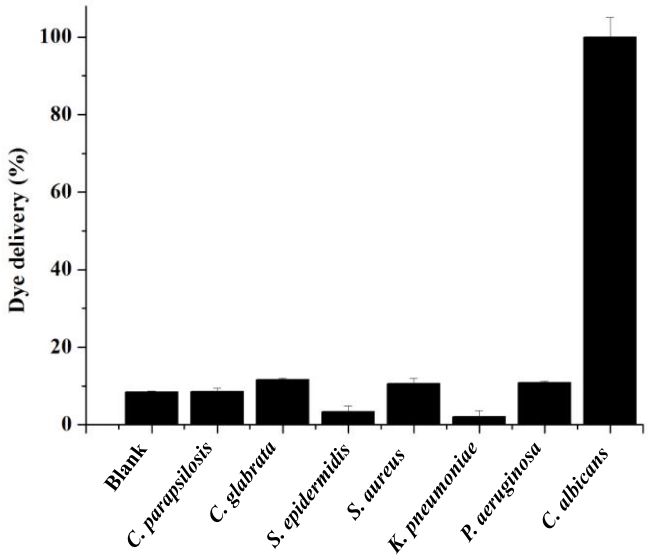

Figure 2. Release of rhodamine B from solid **S3** in the absence (blank) and in the presence of genomic DNA of C. albicans, C. parapsilosis, C. glabrata, S. epidermidis, Staphylococcus aureus, Klebsiela pneumonia, and Pseudomonas aeruginosa (10^{-8} μg mL^{-1}) in TRIS-HCl buffer (pH 7.5).

Detection of C. albicans DNA in yeast-containing samples. In a step forward, we were interested in validate the use of solid **S3** for *C. albicans* detection in samples inoculated with *C. albicans*. In a typical experiment, **S3** was immersed in hybridization buffer and spiked with *C. albicans* to reach a final concentration of 10^3 cfu mL^{-1}. Another **S3** piece was maintained in hybridization buffer as control. Following a similar procedure as before, supernatant fractions were obtained at scheduled times and the amount of rhodamine B measured. These experiments were carried out without any cell lysis pretreatment of the yeast culture. Nevertheless, Figure 3 clearly shows that **S3** remains tightly capped in buffer, yet a clear payload delivery is found in the presence of *C. albicans*. This observation might be explained taking into account that part of genomic DNA of *C. albicans* is released into the extracellular medium. In fact, it has been described that genomic DNA of *C. albicans* can be found in high concentrations in clinical samples

such as plasma, despite minimal presence of viable organisms present in the sample.[37] The absence of a pretreatment makes the procedure especially simple.

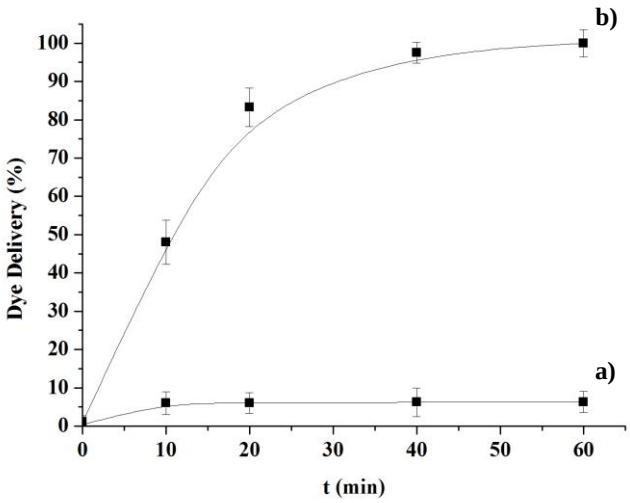

Figure 3. Release profile of rhodamine B from solid **S3** in the absence (a) and in the presence (b) *C. albicans* (10^3 cfu mL^{-1}) in TRIS-HCl buffer (pH 7.5).

Sensitivity studies. Following a similar approach to that described above, cargo delivery from **S3** was studied as a function of the amount of *C. albicans* cells (Figure 4). It was found that the delivered rhodamine B correlates with the different *C. albicans* CFU added, which is in agreement with the uncapping protocol involving a displacement of **O2** in the presence of the *C. albicans* cells. In these experimental conditions a lineal response in the 7-2x10^2 CFU mL^{-1} concentration range was observed. Moreover, a limit of detection (LOD) as low as 8 CFU mL^{-1} was determined for **S3** (Figure 4). This LOD is very similar to commercially available detection systems for *Candida* in the market such as the T2Candida panel in the T2Dx instrument (LOD = 1 CFU mL^{-1}) fromT2 Biosystems based in PCR (Lexington, Massachusetts). Having similar LODs, our system is easier, significantly faster (ca. 30 min compared to ca. 3-5 hours of the T2Dx instrument) and has the advantage that the signal and not the analyte is amplified (*vide infra*).

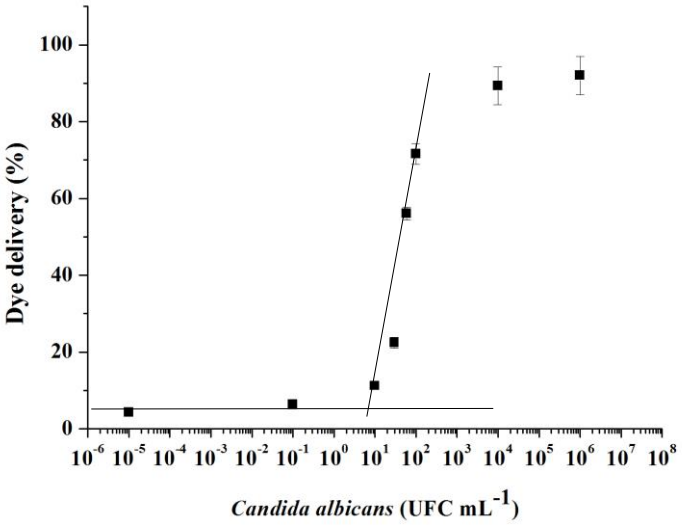

Figure 4. Release of rhodamine B from solid **S3** in the presence of different yeast concentrations of *C. albicans* in TRIS-HCl buffer (pH 7.5).

Amplification assay. One advantage of the use of gated materials in sensing applications is the observation of inherent signal amplification. As stated before, the recognition protocol (hybridization of **O2** with genomic DNA) is separated from the signalling event (dye delivery from the pores). This means that the sensing mechanism is independent of the stoichiometry of the formed host–guest complex and therefore, the event of **O2** hybridization with genomic DNA may be accompanied by the release of a fairly large number of cargo molecules. In terms of signal amplification, in our particular case and for a concentration of genomic DNA of 6.64 x 10^{-8} μg mL^{-1}, it was found that the number of dye molecules released is ca. 80,000 times that of the number of DNA molecules, which is a significant signal amplification. The estimation clearly shows the advantage of this gated material that does not need of pre-amplification procedures such as enzymatic signalling methods or PCR technology, to obtain a substantial signal.

Real sample determination. A step forward was taken and ability of the capped material **S3** for *C. albicans* detection in more competitive media was

tested. Delivery of rhodamine B from **S3** in the presence and absence of *C. albicans* at concentration of 10^3 cfu mL^{-1} was studied in typical fluids where *Candida* can be found such as cerebrospinal fluid (CSF), plasma and peritoneal fluid. As depicted in Figure S2, **S3** is able to detect *C. albicans* in these media; a negligible release (less than ca. 10-20%) in the absence of the yeast was found, whereas a marked delivery (ca. 90%) was observed when the fluids were spiked with 10^3 cfu mL^{-1} of *C. albicans*. These results agree with those obtained in buffered solutions.

Encouraged by these results, and a final step in our research, we were interested to validate the use of **S3** as a potential alternative to the current method for *C. albicans* detection. In a first step, standard procedures such as blood culture were used to determine the presence of C*. albicans* in 16 clinical samples from infected and non infected individuals from Hospital Universitari i Politècnic La Fe. In particular, for microbiological diagnosis, clinical samples were processed by blood culture using an automated system. *C. albicans* isolates were identified by phenotypic and biochemical characteristics, and proteomic profiling technology. In parallel, the same 16 samples were also analyzed using **S3**. To test each sample, a piece of **S3** was immersed in 700 µL of hybridization buffer and then 300 µL of the target sample was added. A control experiment with **S3** immersed in the same volume of hybridization buffer and containing 300 µL of a non-infected fluid (non infected cerebrospinal fluid, plasma or peritoneal fluid) was also performed. After 30 minutes at 25°C, release of rhodamine B was measured by fluorescence at 585 nm (λ_{exc} = 555 nm). Samples were considered positives when the fluorescence intensity at 585 nm was 3-fold higher than that of the control. As a typical result, Figure 5 shows the response (i.e. rhodamine B delivered) obtained for **S3** when in contact CSF infected with *C. albicans* (positive sample) and non infected (negative sample).

Despite its low sensitivity (50-60%), blood culture remains as the gold standard method to diagnose candidemia. Time to positivization of blood cultures varies between different species of *Candida* from 19-22 hours in *C. tropicalis* and *C. krusei* to 60-75 hours in species such as *Candida guillermondii* or *C. glabrata*, with a mean time of growth of 37.6 hours (data from 258 candidemia episodes at

Hospital Universitari i Politècnic La Fe). Once the blood culture is positive, it takes about 15 minutes to learn whether the causing agent of the blood stream infection is yeast with a Gram stain. However, final identification with traditional methods such as AuxaColorTM 2 (Bio-Rad, Marnes-la-Coquette France), Vitek® 2 YST ID card (bioMérieux, Marcy l'Etoile, France) or CHROMagarTM Candida (CHROMagar, Paris, France) takes around 24-48 hours. Some novel strategies to shorten this diagnostic period include Peptide Nucleic Acid Fluorescent In-situ Hybrydization (PNA-FISH) that it is performed from positive blood cultures in 90 minutes; direct MALDI-TOF (MALDI-TOF MS, Bruker Daltonik GmbH Leipzig, Germany; VITEK® MS, bioMérieux, Marcy l'Etoile, France) from the blood culture bottle in 30 minutes; multiplex acid nucleic testing like Filmarray platform (FA; BioFire, Salt Lake City, UT), a closed diagnostic system allowing high-order multiplex PCR analysis with automated readout of results in one hour directly from positive blood cultures or after a 12 hours incubation. Table 2 shows a comparison between the results obtained for the 16 samples using traditional blood culture procedures and with **S3**. In all cases, a complete coincidence was found between the hospital reference method and our procedure using gated mesoporous alumina, revealing the good response of solid **S3** to detect *C. albicans* in highly competitive real samples. Moreover, while blood culture protocols have a typical assay time of ca. 2 to 6 days, the results using **S3** can be obtained in ca. 30 min.

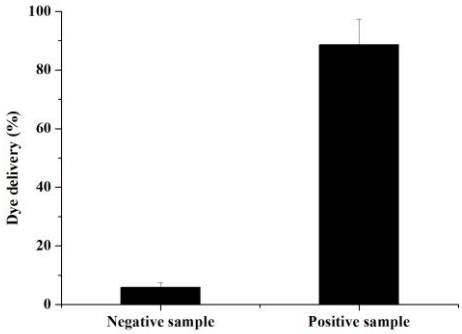

Figure 5. Detection of *C. albicans* in real cerebrospinal fluid samples : Release of rhodamine B from the nanoporous alumina gated material in the presence of cerebrospinal fluids infected with *C. albicans* (positive sample) and non infected (negative sample). The assay was performed in triplicate.

Table 2. Results of real samples analyzed by the reference and the proposed method (mycological culture and **S3** assay, respectively).

Type of Sample	# Sample	Reference method (mycological culture)[a]	Gated material (S3)[b]
Cerebrospinal fluid	**1**	-	-
	2	-	-
	3	-	-
	4	+	+
	5	+	+
	6	+	+
Blood	**7**	-	-
	8	-	-
	9	-	-
	10	+	+
	11	+	+
	12	+	+
Peritoneal fluid	**13**	-	-
	14	-	-
	15	-	-
	16	+	+
	17	+	+
	18	+	+

[a] Samples were considered positives when any C. albicans colony isolated in body fluids culture.

[b] Samples were considered positives when the fluorescence intensity at585 nm was 3-fold higher than that of the control.

Conclusions

Developent of new strategies for sensitive and rapid detection of *C. albicans* is of importance for survival in invasive candidiasis infections. In summary, we report here the preparation of oligonucleotide-capped nanoporous anodic alumina loaded with rhodamine B and its use for the detection of *C. albicans* in

real hospital samples in ca. 40 min from infected patients without previous culture growth or the use of amplification PCR techniques. The oligonucletide used as cap is a sequence of the coding region of the integrin-like alpha Int1p protein from *C. albicans*. In the presence of DNA of *C. albicans* a displacement of the capping oligonucleotide occurs, inducing pore opening and dye release. Besides **S3** shows a selective response to *C. albicans* and yet was unable to respond to the presence of *C. parapsilosis, C. glabrata, S. epidermidis, S. aureus, K. pneumoniae,* and *P. aeruginosa*. By this simple procedure a limit of detection as low as 8 CFU mL^{-1} was calculated. This LOD is very similar to other commercially available detection systems for *Candida*. However, showing similar LODs, our system is easier, significantly faster (an overall assay time of ca. 30 min compared to ca. 12 hours for PCR-based method or to ca. 37.6 hours for blood culture) and cost-effective, and has the advantage that it is not the analyte but the signal that is amplified. In addition, the **S3** capped material allowed an accurate and effective detection of *C. albicans* in different real samples from infected pacients. In conclusion, our reseach suggest that the use of gated materials having a specific biochemical recognition coupled to indicator delivery is an innovative strategy for the easy and quick detection of DNA sequences of pathogens. The proposed method is simple, portable, can be easily tuned via the use of different reporting molecules and may allow the development of simple tests, offering a great potential for clinical applications. In addition, such simple yet highly selective assay shows a high potential in its use in less developed areas of the world.

Aknowledgements

We thank the Spanish Government (projects MAT2015-64139-C4-1-R, TEC2015-71324-R and CTQ2014-52588-R (MINECO/FEDER)), the Generalitat Valenciana (project PROMETEOII/2014/047), Generalitat de Catalunya (2017 SGR 1527), ICREA Academia and Universitat Politècnica de Valencia – Instutito de Investigación Sanitaria la fe (CANDIGATE project) for support. A.R. thanks UPV for her predoctoral fellowship. S.S. thanks the Instituto de Salud Carlos III and the European Social Fund for the financial support “Sara Borrell” (CD16/000237).

References

1. J. Pemán, M. Salavert, G. Quindós, *Rev. Iberoam. Micol*., **2016**, *33*, 131–132.
2. G. P. Bodey, Candidiasis: pathogenesis, diagnosis, and treatment , 2nd Ed. Raven Press, New York (USA), **1993**.
3. H.A. Carneiro, A. Mavrakis, E. Mylonakis, *World J. Surg*., **2011**, *35*, 2650–2659.
4. A. Bacconi, G. S. Richmond, M.A. Baroldi, T.G. Laffler, L.B. Blyn, H.E. Carolan, M.R, Frinder, D.M. Toleno, D. Metzgar, J.R. Gutierrez, C. Massire, *J. Clin. Microbiol*., **2014**, *52*, 3164–3174.
5. J. Guinea, O. Zaragozá, P. Escribano, E. Martin–Mazuelos, J. Pemán, F. Sánchez–Reus, M. Cuenca– Estrella, *Antimicrob. Agents Chemother*., **2014**. *58*, 1529–1537.
6. M. Cuenca–Estrella, P.E. Verweij, M.C, Arendrup, S. Arikan–Akdagli, J. Bille, J.P. Donnelly, H.e. Jensen, C. Lass–Flörl M. D. Richardson M. Akova M. Bassetti T. Calandra E. Castagnola O. A. Cornely J. Garbino A. H. Groll R. Herbrecht W. W. Hope B. J. Kullberg O. Lortholary W. Meersseman G. Petrikkos E. Roilides C. Viscoli A. J. Ullmann, *Clin. Microbiol. Infect.,* **2012**, *9*, 18, 9–18.
7. J. Prattes, S. Heldt, S. Eigl, M. Hoenigl, *Curr. Fungal Infect. Rep*., **2016**, *10*, 43–50
8. I. Willner, B. Shlyahovsky, M. Zayats, B. Willner, *Chem. Soc. Rev*., **2008**, *37*, 1153–1165.
9. F. Sancenón, Ll. Pascual, M. Oroval, E. Aznar, R. Martínez-Máñez, *Chemistry Open,* **2015**, *4*, 418-437.
10. E. Aznar, M. Oroval, L. Pascual, J.R. Murguía, R. Martinez-Máñez, F. Sancenón, *Chem. Rev*., **2016***, 116*, 561–718.
11. E. Bringas, Ö. Köysüren, D.V. Quach, M. Mahmoudi, E. Aznar, J.D. Roehling, M.D. Marcos, R. Martínez-Máñez, P. Stroeve, *Chem. Commun*., **2012**, *48*, 5647–5649.
12. E. Aznar, C. Coll, M.D. Marcos, R. Martínez-Máñez, F. Sancenon, J. Soto, E. Ruiz, *Chem. Eur. J.,* **2009**, *15*, 6877–6888.
13. G. Bayramoglu, V.C. Ozalp, U. Dincbal, M.Y. Arica, *ACS Biomater. Sci. Eng*. **2018**, *4*, 1437−1444.
14. S. Dehghani, N. M. Danesh, M. Ramezani, M. Alibolandi, P. Lavaee, M. Nejabat, K. Abnous, S. M. Taghdisi, *Anal. Chim. Acta*, **2018**, doi.org/10.1016/j.aca.2018.05.003
15. X. He, Y. Zhao, D. He, K. Wang, F. Xu, J. Tang, *Langmuir* **2012**, *28*, 12909−12915.
16. a) A. Ribes, E. Xifré-Perez. E. Aznar, F. Sancenón, T. Pardo, Ll. F. Marsal, R. Martínez-Máñez, *Sci. Rep.,* **2016**, *6*, 38649-38658. b) A. Ribes, E. Aznar, A. Bernardos, M.D. Marcos, P. Amorós, F. Sancenón, R. Martínez-Máñez, *Chem. Eur. J.,* **2017**, *23*, 8581–8584
17. A.Ribes. S. Santiago-Felipe, A. Bernardos, M.D. Marcos, T. Pardo, F. Sancenón, R. Martínez-Máñez, E. Aznar, *ChemistryOpen,* **2017**, *6*, 653–659.
18. E. Climent, R. Martínez-Máñez, F. Sancenón, M.D. Marcos, J. Soto, A. Maquieira, P. Amorós, *Angew. Chem*., **2010**, *122*, 7439–7441.
19. E. Climent, L. Mondragón, R. Martínez-Máñez, F. Sancenón, M.D. Marcos, J.R. Murguia, P. Amorós, K. Rurack, E. Pérez-Payá, *Angew. Chem. Int. Ed*., **2013**, *52*, 8938–8942.

20. Ll. Pascual, I. Baroja, E. Aznar, F. Sancenón, M.D. Marcos, J.R. Murguia, P. Amoros, K. Rurack, R, Martinez-Máñez, *Chem. Comm*., **2015**, *51*, 1414–1416.
21. a) G. Rajeev, B. Prieto Simon, L.F. Marsal, N.H. Voelcker, *Materials*, **2018**, *7*, 1700904; b) A. Santos, M.J. Deen, L.F. Marsal, *Nanotechnology*, **2015**, *26*, 042001; c) E. Xifre-Perez, S. Guaita-Esteruelas, M. Baranowska, J. Pallares, L. Masana, L.F. Marsal, *ACS Appl. Mater. Interfaces*, **2015**, *7*, 18600-18608.
22. L. Pla E. Xifré-Pérez À. Ribes E. Aznar M.D. Marcos, Ll. F. Marsal, R. Martínez-Máñez F. Sancenón, *ChemPlusChem*, **2017**, *82*, 467–467.
23. Y. Chen, A. Santos, W. Wang, C. Wang, D. Losic, *ACS Appl. Mater. Interfaces*, **2015**, *7*, 19816–19824.
24. T. Kumeria, A. Santos, M.M. Rahman, J. Ferré-Borrull, L.F. Marsal, D. Losic, *ACS Photonics,* **2014**, *1*, 1298-1306.
25. L. Vojkuvka, L. F. Marsal, J. Ferré-Borrull, P. Formentin, J. Pallarés, *Superlattices Microstruct*. **2008**, *44*, 577–582.
26. A. De la Escosura-Muñiz, A. Merkoçi, *ACS Nano*, **2012**, *6*, 7556–7583.
27. T. Kumeria, M. Rahman, A. Santos, J. Ferré-Borrull, L.F. Marsal, D. Losic,. *Appl. Mater. Interfaces,* **2014**, 6, 12971−12978.
28. A. Santos, T. Kumeria, D. Losic, Materials, **2014**, 7, 4297–4320.
29. R. Urteaga, C. L. Berli, *In Nanoporous Alumina. Fabrication, Structure, Properties and Applications*; 1st Ed. Springer International Publishing, 249-269, **2015**.
30. J. Ferré-Borrull, J. Pallarès, G. Macías, L.F. Marsal, L. F. Nanostructural Engineering of Nanoporous Anodic Alumina for Biosensing Applications. *Materials*, **2014**, *7*, 5225–5253.
31. D. Gong, V. Yadavalli, M. Paulose, M.; Pishko, C.A. Grimes, *Biomed. Microdevices*, **2003**, *5*, 75–80.
32. L.F. Marsal, L. Vojkuvka, P. Formentin, J. Pallarés, J. Ferré-Borrull, *Optical Materials*, 2009, *31*, 860.
33. M. Baranowska, A.J. Slota, P.J. Eravuchira, G. Macias, E. Xifré-Pérez, J. Pallarès, J. Ferré-Borrull, L.F. Marsal, *Colloids. Surf. B Biointerfaces*, **2014**, *122*, 375–383.
34. Y.H. Lim, D.H. Lee, *J. Microbiol*., **2000**, 105–108.
35. C. Gale, D. Finkel, N. Tao, M. Meinke, M. McClellan, J. Olson, K. Kendrick, M. Hostetter, *Proc. Natl. Acad. Sci.,* **1996**, *93*, 357–361.
36. M. Kasai, A. Francesconi, R. Petraitiene, V. Petraitis, A. M. Kelaher, H. Kim, J. Meletiadis, T. Sein,J. Bacher, T. J. Walsh, *J. Clin. Microbiol.*, **2006**, *44*, 143–150.

SUPPLEMENTARY INFORMATION

A rapid, selective and sensitive probe based in oligonucleotide-capped nanoporous alumina for the detection of infection produced by fungi Candida albicans

Àngela Ribes, Elena Aznar, Sara Santiago-Felipe, Elisabet Xifre-Perez, Maria Angeles Tormo-Maria, Javier Pemán , Lluis F. Marsal and Ramón Martínez-Máñez

FESEM images

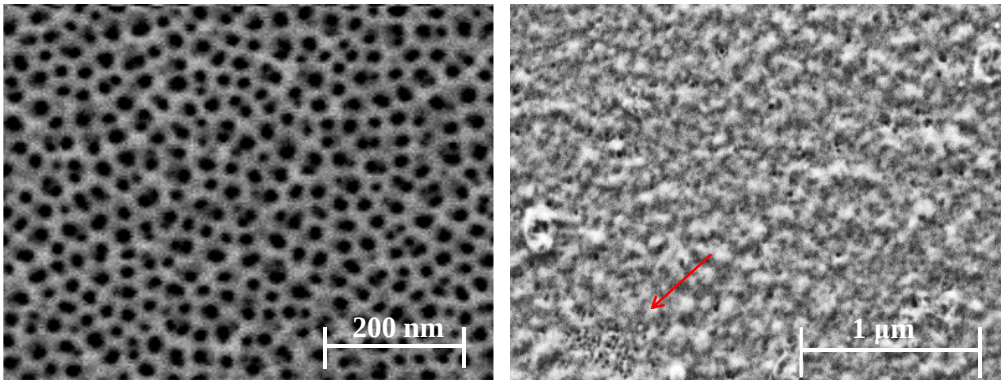

Figure S1. *Representative FESEM image of a) NAA support and b) solid* ***S3.*** *The arrow in figure b, confirmed the preservation of the nanoporous structure in the final device.*

Real media determination

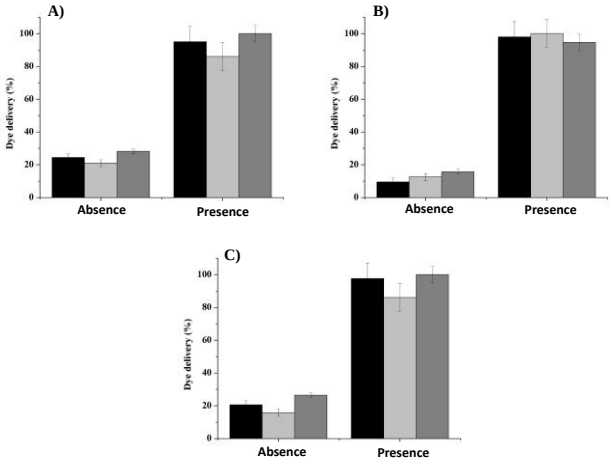

Figure S2. *Release of rhodamine B from solid* ***S3*** *in absence/presence of C. albicans in different organic body fluids, A) cerebrospinal, B) plasma and C) peritoneal. In all media three independent assays with three replicas were carried out.*

7. Design of oligonucleotide-capped mesoporous silica nanoparticles for the detection of miRNA-145 by duplex and triplex formation

Design of oligonucleotide-capped mesoporous silica nanoparticles for the detection of miRNA-145 by duplex and triplex formation

*Àngela Ribes[1,2,3,+], Sara Santiago-Felipe[2,1,3,+], Anna Aviño[2, 4] Vicente Candela-Noguera[1,2,3,5], Elena Aznar[2,1,3,5],Ramón Eritja[2, 4 *], Felix Sancenón[1,2,3,5] and Ramón Martínez-Máñez[1,2,3,5,*]*

[1] Instituto Interuniversitario de Investigación de Reconocimiento Molecular y Desarrollo Tecnológico (IDM). Universitat Politècnica de València, Universitat de València, Departamento de Química, Universitat Politècnica de València, Camino de Vera s/n, 46022, Valencia, Spain.

[2] CIBER de Bioingeniería, Biomateriales y Nanomedicina (CIBER-BBN), Spain.

[3] Unidad Mixta de Investigación en Nanomedicina y Sensores. Universitat Politècnica de València, Instituto de Investigación Sanitaria La Fe, Valencia, Spain

[4] Institute for Advanced Chemistry of Catalonia (IQAC), CSIC, Jordi Girona 18-26, 08034, Barcelona, Spain

[5] Unidad Mixta UPC-CIPF de Investigación en Mecanismos de Enfermedades y Nanomedicina. Universitat Politècnica de València, Centro de Investigación Príncipe Felipe, Valencia, Spain

[+] These authors contributed equally

Submitted

Abstract

The development of new strategies to detect microRNAs (miRNAS) has become an important challenge in the biomedical field. We report herein the use of oligonucleotide-gated silica nanoparticles for the detection of miRNA-145. In the proposed design, mesoporous silica nanoparticles (MSNs) are loaded with a fluorescent reporter (rhodamine B) and pores are blocked by specific DNA oligonucleotides. The opening of the gated system and dye delivery is selectively controlled by DNA-miRNA recognition. Moreover, the use of DNA capture probes able to form duplex or triplex structures between target miRNA and the complementary oligonucleotides has been studied. By this simple procedure a limit of detection as low as 0.25 pM was found for miRNA. The method was successfully applied to detect miRNA-145 in serum samples, which demonstrates the high potential of these capped materials to detect miRNA for diagnostic purposes.

KEYWORDS: Mesoporous silica materials, molecular gates, miRNA-145, biosensor, triplex

Introduction

MicroRNAs (miRNAs) are a class of small (19-25 nucleotides) non-coding RNA with important roles in gene regulation. These post-transcriptional gene regulators were described for the first time in 1993 and, at this time, a large number of them have been identified. According to the miR database, 28645 miRNA entries in 283 species have been identified so far (http://microrna.sanger.ac.uk/) from which 2661 are unique human miRNAs sequences. miRNAs play an important role in many biological processes including development, cell proliferation, differentiation and apoptosis.[1] Alterative expression of miRNAs has been associated with a number of diseases. Thus, detection of circulating miRNAs present in physiological fluids can provide valuable diagnostic and prognostic data.[2] However, measuring miRNAs is a very challenging task due to their intrinsic properties such as short length, high

homologous sequences, low abundance and large variation in base composition and secondary structures.[3] miRNAs are often identified by Northern blotting, microarrays and RT-qPCR, however the practical application of these methods are limited due to their time-consuming and costly labeling techniques, and the expensive and sophisticated instrumental requirements.[4,5] In the recent years, and in addition to these traditional approaches, a large number of protocols involving non-canonical DNA structures and novel nanomaterials have been deployed.[3]

On that regard, the development of efficient and reliable detection strategies for rapid, sensitive and selective identification of miRNAs is of importance. Current works have shown that biosensors technology can offer rapid results with high sensitivity and minimal sample preparations. In this scenario some studies have been published recently based on miRNAs detection by electrochemical or optical biosensors.[4,6-8] Specifically, those based on the hybridization of target miRNA with a DNA probe used as recognition element, have provided excellent characteristics for clinical diagnosis.[9] All these described methods rely on duplex formats between the miRNA and the complementary DNA probe. Nevertheless, other formats such as triple-helix formation based on Hoogsteen base pairing to the Watson-Crick duplex are also interesting alternatives.

Triplex can only be formed at specific polypurine-polypyrimidine sequences, which are widespread within the human genome, especially at promoter regions.[10,11] Previous works have reported the triplex-stabilizing properties of 8-aminopurines and the use of parallel and antiparallel tail-clamps to increase the efficiency of triplex formation with structured DNA and RNA targets.[12,13] This triplex affinity capture strategy has been successfully applied for the detection of Listeria mRNA and miRNA-145 using a SPR biosensor.[14,15]

From a different point of view, in the last years nanomaterials for sensing applications have played a great role due to their capacity to provide rapid, simple and sensitive responses to target analytes. Among nanomaterials used in sensing

protocols, mesoporous silica nanoparticles (MSNs) have been widely employed due to their remarkable properties such as large load capacity, biocompatibility, high inner surface area and the possibility to easily modify their surface. MSNs can be functionalized with a wide range of different (bio)molecules than act as "molecular gates" to obtain hybrid organic-inorganic supports for the design of stimuli-responsive systems.[16] In particular, this type of materials can be used as probes when the support is loaded with a dye and the capping mechanism is designed in a way that only a target analyte is able to trigger the delivery of the cargo.[17] Among the different biomolecules that could act as caps, nucleic acids (DNA or aptamers) have shown excellent performances in sensing applications.[18-20] However, as far as we know, the use of DNA-capped silica materials for the detection of miRNAs has not yet been reported.

Based on these concepts, we report herein a new strategy to detect miRNA-145. miRNA-145 is related with several cardiovascular diseases, atherosclerosis and hypertension, and also acts as a tumor suppressor, showing a clear relationship between its expression and clinic pathological findings in human colorectal tumors.[21.22] Several sensing systems based in gated MSNs loaded with a fluorophore (rhodamine B) and capped with different oligonucleotide probes able to form duplex or triplex structures with miRNA-145 are reported. Best results were found when the capping oligonucleotide used was designed to form an antiparallel triplex, reaching a limit of detection in the low picomolar range. In addition, this direct detection method is compatible with the presence of serum in the samples.

Material and methods

***General techniques*.** Powder X-ray diffraction (PXRD), transmission electron microscopy (TEM), N_2 adsorption-desorption, thermogravimetric analysis (TGA), dynamic light scattering (DLS) and fluorescence spectroscopy were employed to characterize the synthesized materials. PXRD measurements were performed on a D8 Advance diffractometer using Cu Kα radiation (Philips, Amsterdam, The Netherlands). Thermogravimetric analyses were carried out on a TGA/SDTA 851e

balance (Mettler Toledo, Columbus, OH, USA), using a oxidizing atmosphere (air, 80 mL min^{-1}) with a heating program consisting of a gradient of 393-1273 ºK at 10°C min^{-1}, followed by an isothermal heating step at 1273°C for 30 min. TEM images were obtained with a 100 kV CM10 microscope (Philips). N_2 adsorption-desorption isotherms were recorded with a Tristar II Plus 2.03 automated adsorption analyzer (Micromeritics, Norcross, GA, USA). The samples were degassed at 120°C in vacuum overnight. The specific surface areas were calculated from the adsorption data in the low pressure range using the Brunauer, Emmett and Teller (BET) model.[23] Pore size was determined following the Barret, Joyner and Halenda (BJH) method.[24] Dynamic light scattering was used to obtain the particle size distribution of the different solids, using a Zetasizer Nano (Malvern Instruments, Malvern, UK). For the measurements, samples were dispersed in distilled water. Data analysis was based on the Mie theory using refractive indices of 1.33 and 1.45 for the dispersant and mesoporous silica nanoparticles, respectively. An adsorption value of 0.001 was used for all samples. Variation of this adsorption value did not significantly alter the obtained distributions. Measurements were performed in triplicate. Fluorescence spectroscopy measurements were carried out on a Synergy H1 microplate reader (BioTek, Winooski, VT, USA).

Chemicals. Tetraethylorthosilicate (TEOS), n-cetyltrimethylammonium bromide (CTABr), sodium hydroxide (NaOH), triethylamine (TEA), (3-aminopropyl)triethoxysilane, rhodamine B, tris(hydroxymethyl)aminomethane (TRIS), and hydrochloric acid were purchased from Sigma-Aldrich Química (Madrid, Spain) and used as received.

Synthesis of oligonucleotides Oligonucleotides used in this study are listed in **Table 1** and they were prepared using phosphoramidite solid phase synthesis protocols as described peviously.[12-15] Briefly, oligonucleotides were asembled on controlled pore glass (CPG) supports by successive addition of the appropriate phosphoramidites using an autmomated Applied Biosystems 394 DNA synthesizer (Foster City, CA, USA). The addition of 8-amino-2'-deoxyguanosine was done

using the corresponding 8-amino-2'-deoxyguanosine phosphoramidite protected with two dimethylformamidino groups obtained from commercial sources (Berry Associates, USA). The parallel clamps were assembled using standard 3'-phosphoramidites for the polypurine stretch and reversed C and T 5'-phosphoramidites and 5'-reversed-C solid support for the C,T-Hoogsteen strand. After the assembly of the sequences, the supports were treated with concentrated ammonia (overnight, 55ºC) except for the sequences carrying 8-amino-dG that were treated with 0.1M mercaptoethanol in concentrated ammonia (24 hr, 55 ºC).[12] RNA oligonucleotides were prepared by standard solid phase protocols using the tert-butyldimethylsilyl group for the protection of the 2'-OH group. Oligonucleotides were purified by Glen-PackTM DNA/RNA purification cartridges (Glen Research, USA) and analyzed by mass spectrometry (Table S2, supplementary section).

Table 1. Sequences of the oligonucleotides prepared in this work.

Code	Name	Sequence (5'-3')
O1	Compl duplex	5'-AGGGATTCCTGGGAAAACTGGAC-3'
O2	Antiparallel-8AG Clamp	5`-AG*G*G*ATTCCTGGGAAAA-TTTT-AAAAGGG-3'
O3	Antiparallel Clamp	5'-AGGGATTCCTGGGAAAA-TTTT-AAAAGGG-3'
O4	Parallel-8AG Clamp	5'-AG*G*G*ATTCCTGGGAAAA-TTTT-3'-3'TTTTCCC-5'
O5	Parallel Clamp	5'-AGGGATTCCTGGGAAAA-TTTT-3'-3'TTTTCCC-5'
O6	miRNA-145	5'-GUCCAGUUUUCCCAGGAAUCCCU-3'
O7	miRNA-141	5'-UAACACUGUCUGGUAAAGAUGG-3'
O8	miRNA-let 7A	5'-UGAGGUAGUAGGUUGUAUAGUU-3'

Synthesis mesoporous silica nanoparticles (MSNs). For the synthesis of mesoporous silica nanoparticles n-cetyltrimethylammoniumbromide (CTABr, 1.00 g, 2.74 mmol) was first dissolved in 480 mL of deionized water. 3.5 mL of NaOH 2.00 M in deionized water was added to the CTABr solution, followed by adjusting the solution temperature to 80°C. TEOS (5 mL, 25.7 mmol) was then added dropwise to the surfactant solution. The mixture was allowed stirred for 2 h to give a white precipitate. Finally the solid product was centrifuged, washed with

deionized water and dried at 60°C (as-synthesized). To prepare the final porous material, the as-synthesized solid was calcined at 550°C using oxidant atmosphere for 5 h in order to remove the template phase.

Synthesis of S1. In a typical synthesis, calcined MSNs (200 mg) and rhodamine B (766.4 mg, 0.16 mmol) were suspended in CH_3CN (10 mL) and stirred at room temperature for 24 h. Then (3-aminopropyl)triethoxysilane (292.5 µl, 1 mmol) was added, and the final mixture was stirred at room temperature for 5.5 h. The resulting pink solid (**S1**) was isolated by filtration, washed with CH_3CN (5 mL) and dried at 38°C for 18 h.

Synthesis of (S2-S6). For the preparation of the sensing materials, 500 µg of solid **S1** were capped by adding an aqueous solution (100µM) of the corresponding oligonucleotide (**O1**-**O5**) following the data shown in **Table 2**. Volume was completed to 500 µL with hybridization buffer (20 mM Tris-HCl, 37.5 mM $MgCl_2$, pH 7.5) and the mixtures were stirred 60 minutes at 37°C. The resulting materials were isolated by centrifugation, washed with hybridization buffer to eliminate residual dye and free oligonucleotides and dried at vacuum.

Table 2. Volume of the oligonucleotides used to synthesize **S2-S6**.

Solid	**S2**	**S3**	**S4**	**S5**	**S6**
Oligonucleotide	**O1**	**O2**	**O3**	**O4**	**O5**
Volume (µL)	100	20	10	25	25

Assay protocol. The response of solids **S2**-**S6** was tested in the presence of miRNA-145 by measuring the emission of rhodamine B dye delivered from the pores to the solution. In a typical experiment, 500 µg of each solid were suspended with 400 µL of hybridization buffer and separated in 2 aliquots of 200

µL. Then, 10 µL an aqueous solution of miRNA-145 (100 µM) were added to one of the aliquots whereas 10 µL of water were added to the other aliquot. Both samples were completed to a final volume of 1000 µL of hybridization buffer. Suspensions were stirred at 37°C and, at certain times, fractions were taken and centrifuged 2 min at 10000 rpm to separate the solid. Cargo release was then determined by measuring the rhodamine B fluorescence in the supernatant at 585 nm (λexc = 555 nm).

Calibration curve. The response of materials **S2**-**S6** to different concentrations of miRNA-145 was studied. For that, 500 µg of each solid was suspended in 1000 µL of hybridization buffer and separated into 10 aliquots of 100 µL. Different amounts of miRNA-145 standard solution were added to each aliquot and the volume was completed to 1000 µL with hybridization buffer. All samples were stirred at 37°C for 30 min and centrifuged 2 min at 10000 rpm to separate the solid. The fluorescence of the released rhodamine B was then measured at 575 nm (λexc 555 nm).

Selectivity studies with S2-S6. In order to carry out these experiments, 500 µg of each solid were suspended in 500 µL of hybridization buffer and 6 aliquots of 100 µL each one were separated. The solid suspensions were spiked with 5 µL of 10 µM solution of miRNA-145, miRNA-Let7A and miRNA-141 in order to obtain a final concentration of 0.1 µM of each analyte. One fraction was treated as control by adding 10 µL of water. In all cases volume was completed to 1 mL with hybridization buffer. All samples were stirred at 37°C for 30 min and centrifuged 2 min at 10000 rpm to separate the solid. The fluorescence of the released rhodamine B was then measured at 575 nm (λ_{exc} = 555).

Real sample experiments. In order to study the applicability of the method in a more realistic context, **S2** and **S4** performance was tested in human serum samples. For that, 500 µg of each solid were suspended in 1980 µL of human serum and separated in 2 aliquots of 990 µL. Then, 10 µL of miRNA-145 (100 µM) were added to one of the fractions whereas 10 µL of water were added to the

other aliquot. Suspensions were stirred at 37°C for 30 min, centrifuged 2 min at 10000 rpm to separate the solid, and the fluorescence of the released rhodamine B was measured.

Results and discussion

***Preparation and characterization of the sensing supports*.** MSNs with a diameter of ca. 100 nm were selected as inorganic scaffolds and pores were loaded with a fluorophore (rhodamine B). This type of reporter has been extensively used in gated materials for the detection of several types of analytes including proteins, small molecules and genomic sequences [17-20]. The external surface was functionalized with (3-aminopropyl)trimethoxysilane, to yield **S1**. Aminopropyl moieties are partially charged at a neutral pH and are known to display electrostatic interactions with negatively charged oligonucleotides [18, 19]. Based on this, addition of oligonucleotides **O1-O5** to solution of **S1** yielded the capped solids **S2-S6**. It was expected that in the presence of miRNA145, the capping oligonucleotide will be displaced to form a hibridized structure with miRNA145, allowing the release of the entrapped dye as depicted in Scheme 1.

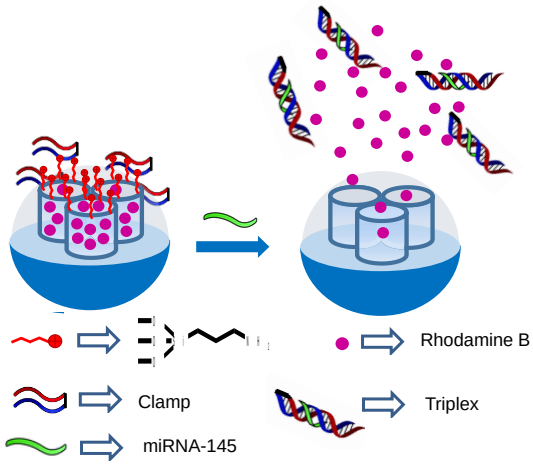

Scheme 1. Representation of the gated materials capped with oligonucleotides. Delivery of the entrapped rhodamine B was selectively observed in the presence of miRNA-145 via formation of duplex or triplex structures.

The starting MSNs and the synthetized solids **S1**-**S6** were characterized following standard techniques, including powder X-ray diffraction (PXRD), transmission electron microscopy (TEM), N_2 adsorption–desorption isotherms, thermogravimetric analysis (TGA), and dynamic light scattering (DLS). PXRD and TEM carried out on calcined MSNs clearly showed the presence of a mesoporous structure that persisted in solids **S1**-**S6** regardless of the loading of the porous with rhodamine B, further functionalization with (3-aminopropyl)trimethoxysilane and capping with the oligonucleotides **O1**-**O5** (see Figure S1). In particular, PXRD pattern of the as-synthesized MSNs (Figure S1, curve a) showed four low-angle reflections typical of a hexagonal array, indexed as (100), (110), (200), and (210) Bragg peaks. A significant displacement of the (100) peak in the PXRD pattern of the calcined MSNs is showed in curve b, related to a cell contraction (5Å) due to the condensation of silanol groups during calcination. Curve c and d correspond to the XRD pattern of **S1** and **S3**. A decrease of the intensity of the (100) peak and a broadening of the (110) and (200) reflections was observed, related to a loss of contrast. Results for solids **S2**, **S4**, **S5** and **S6** were similar to that for **S3**. BET specific surface area, pore volume and pore size were calculated from de N_2 adsorption-desorption measurements.[23,24] For the starting calcined MSNs a value of BET specific surface of 1027.53 $m^2\ g^{-1}$ was obtained, while for **S1** a decrease of the specific surface was observed (278.21 $m^2\ g^{-1}$), which is agreement with the presence of the rhodamine B dye inside the pores and surface functionalization (see Figure S2 and Table S1 in the Supporting Information). The size of the nanoparticles was determined by dynamic light scattering (DLS) studies. Diameters of 105.7, 141.8, 278.6, 275.9, 289.8, 296.9 and 295 nm were found for starting calcined MSNs, **S1**, **S2**, **S3**, **S4**, **S5** and **S6**, respectively, showing a progressive diameter increase in each functionalization step from calcined MSNs to final sensing solids **S2**-**S6** (see Figure S3 in the Supporting Information). Moreover, the content of 3-aminopropyl moieties, rhodamine B, **O1**, **O2**, **O3**, **O4** and **O5** in the different prepared solids was calculated from thermogravimetric analysis (Table 3).

Table 3. Contents (mmol mg^{-1}) of 3-aminopropyl, rhodamine B, **O1, O2**, **O3**, **O4** and **O5** in the different prepared solids.

	Rhodamine B	3-aminopropyl	O1	O2	O3	O4	O5
S1	$6.86 \cdot 10^{-3}$	$5.90 \cdot 10^{-2}$	-	-	-	-	-
S2	$2.90 \cdot 10^{-3}$	$5.70 \cdot 10^{-2}$	$2.50 \cdot 10^{-4}$	-	-	-	-
S3	$2.57 \cdot 10^{-3}$	$5.70 \cdot 10^{-2}$	-	$2.20 \cdot 10^{-4}$	-	-	-
S4	$3.57 \cdot 10^{-6}$	$5.80 \cdot 10^{-2}$	-	-	$1.05 \cdot 10^{-4}$	-	-
S5	$2.43 \cdot 10^{-6}$	$5.90 \cdot 10^{-2}$	-	-	-	$1.93 \cdot 10^{-4}$	-
S6	$1.83 \cdot 10^{-6}$	$6.00 \cdot 10^{-2}$	-	-	-	-	$2.58 \cdot 10^{-4}$

Synthesis of oligonucleotide capture probes for duplex and triplex formation. Based on our previous work on triplex-affinity capture of miRNA-145 for SPR detection,[15] several DNA probes carrying a complementary sequence to the polypyrimidine track (5'-UUUUCCC-3') of miRNA-145 were prepared (Table 1, Scheme 2). The complementary sequence (**O1**, duplex) is a 23-bases long oligonucleotide designed to form the full 23-bases long duplex (Scheme 2). The antiparallel clamps (**O2**, **O3**) contain a complementary sequence of 17 bases followed by a tetrathymidine loop and the reverse Hoogsteen sequence (5'-AAAAGGG-3', Scheme 2).

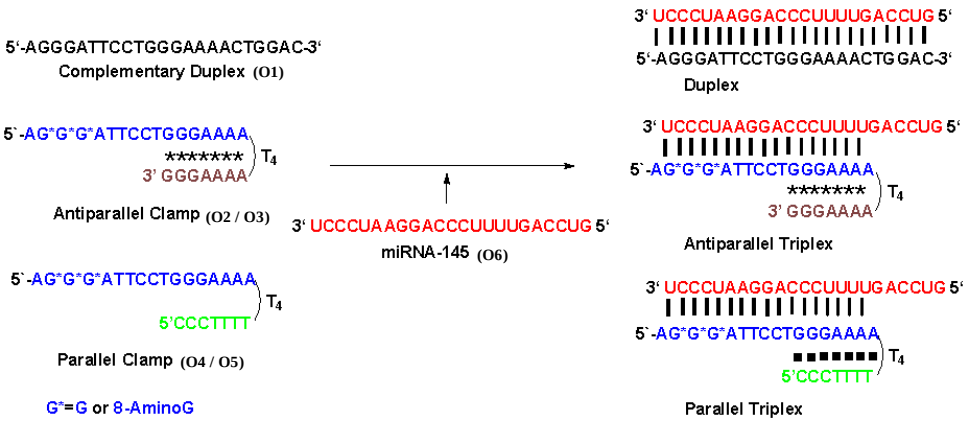

Scheme 2. Schematic representation of binding of miRNA-145 with Compl duplex and Antiparallel and Parallel Clamps to form duplex and Antiparallel and Parallel triplex.

Oligonucleotide **O2** carries three modified 8-aminoguanine residues replacing 3 guanines (see Table 1). It has been described that the change of guanine by 8-aminoguanine may increase the stability of the antiparallel triplex as shown in thermal denaturation studies.[25] These oligonucleotides (**O2**, **O3**) are designed to form an antiparallel triplex with miRNA-145. The parallel clamps (**O4**, **O5**) contain the same complementary sequence of 17 bases followed by a tetrathymidine loop and the Hoogsteen sequence (3'-TTTTCCC-5'). The Hoogsteen sequence has the opposite polarity to the Watson-Crick sequence and has been characterized by denaturation studies.[15] Thus, these oligonucleotides (**O4**, **O5**) are able to form a parallel triplex with miRNA-145. Oligonucleotide clamp **O4** carries also the three modified 8-aminoguanine residues because it has been described that parallel triplexes are stabilized by the 8-amino group of the guanine [12]. All together, these DNA capture probes will show whether the formation of parallel or antiparallel triplex is advantageous or not in the capture of the target microRNA and subsequent release of the dye.

We also expect to answer whether the stabilization properties of triplex of 8-aminopurines observed in solution is maintained or not in the capture of the target miRNA on the surface of mesoporous materials.

Release experiments.

As an example, Figure 1 shows the delivery kinetics profile of rhodamine B from solid **S4** in the presence and in the absence of miRNA-145. In the absence of miRNA-145 (curve a), a poor rhodamine B release (less than 10% in one hour) was observed, indicating tight pore closure. In contrast, when miRNA-145 was present in the solution, the delivery of the dye was induced due to the displacement of the capping oligonucleotide from the nanoparticle to the solution (curve b).

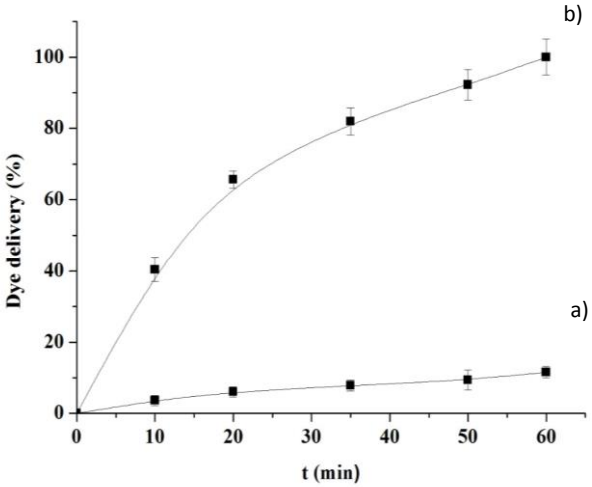

Figure 1. Release profile of rhodamine B from solid **S4** in the absence (a) and the presence (b) of miRNA-145.

A similar response was observed for solids **S2**, **S3**, **S5** and **S6**, showing a selective pore opening and dye delivery regardless the recognition between the oligonucleotide and miRNA-145 formed a duplex or a triplex structure (see Figure S-4 in the ESM). As depicted in Figure S-4, dye delivery from solids capped with oligonucleotides designed to form an antiparallel triplex (**S3** and **S4**), showed better performance and a slightly faster response to the presence of miRNA-145. In addition, in the case of solids **S3** and **S4**, a flat release curve was observed in the absence of miRNA-145 (curves a), indicating a more stable pore closure. These

differences are an indication of the efficiency of triplex or duplex formation, as the release of the dye is caused by the displacement of the capped oligonucleotide from the surface due to triplex or duplex formation. Antiparallel triplexes shaped when using solids **S3** and **S4**, can be more rapidly formed than duplexes and parallel triplexes. Also, it is important to notice than duplex probe in **S2** is 23 base pairs long while the triplex probes are only 17 base pairs long. Despite that, antiparallel triplexes are formed more efficiently than duplex and parallel triplex. The more efficient release of the antiparallel triplexes (solids **S3** and **S4**) may be due to the fact that antiparallel tail-clamps have the reversed Hoogsteen duplex structure already formed before the addition of the target RNA. This may facilitate the capture of miRNA oligonucleotide to form the corresponding antiparallel triplex. The formation of parallel triplexes needs the protonation of cytosines that occur at acid pH [26]. We have analyzed the release of parallel triplex (solids **S5** and **S6**) at pH 5.5 but we were unable to observe any improvement at this pH. On the other hand, no significant differences are observed with the presence of the 8-aminoguanine residue, indicating that the higher stability of the triplex observed in thermal denaturation studies [12, 25] does not increase the efficiency of dye release in the present system.

Anlytical performance: sensitivity and specificity studies.

To assess the sensitivity of the method, the response of **S2-S6** to different concentrations of miRNA-145 was studied. It was found that the amount of delivered rhodamine B was proportional to miRNA-145 concentration in all cases, which is in agreement with the uncapping protocol detailed above (see Figure S-5 in the ESM). Results of the sensitivity obtained with all the sensing solids are displayed in Table 4. A limit of detection of 2.5 pM, 5.0 pM and 8.0 pM was calculated for duplex (solid **S2**), parallel triplex (solid **S5**) and parallel-8Ag triplex (solid **S6**), respectively, whereas antiparallel (solid **S3**) and antiparallel-8Ag triplex (solid **S4**) exhibited more than 10 times lower LODs (0.30 pM and 0.25 pM, respectively). The higher sensitivity of the solids carrying the antiparallel probes (**S3** and **S4**) is in agreement with the release experiments described above. The higher sensitivity provided by the antiparalel triplex format (solids **S3** and **S4**) may

be due to a combined effect of the structure of the antiparallel clamps, which are more efficient in bloking MSNs, and a more rapid formation of the triplex due to the existence of a preformed reversed Hoogsteen antiparalel structure in the capping oligonucleotides **O2** and **O3**.The obtained LODs fell within the expected concentrations for circulating miRNAs in human serum (0-1 pM), demonstrating the potential of the method for its application in clinical diagnostics. Compared with the SPR protocol using similar triplex-forming capture probes[15] the systems described herein show an increase of 3 orders of magnitude. This increase could be ascribed to the amplification of the signal induced by the release of a large number of fluorescent rhodamine molecules per recognition event when using gated materials. The limits of detection obtained are in the range of Northern blotting or microarray,[2] however, our proposed method is simpler, faster and no especial instrumentation is needed nor labeling of the sample.

Table 4. Limits of detection of the solids **S2-S6**.

Solid	Oligonucleotide	Limit of Detection (pM)
S2	Duplex	2.5
S3	Antiparallel-8Ag	0.30
S4	Antiparallel	0.25
S5	Parallel-8Ag	5.0
S6	Parallel	8.0

In a step forward, the specificity of the solids was confirmed by studying the response of **S2-S6** to different possible interferent miRNAs (see **Table S2** in the Supporting Information). As it is shown in **Figure 2**, miRNA-145 is the only molecule able to induce a notable dye delivery, whereas all the interferents induced less pore opening and poor payload release. This observation supports a selective oligonucleotide-miRNA-145 interaction as mechanism of the observed optical response, and corroborates the preferential binding of the used oligonucleotides with the miRNA-145 sequence, which resulted in uncapping of the pores and payload delivery.

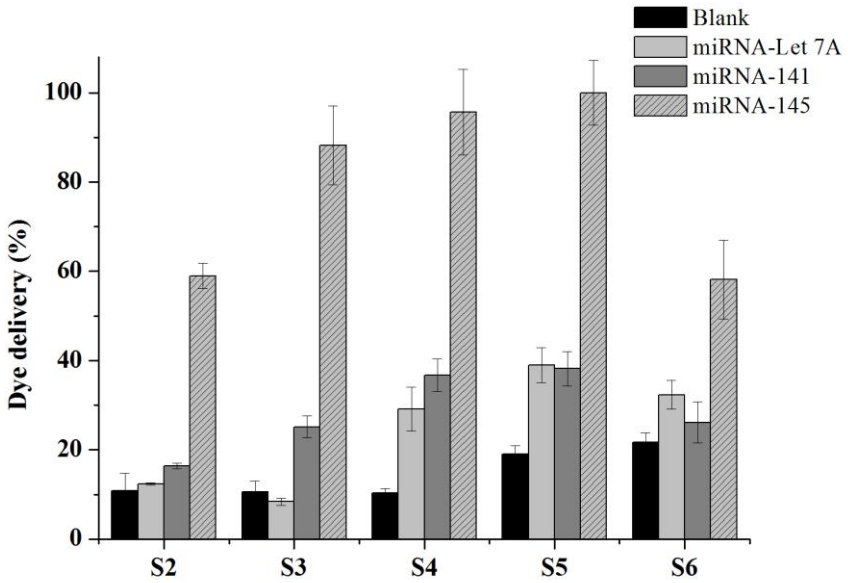

Figure 2. Release of rhodamine B from solid **S2**, **S3**, **S4**, **S5** and **S6** in the absence and the presence of miRNA-Let7A, miRNA-141 and miRNA-145.

MiRNA-145 detection in real media

The detection of miRNA-145 directly in real samples is a topic of high interest. New strategies to help medical professionals to obtain accurate and rapid results to early diagnose and made a prognosis of their patients is a decidedly pursued goal. Therefore, the potential use of the sensing solids to detect miRNA-145 in more competitive samples was studied. In particular, delivery of rhodamine B from S2 and S4 in the presence and in the absence of miRNA-145 was carried out in human serum samples (see Experimental section for details). Figure 3 shows a selective displacement of the oligonucleotide, pore opening and dye release in the presence of miRNA-145 for both solids after 30 min (grey columns). Although a slightly higher background was observed in serum samples when compared with that obtained in hybridization buffer (ca. 20% and 10%, respectively), a clear larger amount of dye was delivered in the presence of miRNA-145 which resulted in a flawless miRNA-145 detection. These results show that the proposed method

may be a promising alternative to classical procedures for the detection of target miRNA in clinical relevant samples.

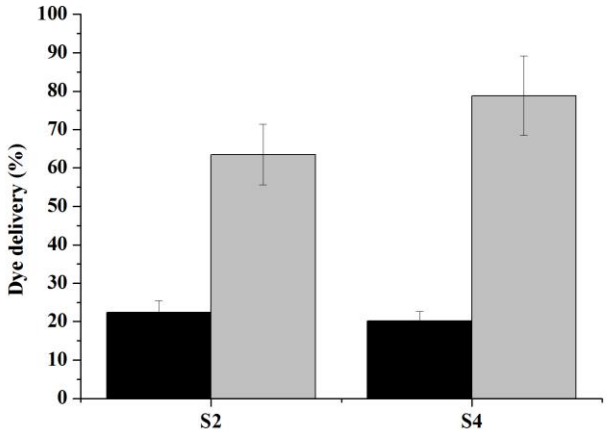

Figure 3. Release of rhodamine B from solid **S2** and **S4** in the absence (in black) and the presence (in grey) of miRNA-145 in human serum samples.

Conclusions

Developing new strategies for sensitive and label-free detection of miRNA has become an important issue in the clinical field. Here we present a new protocol for the detection of miRNA-145 by using MSNs loaded with a dye and capped with selective oligonucleotides. The response of the detection systems is related with the recognition between the capping oligonucleotide and miRNA-145, which induced a displacement of the oligonucleotide from the solid, pore opening and dye release. The use of duplex or triple-helix formats between the miRNA and the complementary DNA probe was studied. In particular, we analyzed the use of antiparallel and parallel clamps and the effect of introducing 8-amino-2'-deoxyguanosine in these clamps. All proposed solids presented excellent analytical performances in terms of sensitivity and selectivity. Specifically, the antiparallel triplex formation (**S3** and **S4**) resulted in a more efficient approach when compared with parallel triplex or duplex formation, reaching LODs as low as

0.25 pM. In addition, the capped nanomaterial allowed an accurate determination of miRNA-145 in realistic human serum samples. The achieved results are of interest towards the detection of miRNA in a realistic manner. The method is simple, portable, can be easily tuned via the use of different reporting molecules (e.g. dyes, fluorophores or electroactive species) and may allow the development of simple tests, offering a great potential for clinical applications.

Acknowledgements

We thank the Spanish Government (projects MAT2015-64139-C4-1-R, AGL2015-70235-C2-2-R and CTQ2014-52588-R (MINECO/FEDER)), the Generalitat Valenciana (project PROMETEOII/2014/047) and the Generalitat de Catalunya (2014/SGR/624) for support. A.R. thanks UPV for her predoctoral fellowship. S.S. thanks the Instituto de Salud Carlos III and the European Social Fund for the financial support "Sara Borrell" (CD16/000237). The authors also thank the Electron Microscopy Service at the UPV for support.

Author contributions statement

L.M, and R.M proposed the idea. A.R, S.S and E.X carried out the experiments. E.A, F.S and T.P analysed the results. All authors discussed the results, wrote and reviewed the manuscript.

Additional Information

Competing financial interests: The authors declare no competing financial interests.

References

1. a) S.L. Ameres, P.D. Zamore, Nat. Rev. Mol. *Cell Biol*., **2013**, *14*, 475–488; b) S. Jonas, E. Izaurralde, *Nat Rev. Genetics*, **2015**, *16*, 421-433; c) A. Alagia, E. Eritja, The biochemistry of gene silecing. Encyclopedia Life Sciences, eLS, John Willey & Sons, Ltd. Chichester, 2017, a0021019.
2. H. Dong, J. Lei, L. Ding, Y. Wen, H. Ju, X. Zhang, *Chem. Rev*., **2013**, *113*, 6207-6233.

3. a) T. Tian, J. Wang, X. Zhou, *Org. Biomol. Chem*., **2015**, *13*, 2226-2238; b) M. Mahdiannasser, Z. Kamari, *Biosensors Bioelect*., **2018**, *107*, 123-144.
4. L. Liu, N. Xia, H. Liu, X. Kang, X. Liu, C. Xue, X. He, *Biosens. Bioelect*., **2014**, *53*, 399-405.
5. M. Kaplan, T. Kilic, G. Guler, J. Mandli, A. Amine, M. Ozsoz, *Biosens. Bioelect*., **2017**, *92*, 770-778.
6. F. Khakbaz, M. Mohamad, *Anal. Biochem*., **2017**, *523*, 32-38.
7. S. Azzouzi, W.C. Mak, K. Kor, A.P.F. Turner, M.B. Ali, V. Beni, *Biosens. Bioelect*., **2017**, *92*, 154-161.
8. T. Kilic, A. Erdem, M. Ozsoz, S. Carrara, *Biosens. Bioelect*.,**2018**, *99*, 525-546.
9. S. Fang, H.J. Lee, A.W. Wark, R.M. Corn, *J. Am. Chem. Soc*., **2006**, *128*, 14044.
10. J.R. Goñi, X. De La Cruz, X. Orozco, *Nucleic acids res*.,**2004**, *32*, 354-360.
11. J.R. Goñi, J.M. Vaquerizas, J. Dopazo, M. Orozco, *BMC genomics*, 2006, *7*, 63.
12. A. Aviñó, M. Frieden, J.C. Morales, B. García de la Torre, R. Güimil Garcia, F. Azorín, J.L. Gelpi, M. Orozco, C. González, R. Eritja, *Nucleic Acids Res*., **2002**, *30*, 2609-2619.
13. A. Nadal, R. Eritja, T. Esteve, M. Pla, *ChemBioChem.*, **2005**, *6*, 1034-1042.
14. L.G. Carrascosa, S. Gomez-Montes, A. Aviño, A. Nadal, M. Pla, R. Eritja, L.M. Lechuga, *Nucleic Acids Res*., **2012**, *40*, 56.
15. A. Aviñó, C.S Huerta, L.M. Lechuga, R. Eritja, *Anal. Bioanal. Chem*., **2016**, *408*, 885-893.
16. a) E. Aznar, M. Oroval, L. Pascual, J.R. Murguía, R. Martinez-Máñez, F. Sancenón, *Chem. Rev*., **2016**, *116*, 561-718; b) J. Wen, K. Yang, F. Liu, H. Li, J. Xu, S. Sun, *Chem. Soc. Rev*., **2017**, 46, 6024; c) C. Li, M. Qian, S. Wang, H. Jiang, Y. Du, J. Wang, W. Lu, N. Murthy, R. Huang, *Theranostics*, **2017**, *7*, 3319; d) R. Bhat, I. García, E. Aznar, B. Arnaiz, M.C. Martínez-Bisbal, L.M. Liz-Marzán, S. Penadés, R. Martínez-Máñez, *Nanoscale*., **2018**, *10*, 239-249; e) T. Ribeiro, E. Coutinho, A.S. Rodrigues, C. Baleizão, J.P.S. Farinha, *Nanoscale*., **2017**, *9*, 13485.
17. a) F. Sancenón, L. Pascual, M. Oroval, E. Aznar, R. Martínez-Máñez, *ChemistryOpe*n, **2015**, *4*, 418-437; b) Q. Tan, R. Zhang, R. Kong, W. Kong, W. Zhao, F. Qu, *Microchim. Acta*, **2018**, *185*, 44.
18. a) M. Ercan, V.C. Ozalp, B.G. Tuna, *Anal. Biochem*., **2017**, *537*, 78; b) L. Pascual, I. Baroja, E. Aznar, F. Sancenón, M.D. Marcos, J.R. Murguia, P. Amoros, K. Rurack, R. Martinez-Máñez, *Chem. Comm*., **2015**, *51*, 1414-1416.
19. P. Zhang, F. Cheng, R. Zhou, J. Cao, J. Li, C. Burda, Q. Min, J.J. Zhu,. *Angew. Chem. Int. Ed*., **2014**, 53, 2371-2375.
20. a) Z. Zhang, F. Wang, D. Balogh, I. Willner, *J. Mater. Chem. B*, **2014**, *2*, 4449; b) A. Aviñó, M. D. Marcos, F. Sancenón, R. Martínez-Máñez, P. Amorós, *Chem. Comm*., **2013**, *49*, 5480-5482; c) A. Ribes. E. Xifré-Pérez, E. Aznar, F. Sancenón, T. Pardo, L.F. Marsal, R. Martínez-Máñez, *Sci. Rep*., **2016**, *6,* 38649.
21. D. Santovito, C. Mandolini, P. Marcantonio, V. de Nardis, M. Bucci, C. Paganelli, Expert *Opin. Ther. Targets*, **2013**, *17*, 217-223.
22. T. Takagi, A. Iio, Y. Nakagawa, T. Naoe, N. Tanigawa, Y. Akao, *Oncology*, **2009**, *77*, 12-21.
23. E.P. Barrett, L.G. Joyner, P.P. Halenda, *J Am. Chem. Soc*., **1938**, *73*, 373-380.
24. S. Brunauer, P.H. Emmett, E. Teller, *J. Am. Chem. Soc*., **1938**, *60*, 309-319.
25. A.Aviñó, E. Cubero, C. González, R. Eritja, M. Orozco, *J. Am. Chem. Soc*., **2003**, *125*, 16127-16138.
26. J. Robles, A. Grandas, E. Pedroso, F.J. Luque, R. Eritja, Orozco, M. *Curr. Org. Chem*., **2002**, *6*, 1333-1368.

SUPPLEMENTARY INFORMATION

Design of oligonucleotide-capped mesoporous silica nanoparticles for the detection of miRNA-145 by duplex and triplex formation

Àngela Ribes, Sara Santiago-Felipe, Anna Aviño, Vicente Candela-Noguera, Elena Aznar, Ramón Eritja, Felix Sancenón and Ramón Martínez-Máñez

1. ***MSNs structure characterization***

Powder x-ray diffraction and electron transmission microscopy

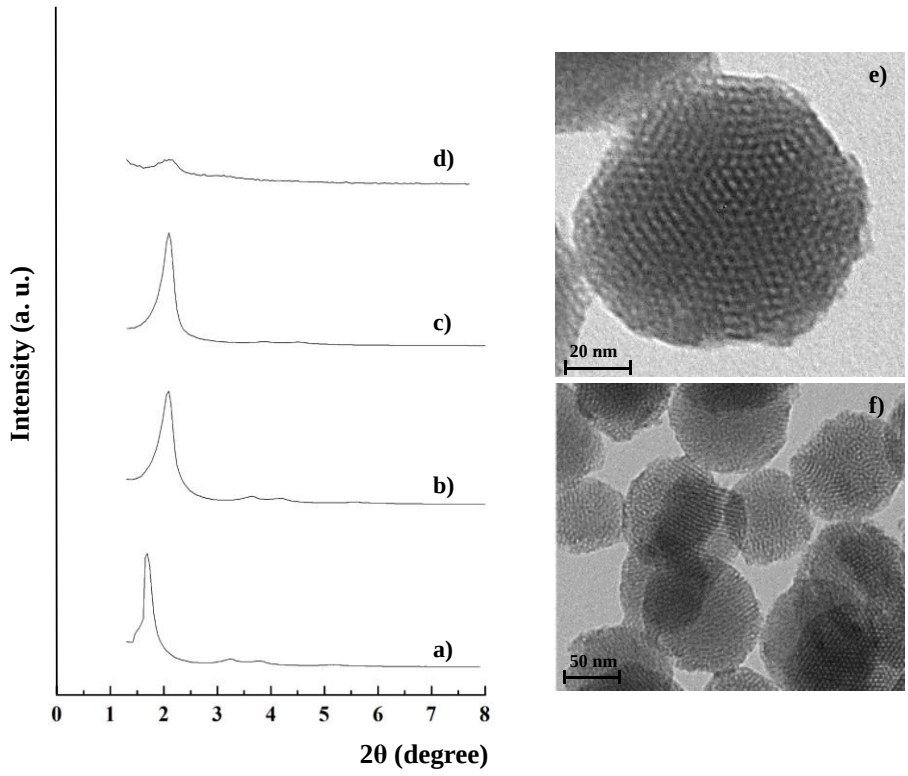

Figure S1. Powder X-ray patterns of MSNs as synthesized (a), calcined MSNs (b), **S1**(c) and **S3** (d). Inset: TEM images of (e) calcined MSNs and (f) **S4**.

N_2 adsorption–desorption characterization

Mesoporosity was analysed by N_2 adsorption–desorption isotherms. Calcined MSNs showed an adsorption step at an intermediate P/P_0 value (0.1–0.5) typical

of this type of solid (see **Figure S2**). This step can be related to the nitrogen condensation inside the mesoporous by capillarity. The absence of a hysteresis loop in this interval and the narrow BJH pore suggest the existence of uniform cylindrical mesopores with a total pore volume of 0.38 $cm^3\ g^{-1}$ calculated by using the BJH model on the adsorption branch of the isotherm. The application of the BET model resulted in a value for the total specific surface of 1027.53 $m^2\ g^{-1}$. From the XRD, porosimetry and TEM studies, a pore diameter of 2.54 nm was determined. In addition to this adsorption step associated to the micelle generated mesopores, a second feature appeared in the isotherm at a high relative pressure (P/P0 > 0.6). This corresponded to the filling of the large voids among the particles and presented a volume of 0.29 $cm^3\ g^{-1}$ (calculated by using BJH model), which must be considered as a textural-like porosity. In this case, the curves showed a characteristic H1 hysteresis loop and a wide pore size distribution.

The N_2 adsorption–desorption isotherm of **S1** (see **Figure S2**) is typical of mesoporous systems with filled mesoporores, and a decrease in the N_2 volume adsorbed (0.10 $cm^3\ g^{-1}$) and surface area (278.21 $m^2\ g^{-1}$) were observed. The most relevant feature in the N_2 adsorption–desorption isotherm of these solids is the absence of a sharp step at low-medium relative pressure ($0.1 < P/P_0 < 0.6$). In fact, this solid showed flat curves when compared (at the same scale) to those of the starting MSNs parent material, this indicates a significant pore blocking and the subsequent absence of appreciable mesoporosity.

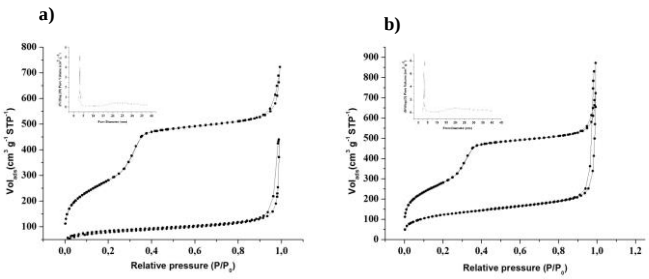

Figure S2. Nitrogen adsorption-desorption isotherms for (a) calcined MSNs (b) solid **S1** Inset: Pore size distribution of calcined MSNs.

Table S1. BET Specific Surface Values, Pore Volumes, and Pore Sizes Calculated from the N_2 Adsorption−Desorption Isotherms for Selected Materials.

	S_{BET} ($m^2\ g^{-1}$)	BJH pore size ($P/P_0 < 0.6$)[a] (nm)	Pore volume ($P/P_0 < 0.6$)[b] ($cm^3\ g^{-1}$)	BJH pore size ($P/P_0 > 0.6$)[c] (nm)	Pore volume ($P/P_0 > 0.6$)[d] ($cm^3\ g^{-1}$)
Calcined MSNs	1027.53	2.42	0.38	54.28	0.29
S1	278.21	2.54	0.10	28.51	0.18

[a]Pore size estimated by using the BJH model applied on the adsorption branch of the isotherm, for $P/P_0 < 0.6$, which can be associated with the surfactant generated mesopores. [b]Pore volume estimated by using the BJH model applied on the adsorption branch of the isotherm, for $P/P_0 < 0.6$, which can be associated with the the surfactant generated mesopores. [c]Pore size for $P/P_0 > 0.6$, which can be associated with the textural porosity. [d]Pore volume for $P/P_0 > 0.6$, which can be associated with the textural porosity.

2. Dynamic Light scattering characterization

The progressive diameter increase in each functionalization step from calcined MSNs to final solids **S2**-**S6** is shown in **Figure S3**.

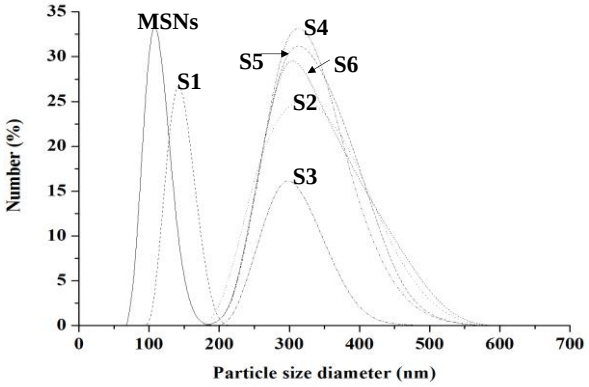

Figure S3. Size distribution obtained by DLS studies for calcined MSNs, **S1**, **S2**, **S3**, **S4**, **S5** and **S6** solids.

3. Release experiments

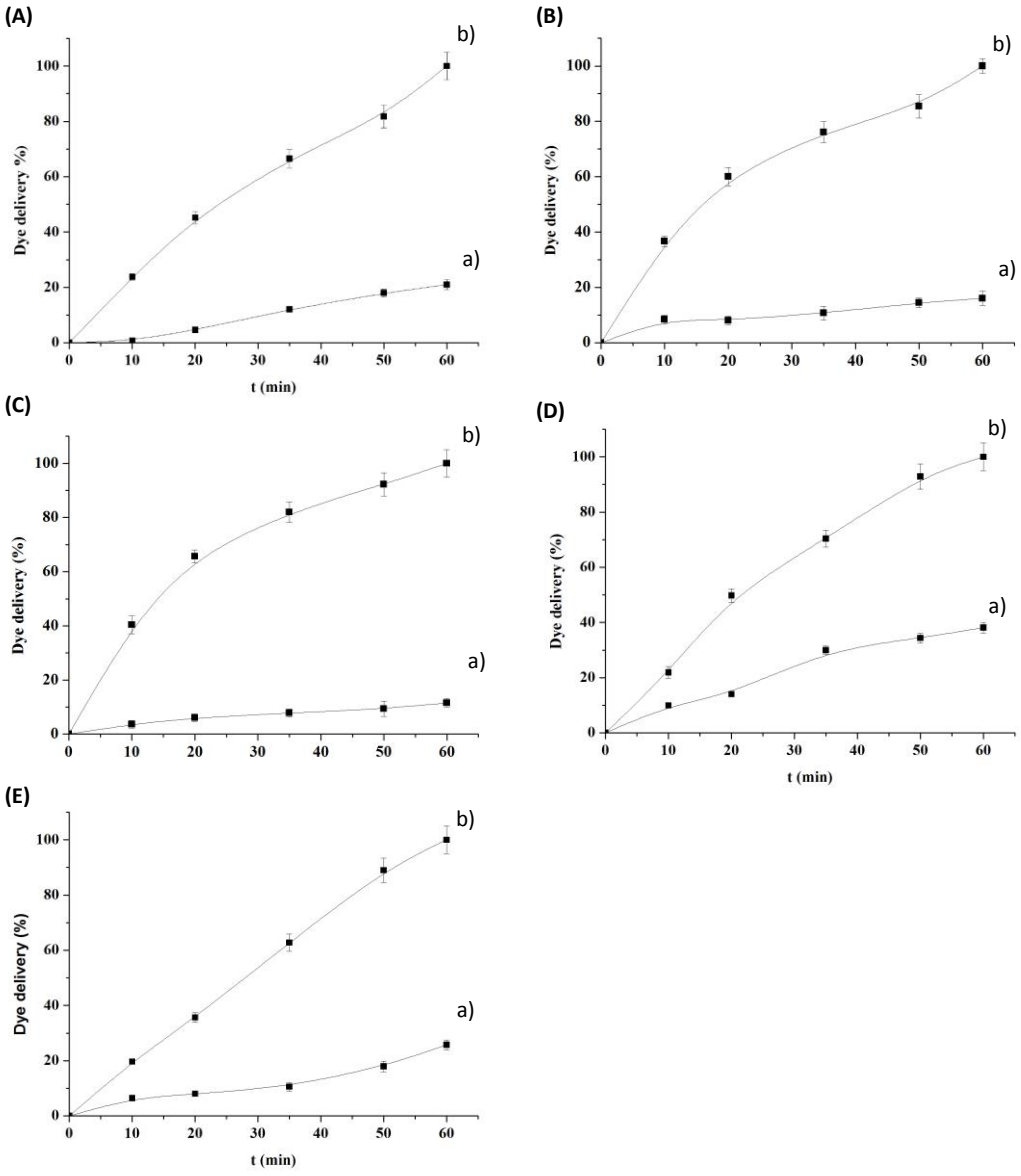

Figure S4. Release profile of rhodamine B from solids **S2** (A), **S3** (B), **S4** (C), **S5** (D), **S6** (E) in the absence (a) and the presence (b) of miRNA-145.

4. Limit of detection

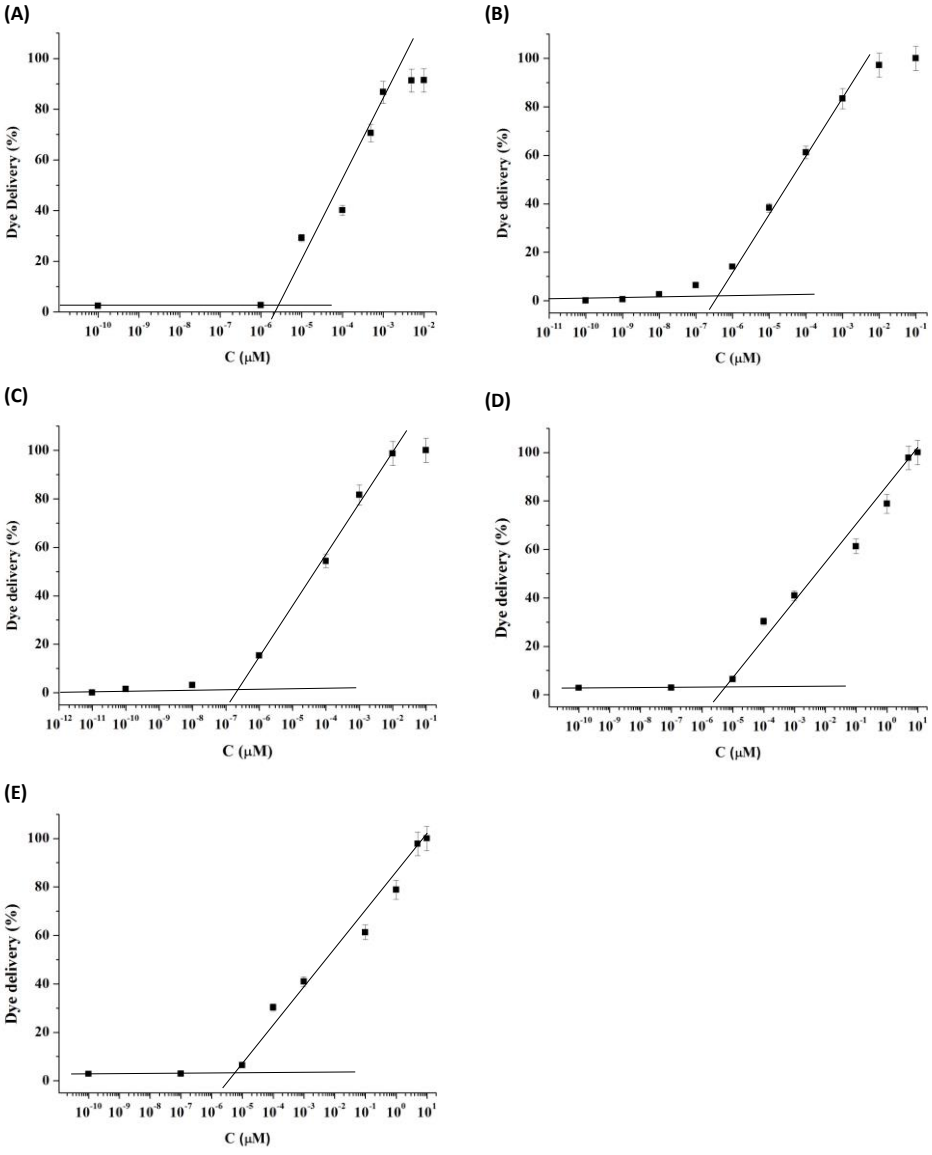

Figure S5. Release of rhodamine B from solids **S2** (A), **S3** (B), **S4** (C), **S5** (D) and **S6** (E) in the presence of different concentrations of miRNA-145.

Table S2. Mass spectrometry analysis of the oligonucleotides prepared in this work obtained by Matrix-Assisted Laser Desorption Ionization Time-Of-Flight (MALDI-TOF).

Code	Name	M calculated (g/mol)	M found (g/mol)
O1	Duplex	7137.7	7140.8
O2	Antiparallel-8AG Clamp	8785.7	8784.8
O3	Antiparallel Clamp	8740.7	8737.8
O4	Parallel-8AG Clamp	8625.2	8628.6
O5	Parallel Clamp	8580.2	8584.2
O6	miRNA-145	7216.1	7216.2
O7	miRNA-141	7066.4	7063.5
O8	miRNA-let 7A	7101.4	7097.4

8. Conclusions and perspectives

The reports of functional nanomaterials have been exponentially increasing over the last decades. In this field, a significant attention has been paid to the development of new hybrid materials for chemical and biomedical applications. Gated materials have specially contributed to this area with clever designs and new approaches with high impact in the fields of drug delivery and, more recently, in sensing. This PhD thesis has tried to contribute to the knowledge in this field with the development of innovative gated hybrid materials that use new recognition strategies and with potential practical application in certain detection and diagnosis protocols

In particular, in this thesis, a new fluorogenic probe for the detection of BPA using MSNs loaded with a dye and capped with a BPA-selective aptamer has been developed. The response of the probe is related with the interaction between the capping aptamer and BPA that induced a displacement of the aptamer, pore opening and dye release. A LOD as low as 3.5 μM for BPA was calculated. Moreover, the probe displayed an amplification of the signal and it was found that a unique molecule of BPA was able to induce the delivery of about 10 molecules of the dye. In addition, the capped nanomaterial allowed accurate BPA determination in tap water samples. As far as it is know, this is the first time that aptamer-capped mesoporous supports have been used for the detection of BPA.

This thesis also presents the design, preparation and evaluation of two new fluorogenic aptasensors for the detection of OTA by using MSNs loaded with a dye and capped with an OTA-selective aptamer. Two approaches, based on an electrostatic or covalent protocol, were used to cap the pores. The response of both probes is related with the interaction between the capping aptamer and OTA, which induces displacement of the aptamer from the solid, with the subsequent pore opening and dye release. The covalent approach displayed dye delivery in a shorter time than the sensing using an electrostatic approach. A LOD of 0.5 and 0.05 nM for the covalent and electrostatic supports were calculated, respectively. In addition, the capped nanomaterials allowed an accurate

determination of OTA in realistic wheat samples. The method is simple, portable, can be easily tuned through the use of different reporting molecules (e.g., dyes, fluorophores, or electroactive species) and may allow the development of a simple test for the detection of OTA in food samples.

The next chapter in this thesis demonstrated that the combination of nanoporous anodic alumina (NAA) supports and selected aptamers can be used to prepare gated probes to detect specific molecules. In particular, the NAA support was loaded with rhodamine B and capped using a specific oligonucleotide sequence capable to recognize cocaine. The studies demonstrated that the functionalized support was able to retain the cargo in an aqueous buffered solution, yet a clear delivery of the entrapped dye was selectively observed in the presence of cocaine. The response of the gated material to different cocaine concentrations was evaluated and a LOD of 5×10^{-7} M was determined. Furthermore, the selectivity of the system was assessed, which demonstrated that heroin and morphine drugs were unable to induce remarkable dye delivery. In addition, the potential applicability of the capped support was confirmed by the detection of cocaine in a competitive matrix such as saliva. As a final point, the possible re-use of NAA support was tested. This procedure, based on measuring an easy-to-detect fluorescent molecule that is delivered when cocaine is present, avoids analyte pre-treatment steps, such as extraction or derivatization and it is appropriate for rapid analyses by non-specialized personnel. The study also demonstrated that NAA is a suitable support to prepare optical gated probes with a synergic combination of the favorable features of gated sensing systems and NAA, which is easy to prepare and handle, and can be easily recovered.

In a step forward, the next chapter reported the development of a robust, sensitive and competitive sensing system to detect the infection produced by *Candida albicans* in clinical samples. The system consisted in the use of nanoporous anodic alumina (NAA) as support, loaded with Rhodamine B and capped with an oligonucleotide complementary to a specific region from *Candida albicans* genome. The response of the probe is related with the hybridization

between the capping oligonucleotide with the genomic DNA of *Candida albicans*, which induced pore opening and dye release. By this simple procedure a limit of detection as low as 8 CFU mL^{-1} was calculated. In addition, this capped nanomaterial allowed an accurate and effective detection of DNA of *Candida albicans* in different real samples from infected patients. The proposed method is simple, portable, can be easily tuned via the use of different reporting molecules and may allow the development of simple tests, offering a great potential for clinical applications.

The final chapter presented a new protocol for the detection of miRNA-145 by using MSNs loaded with a dye and capped with specific oligonucleotides. The response of the detection systems is related with the recognition between the capping oligonucleotide and miRNA-145, which induced a displacement of the gating oligonucleotide from the solid. The use of duplex or triple-helix formats between the miRNA and the complementary oligonucleotides was studied. All proposed solids presented excellent analytical performances in terms of sensitivity and selectivity. Specifically, the antiparallel triplex formation resulted in a more efficient approach when compared with parallel triplex or duplex formation, reaching LODs as low as 0.25 pM. In addition, the capped nanomaterial allowed an accurate determination of miRNA-145 in realistic human serum samples.

In summary, this PhD thesis presented a new set of hybrid organic-inorganic materials that are successfully applied in molecular recognition protocols in different areas. These or similar materials could be implemented in laboratory tests and could be the basis for the development of practical portable new kits for in situ detection of certain species or for the diagnosis of diseases. The procedure used in these new systems, based on the detection of fluorescent molecules delivered from capped materials, avoids undesired pre-treatment steps, such as extraction, derivatization or amplification and it is suitable for rapid analyses by non-specialized personnel. Due to the versatility, simplicity and portability of this

sensing approach, it envisioned the future design of simple tests to detect a large variety of species in different areas such as clinical diagnosis or quality control.

Gracias a la Universitat Politècnica de València por concederme una beca pre-doctoral para la Formación de Personal Investigador (FPI)